FACULTY OF SCIENCE AND TECHNOLOGY
Department of Physics and Technology

Mapping of Solar Energy Potential on Tromsøya Using Solar Analyst in ArcGIS

—

Erlend Homme Falklev

EOM-3901: Master's thesis in Energy, climate and environment, December 2017

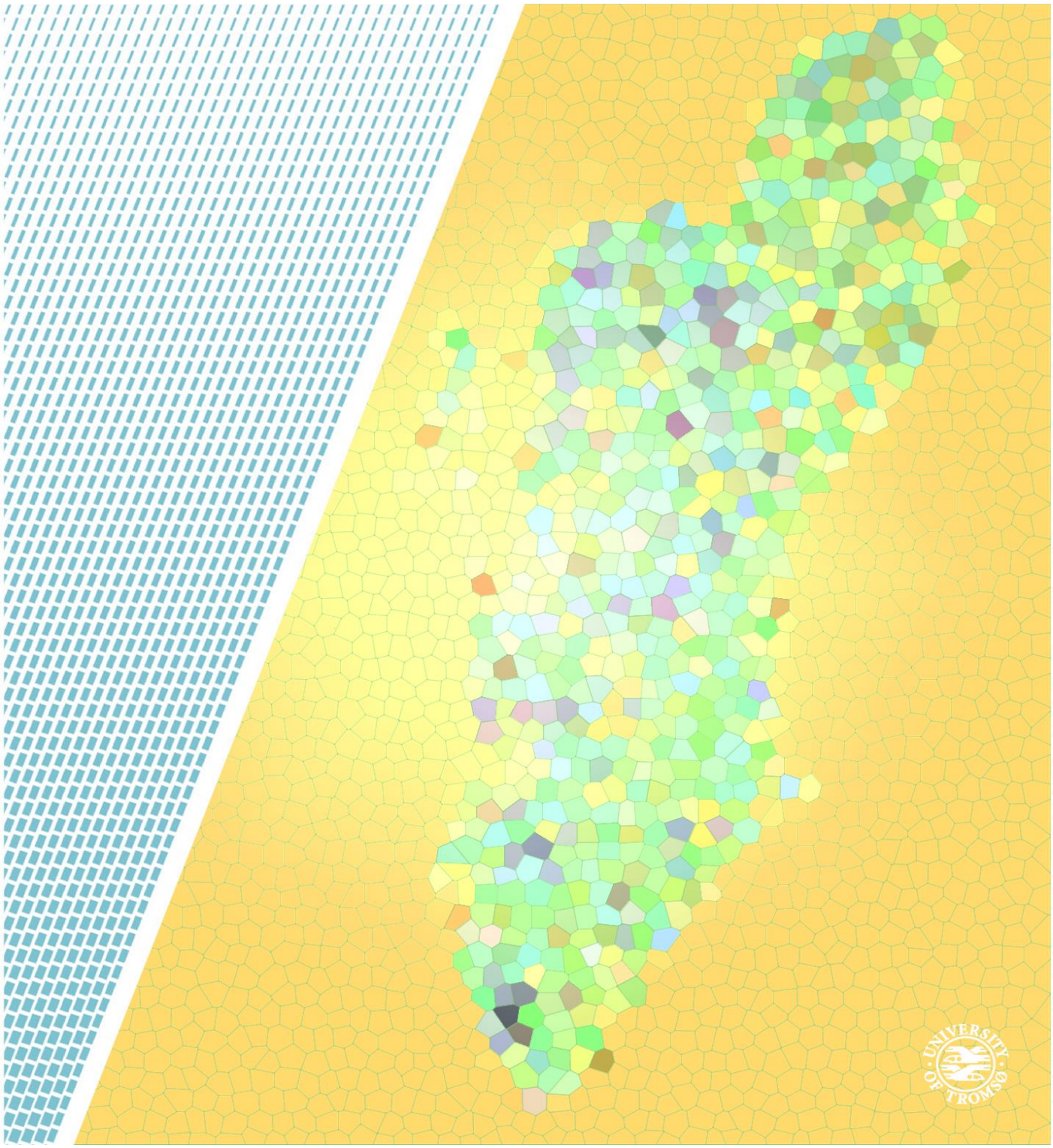

Front page created by Trond-Ola Hågbo.

The truth is: the natural world is changing.
And we are totally dependent on that world.
It provides our food, water and air.
It is the most precious thing we have and we need to defend it.
Sir David Attenborough

Abstract

The price of solar energy is declining, and will continue to decline the coming years. This will make it easier for households and companies to utilize solar energy. Because of this, several solar map projects have been established in the recent years. The aim of this study is to create a solar map of Tromsøya, and thoroughly explain the process in doing so. The process chosen for making the map is the same as used by Oslo Solar Map, made by Oslo Housing and Building Department. This involves the ArcGIS based package Solar Analyst Tools, which includes the tools Solar Radiation Graphics, Points Solar Radiation and Area Solar Radiation. These tools are created for modeling solar radiation at landscape scales. Solar Analyst require input of diffusion fraction and transmittivity value, which have an important effect on the results. These values are calculated by combining weather station measurements with calculation in Solar Analyst. One of the crucial issues in the creation of the solar map with this process is excessive computing times. Reducing computing time is investigated with the use of sectoring and investigating how the tools operate and utilizes computing power.

Acknowledgements

I have always wanted to do my best to fight climate change. I hope this thesis can provide a small part of the solution, as well as giving me a path to a meaningful job, in which I can continue to work towards a safe planet for future generations.

I am deeply indebted to my fellow students for giving me a family 2000 kilometers from home. Thank you for five awesome years.

I specifically want to thank my supervisor Clara Good for great advice and support through the process of writing this thesis. I also want to thank Rolf Andersen and Espen Tangen at the Section for Digital Research Services for invaluable input and inspiration in reducing computing time for solar maps. Stefanie Adamou from Oslo Housing and Building Department have been available throughout the last 3 months, and provided necessary and valuable information for this thesis. In addition, Marta Kováčová deserves recognition for motivation and encouragement in the last month of writing, along with my brother Anders Homme for proofreading this thesis.

Lastly, I want to express gratitude to my family. You are the most important part of my life.

Table of Contents

List of Abbreviations

AM	Air mass
ASR	Area Solar Radiation
CPU	Central processing unit
DEM	Digital elevation model
DIF	Diffuse solar radiation
DIR	Direct solar radiation
DSM	Digital surface model
DTM	Digital terrain model
ETRS	European Terrestrial Reference System
GDB	Geodatabase
GIS	Geographic Information System
LiDAR	Light detection and ranging
MET	Norwegian Meteorological Institute
NIBIO	Norwegian Institute for Bioeconomy
OHBD	Oslo Housing and Building Department
PSR	Point Solar Radiation
PV	Photovoltaic
PVGIS	Photovoltaic Geographic Information System
RADAR	Radio detection and ranging
SDM	Standard overcast diffuse model
SRG	Solar Radiation Graphics
TDIF	Total diffuse solar radiation

TDIR	Total Direct solar radiation
TGSR	Total Global Solar Radiation
TIN	Triangulated irregular network
UDM	Uniform diffuse model
USA	United States of America
UTM	Universal Transverse Mercator

1 Introduction

The price of solar energy is declining, and will continue to decline the coming years. This will make it easier for households and companies to utilize solar energy. Even in high-latitude areas like Northern Norway, the potential use of photovoltaic (PV) systems needs to be assessed. Municipalities like Stockholm and Oslo have developed solar maps to investigate the potential for solar energy on buildings and surfaces. The results will have significance for all building owners that consider utilizing solar energy, in addition to the planning of new buildings. The use of PV installations in Norway has significantly increased over the past years. Although the increase is not as significant in Northern Norway, a solar map will help map the potential and see if PV installations can be beneficial.

Oslo Municipality created their solar map based on weather data and the use of Solar Analyst in the Geographic Information System (GIS) ArcGIS. This method can be used for all locations, and has been used as a starting point for the work in this thesis. (PBE 2017)

1.1 Objective

The objective of this thesis is to determine the potential global solar radiation at Tromsøya using GIS. The results will be presented in the form of a solar map, which is a representation of solar insolation. The ultimate goal for creating such a map is to determine energy yield for solar modules. The results from this thesis is to be a step towards achieving that goal. It is important to thoroughly explain the processes included in the thesis to make it possible for others to use the same technique, as a solar map can be of benefit to everyone living in the mapping area.

The strategy for the thesis is chosen from using the same procedure as Oslo Housing and Building Department (OHBD) did in the making of Oslo Solar Map. They have been available for questions and shared information about programs and inputs they used for their map. The thesis is therefore based on the same process, but with individual inputs. A sensitivity analysis is necessary to find limiting factors and discuss what could have been done better to ensure the reliability and quality of the results in this thesis. Most of the info about Oslo Solar Map from the OHBD is based on personal communication through e-mail or phone calls with Stefanie Adamou. Some of the information for this thesis must be based on personal communication, as only small parts of the information are available online.

Oslo Solar Map used Solar Analyst in ArcGIS to calculate global solar radiation. Solar Analyst includes three tools: Area Solar Radiation (ASR), Point Solar Radiation (PSR) and Solar Radiation Graphics (SRG). They are crucial for this thesis, and include multiple calculations and assumptions that needs to be explained. ASR, PSR and SGR are tools for modeling solar radiation at urban and landscape scales.

An additional objective is look at options for reducing computing time for the main simulations in this thesis. The reason for this is the concern that excessive computing times will complicate the process of making such a map. This has been done in collaboration with Espen Tangen and Rolf Andersen in Section for Digital Research Services at The University of Tromsø. The reason for this goal was the extreme processing time the creators of Oslo Solar Map needed to make the map. Reduced computing time will make it possible to increase resolution and area, as well as updating the solar maps when necessary.

1.2 Existing Solar Map Projects

Several solar map projects have been established in the recent years. Some of these are mentioned here, to get an overview of a few existing projects and what type of data they are based on. The purpose of these maps is to give the residents easy access to info concerning the global radiation potential and potential solar energy output for their own homes. However, solar maps can also be used for planning new buildings, taking roof angles and roof orientation into account. All the maps below give the opportunity to search for addresses, thus making it easier to find the area in question.

1.2.1 Oslo Solar Map

Oslo Sunmap was created in 2016 by Oslo Municipality, more exactly the Unit for Planning and Thematic Maps, under the OHBD. The creators of Oslo Solar Map have been open about the process of making the map, thus making it possible to use the same strategy. The map is based on LiDAR measurements and Solar Analyst in ArcGIS, and rendered with the use of NT3D Builder, which is a help tool for ArcGIS made by Geodata. (PBE 2017) (ESRI Norsk Brukerkonferanse 2017)

1.2.2 Solkart.no

Solkart.no is a solar map of Norway. It is based on data from PVGIS, together with roof angles, roof sky orientation and the area of the roof. In addition, the creators include outputs for existing

solar module systems in calculating data. One of the goals for this map is to sell PV systems. (Solkart.no 2016)

1.2.3 Stockholm Solar Map

This solar map is for the whole of Stockholm County. Topography elements like vegetation and elements like chimneys on roofs are not considered. The solar map also calculates how well a solar panel would work according to temperature and the global solar radiation in real time. (Stockhols Stad 2017)

1.2.4 Google Project Sunroof

Project Sunroof was started up by Google in the United States of America (USA). One of their goals is to cover the entire Earth, but so far only a few cities have been mapped. Their map is based on 3D modeling of roofs and shade from nearby topography or buildings, together with imagery from Google's database. They also use historical weather patterns that may affect solar energy production. In addition, this sunmap recommends certain PV installers and computes savings for the roof in question. (Google Project Sunroof 2017)

1.3 Study Area

The chosen study area for this thesis is the island Tromsøya, located in Troms County. Figure 1-1 show a satellite picture of the island, with Holt weather station marked. Because of time-concerning issues with computing time, the initial study area of the whole municipality of Tromsø was scrapped. Tromsøya has an area of 22 km^2.

Figure 1-1: Overview map of Tromsøya, with Holt Weather Station marked. Made in ArcGIS. Projection: UTM Z-33N.

1.4 Structure of the Thesis

Chapter 2 will provide the reader with sufficient theoretical background to understand all aspects of the thesis. Properties of solar radiation and photovoltaics are introduced, together with basics of GIS. In addition, GIS programs and tools used are introduced for the reader to get the background required to understand how they work and what they are used for.

Chapter 3 presents the methodology. It describes the processes of creating the solar map, including how the issue of computing time was assessed.

Chapter 4 covers the results and discussion of the thesis. This includes a sensitivity analysis to validate final outputs and choices made during the process.

Chapter 5 contains the conclusion. Results are summarized, and future work concerning the solar map are proposed.

Chapter 6 contains the bibliography.

Chapter 7 contains the appendix.

2 Theory

2.1 Solar Energy

2.1.1 Properties of Solar Radiation

The total radiation from the sun is close to constant. In this thesis, it will be represented by the solar constant (S_{const}). The solar constant is a measurement of solar radiation at the average sun-earth distance on the top of the atmosphere, at a surface perpendicular to the Sun. Although solar radiation varies over time because of 11-year cycles in solar activity, the average value will be used. With measurements of extra-terrestrial (outside Earth's atmosphere) solar radiation from satellites through decades, the average value was selected to be:

$$S_{const} = 1367 \frac{W}{m^2} \quad (1)$$

In this formula, we see that the solar constant is a measurement of watts (W) per square meter (m^2). Note that radiation is used as a term related to solar in this thesis. It is necessary to define the difference between solar radiation power and solar radiation energy. The solar constant is a measurement of irradiance, which is solar radiation power. Solar radiation energy is called irradiation or insolation, and the unit $\frac{Wh}{m^2}$, where h is hours. Thus, irradiation is the integrated irradiance over a time. (Solanki 2011)

The radiation must travel through the atmosphere to reach the surface, and as the atmosphere consists of molecules like water vapor, carbon dioxide and ozone, there is scattering and absorption of radiation that leads to lower radiation at the surface. (Sengupta, et al. 2015)

The amount of scattering and absorption is dependent on the path length of the atmosphere the radiation must travel before reaching the surface. As the Sun's position relative to a place on Earth change throughout the year, so does the incoming irradiance. Air mass (AM) is the path length that the solar radiation must travel through the atmosphere, compared to the path length it must travel through at the zenith. See description of this in Figure 2-1, and the following equation (2). The zenith angle is the angle between the sun and the vertical from a location (θ). When the sun is located directly above a location at sea level, it is called air mass one (AM1), thus when $X = Y$.

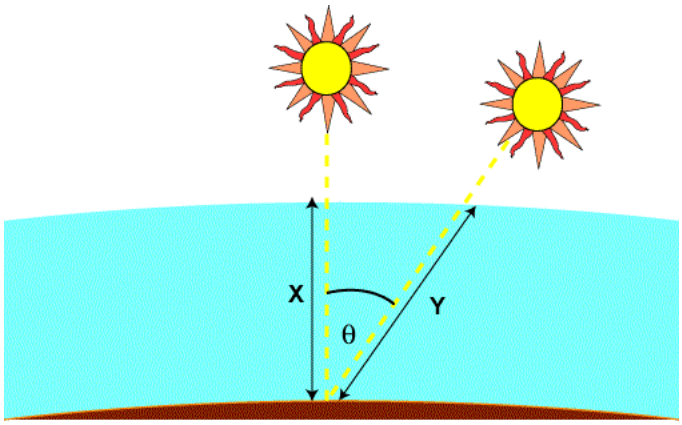

Figure 2-1: Illustration of AM differences and the zenith angle. (Honsberg and Bowden 2015)

$$AM = \frac{Y}{X} = \frac{1}{\cos(\theta)} \quad (2)$$

The further away the sun is from the vertical, the longer the path length is. At $\theta = 60°$, AM will be doubled from AM1, and is called AM2. Thus, the radiation must travel twice the path length in the atmosphere to reach the surface, and more radiation will be lost due to scattering and absorption (Sengupta, et al. 2015).

The highest sun angle at Tromsøya is around 43.8°, which gives a zenith angle of 46.2° and the following AM Tromsø (AM_T):

$$AM_T = \frac{1}{cos(46.2)} = 1.44 \quad (3)$$

The further the distance the radiation must travel, the more is lost to absorption and scattering. The probability of loss increases with the path length, so Tromsøya with its AM being as high as it is, will have more of these losses. It is important to note that weather conditions and atmospheric constituents have high influence on the total irradiance reaching the surface.

2.1.2 Direct, Diffuse and Global Radiation

The radiation reaching the surface is divided into two components: direct radiation and diffuse radiation. Direct radiation is the photons reaching the surface without any influence from absorption and scattering. It is necessary to distinguish between direct normal radiation and direct radiation. Direct normal radiation is direct radiation on a surface always angled towards the sun, so direct radiation is the direct normal multiplied with cosine of the zenith angle. Diffuse radiation is the photons reaching the surface after interacting with the atmosphere. Global radiation is the geometric sum of diffuse and direct radiation. This gives the calculation in equation (4) (Sengupta, et al. 2015)

$$GHI = DNI \times \cos(\theta) + DHI \quad (4)$$

The different components of solar irradiance are displayed in Figure 2-2.

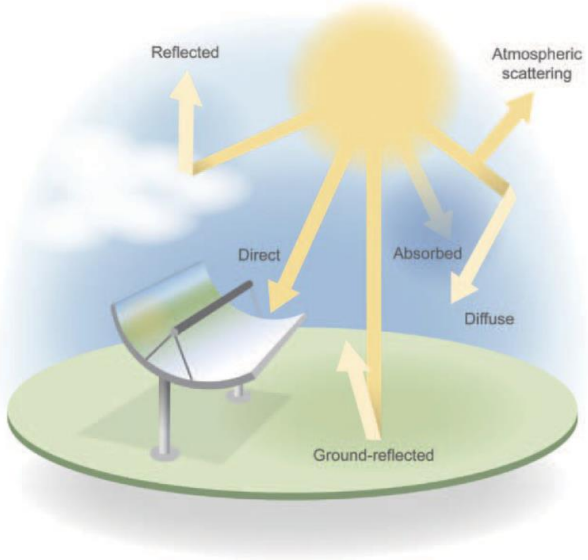

Figure 2-2: Illustration of the solar radiation components inside the atmosphere. (Sengupta, et al. 2015)

2.1.3 Solar Radiation in Norway

There are few measurements of solar radiation above 60° north latitude. This is a consequence of the trajectory of satellites around the earth, as they usually do not pass 60° north. Because of this, calculations will potentially have large insecurities for these areas. The online calculation tool called Photovoltaic Geographic Information System (PVGIS) is one of the main used sources to calculate solar radiation. They estimate global radiation for locations picked by the user. Their website consists of several tools to calculate values for optimally inclined surfaces, horizontal surfaces, and different solar cell technologies. Two versions of PVGIS is available at their website, the original PVGIS and the latest version PVGIS5. (PVGIS 2017) (PVGIS5 2017)

When using the original version, PVGIS give a horizontal global radiation value of 719 kWh/m^2 for the location of Holt weather station. (PVGIS 2017)

The new PVGIS5 show results for each year. These data are presented in Table 2-1, with values of kWh/m^2. (PVGIS5 2017)

Table 2-1: Estimated global solar radiation for Holt weather station. Created from PVGIS5 for a horizontal and optimally inclined surface. Values in kWh/m²

Year	Horizontal surface	Optimally inclined surface
2011	731	917
2012	709	900
2013	746	974
2014	758	973
2015	685	958
2016	670	870

Figure 2-3 shows estimated solar insolation per day in January and June.

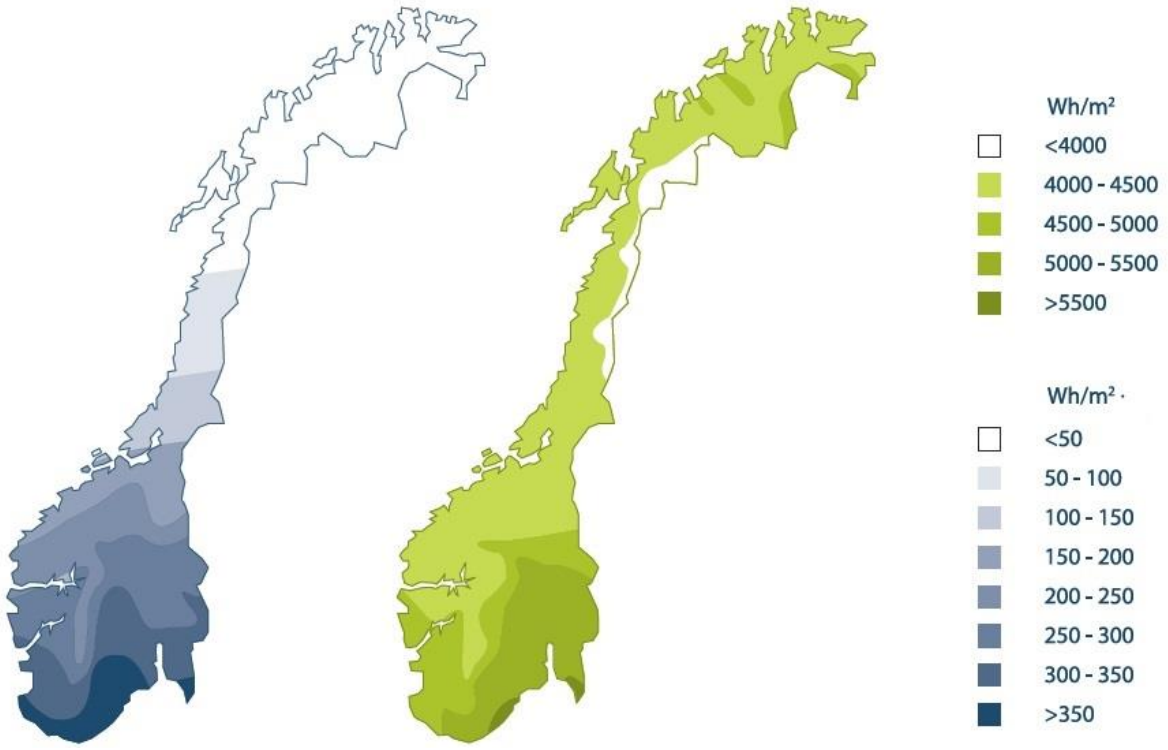

Figure 2-3: Global solar radiation per day for January (left map) and June (right map). Legend shows expected values of Wh/m² for each day, with the top legend being for June and the bottom for January. (Barstad 2016)

2.2 Photovoltaics

Introducing photovoltaics (PV) theory is important for this thesis as an ultimate goal of the solar map is to connect it to solar energy, and whether it would be appropriate with solar energy systems in conditions as far north as Tromsøya. Knowing how much of the solar radiation that can be used is a part of this understanding.

Solar cells are somehow looked upon as not suitable for areas like the Arctic, as the global irradiation is lower there compared to areas closer to the equator. Ever since space operations

needed solar cells to access electricity in space, the investments and research in the photovoltaics field has been expanding. In 2016, there was a growth of over 50% for the photovoltaics (PV) market. This brought the total installations of the year to 75 GW, after a limited rise in 2014 and 25% growth in 2015. The total installed capacity by the end of 2016 is around 300 GW. This emphasizes the growth in 2016, with it being 25% of the installed capacity. The PV industry is expected to continue its growth over the next years. (IEA-PVPS 2017)

A photovoltaic solar cell is made of semiconductor materials, most commonly crystalline silicon which dominates the market today. Most cells have a thickness of around 160 µm (10^{-6} meters), and all cells have a width of 156 mm. A basic cell consists of several important parts: the substrate material (silicon), doped base and emitter, texturing and reflection coating, finger and busbar. (Honsberg and Bowden 2015)

See Figure 2-4 for a sketch of the components of a solar cell.

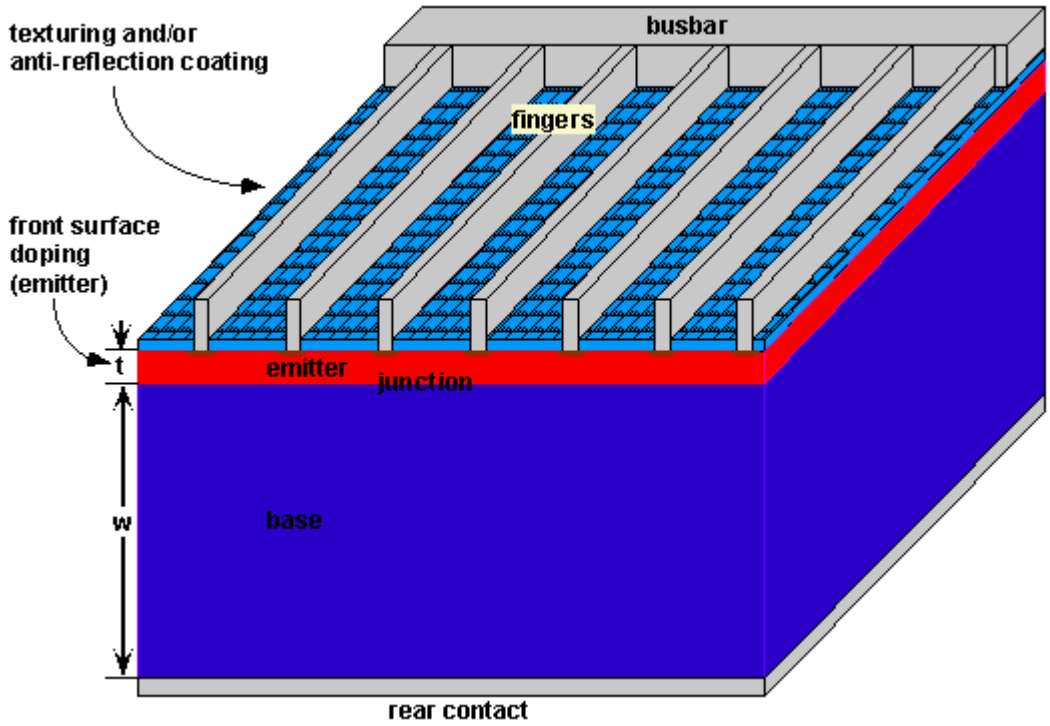

Figure 2-4: A sketch of the components in a silicon solar cell. (Honsberg and Bowden 2015)

Regular silicon solar cells today have an efficiency of around 20%. Efficiencies as high as 44.7% have been achieved by using quadruple junction, although these cells are too expensive for commercial sale. There is a lot of research going on in the photovoltaics community, and

cell efficiencies and cost will continue to rise and decrease respectively. (Andrews and Kais 2015)

The efficiency of a solar cell is dependent on factors like temperature and albedo, and the output can be increased by using tracking systems or reducing snow and ice cover.

2.2.1 Photovoltaics in Arctic conditions

Solar energy generation in the Arctic is different from other areas around the Earth. This alters how solar energy should be looked upon, as several aspects will decide how the output changes. The following is a brief introduction to what makes photovoltaics in Arctic conditions different than others.

2.2.1.1 Efficiency Temperature Dependence

An important aspect to solar cells used in the Arctic, is the fact that solar cell efficiency is dependent on temperature. What is important to note from this is that PV modules have higher performance in lower temperatures. Most modules are sensitive to temperature, and will have a higher power output with lower operating temperatures. (Dubey, Sarvaiya and Seshadri 2013)

2.2.1.2 Snow

When discussing potential use of photovoltaics in northern parts of the world, snow is an important aspect to include. Snow can be both negative and positive for the efficiency of the cell. Negative aspects are snow and ice coverage on the solar modules. Snow is a very reflective medium, so only a thin layer of snow on a solar panel can greatly alter the energy generation. This is a problem for solar energy generation where there are a lot of snow days. A coating to remove snow from solar panels and work properly has not been made yet. (Andenæs, et al. 2018)

A positive aspect is the effect of albedo. Albedo is the fraction of solar radiation reflected from a surface. If 100% of the radiation is reflected, the surface has an albedo of 1. A black body, which absorbs all radiation, has an albedo of 0. This is important because northern areas like Tromsøya have vast amounts of snow cover days (days of snow on the ground) in a year. The reflection contributes to more photons reaching the solar cell. Different types of surface albedo are illustrated in Figure 2-5. (Quaschning 2005)

Surface	*Albedo A*	*Surface*	*Albedo A*
Grass (Summer)	0.25	Asphalt	0.15
Lawn	0.18–0.23	Woods	0.05–0.18
Dry grass	0.28–0.32	Heathland and sand	0.10–0.25
Uncultivated fields	0.26	Water surface ($\gamma_S > 45°$)	0.05
Soil	0.17	Water surface ($\gamma_S > 30°$)	0.08
Gravel	0.18	Water surface ($\gamma_S > 20°$)	0.12
Concrete, weathered	0.20	Water surface ($\gamma_S > 10°$)	0.22
Concrete, clean	0.30	Fresh snow cover	0.80–0.90
Cement, clean	0.55	Old snow cover	0.45–0.70

Figure 2-5: Different types of surface albedo ((Quaschning 2005)

Figure 2-6 illustrates the effects of several types of spectral albedo have on a variety of cells. Silicon cells, that have low band-gap, corresponds to short wavelengths. Snow is very reflective in the UV spectrum, which is short wavelengths, thus increasing the efficiency of the cell. The authors conclude that crystalline silicon cells may be a better option in areas with more snow. (Brennan, et al. 2014)

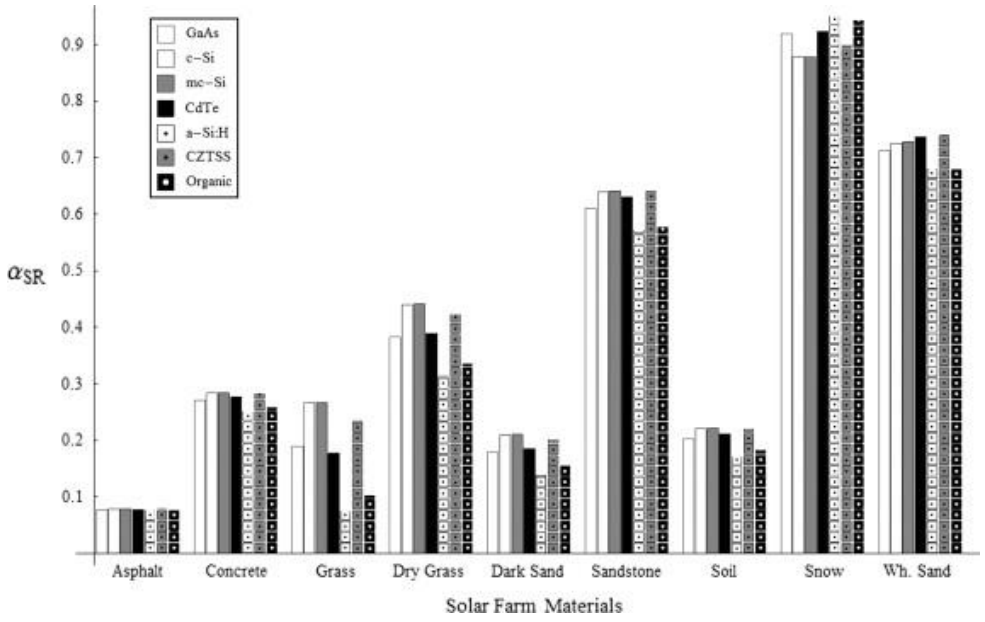

Figure 2-6: Different albedo effects on a variety of solar cells. (Brennan, et al. 2014)

2.2.1.3 Tracking Systems

The use of tracking systems can potentially make a significant difference for solar energy generation. In parts of summer, when there is midnight sun in Arctic areas, a tracking system will be able to follow the sun around the horizon. There are different tracking systems available,

either one-axis tracking or two-axis. A one-axis tracking system can either have vertical or horizontal tracking, while a two-axis system has both. The horizontal tracking system might not create a momentous change to the overall power output in high latitudes, but the vertical tracking system will follow the sun as it turns 360° in summer. In a potential question of cost, the horizontal one-axis system will be cheaper than the two-axis system, and can therefore be favorable. (Quaschning 2005)

Figure 2-7: Picture of a two-axis tracking system in Piteå, Sweden. (Christensen 2012)

2.3 Geographic Information System

Geographic Information System (GIS) is a system that presents, manages, stores and analyzes geographic and spatial data. A GIS lets the user interpret data to visualize pattern and trends, and is used for a wide range of tasks in different businesses around the world. This can be everything from mapping flood areas and evacuation planning, to planning what a new city center is going to look like. (ESRI, What is GIS? 2017)

2.3.1 Data input in GIS

GIS requires the input of data to produce maps with layers of information. Map data are usually produced by high altitude satellites like the Landsat satellite, or low altitude aircrafts. It is common to distinguish between active and passive sensors in remote sensing. Active sensors are the ones that sends out a signal and measures the signal that returns. This is used for radio detection and ranging (RADAR) and light detection and ranging (LiDAR) sensors. Passive sensors like satellites use the sun as the source, and measure the light in different wavelengths like visible and infrared light. (Polat and Uysal 2015) (NASA 2017)

LiDAR sensors are used to produce high resolution digital elevation models (DEMs), like the one used in this thesis. This is done by sending out a pulse of light, and then detecting the precise time for its return. By sending up to 20 pulses per square meter, the LiDAR sensors can detect minor changes in elevation, and thus provide a model with high resolution. (Portland State University 2017)

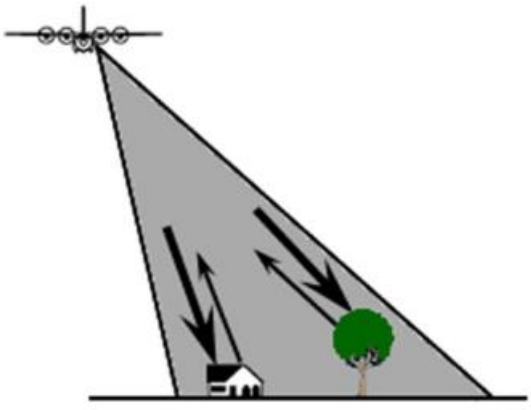

Figure 2-8: Illustration of airborne LiDAR. (Portland State University 2017)

The GIS community uses the terminology “layers” as the mechanism of displaying geographic datasets. This means that each map produced using GIS is a series of layers where each layer provides additional information to the map. Every layer is georeferenced, meaning that it has a

reference to where it is present on the globe. The only georeference used in this thesis is the European Terrestrial Reference System (ETRS) of 1989, Universal Transverse Mercator (UTM) Zone 33 North, more commonly called UTM Z-33N. This is the UTM zone Tromsøya is located in.

There are two different layers in GIS: vector layers and raster layers. Both are used in this thesis. A raster layer consists of pixels (or cells) organized in rows and columns, with each pixel containing a value representing information. This information can be anything from temperature, to global radiation, to land use features and elevation. Rasters can also be base maps, such as orthophotographs. All photographs consist of pixels, and when zoomed in enough is will be possible to see that each pixel have a certain color (Figure 2-9). (ESRI, What is raster data 2017)

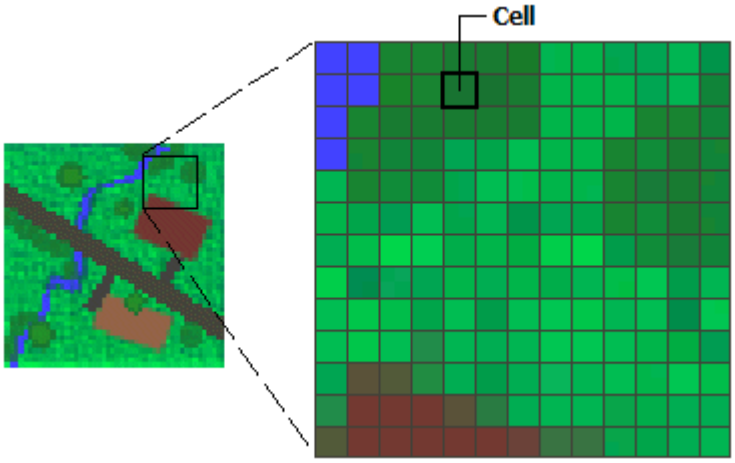

Figure 2-9: Illustration of a raster layer, with cells combined in columns and rows. (ESRI, What is raster data 2017)

Vector layers consists of geometrical shapes combined to form a map. Usually this is two-dimensional polygons, lines or points that represent a certain feature. In Figure 2-10, the lake is defined as a polygon, the river is defined as a line, and the wells are featured by points.

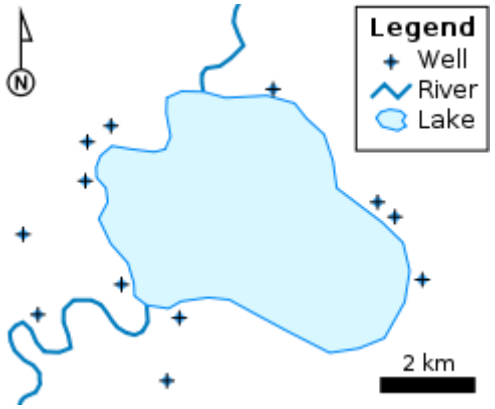

Figure 2-10: Illustration of vector layer with distinctive features. (Wikimedia 2017)

This is only one representation of what a vector layer can look like. Another example of a vector layer is a triangulated irregular network (TIN) model, which makes a three-dimensional surface exclusively of triangles in a three-dimensional perspective. An example of a TIN model of Tromsøya is displayed in Figure 2-11. (ESRI, What is a TIN surface 2017)

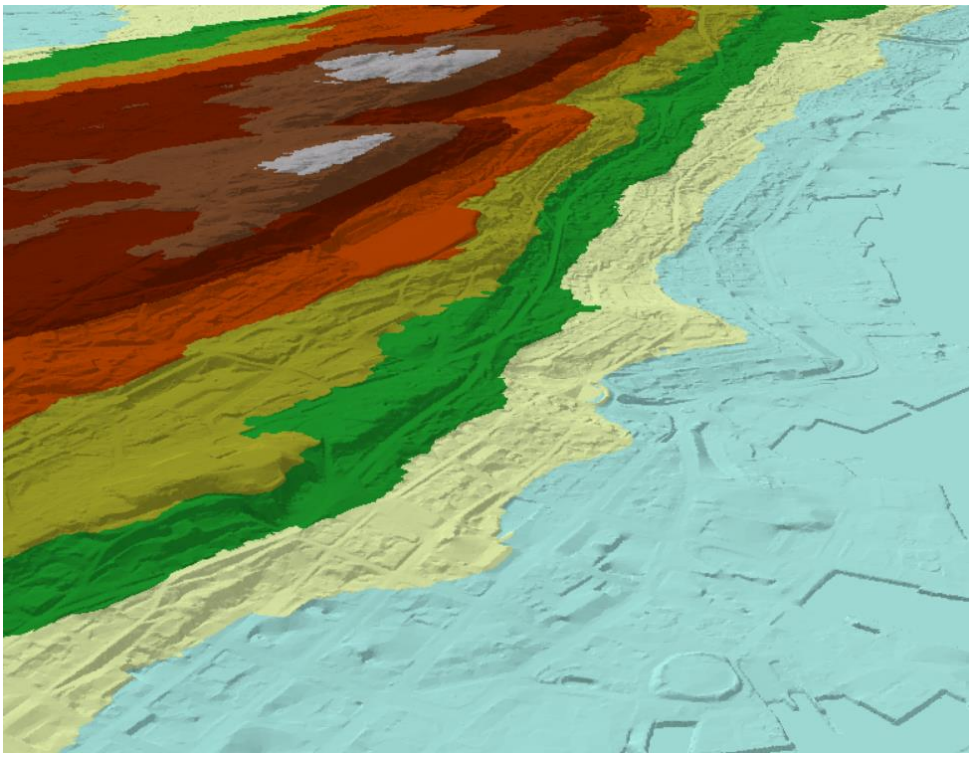

Figure 2-11: Snapshot of a high-resolution TIN model created in ArcGIS. The snapshot shows the eastern part of Tromsøya. Light blue color represents elevation close to the sea surface, and white color represent an altitude over 150 meters. Picture created in ArcGIS.

2.3.1.1 Digital Elevation Model

A digital elevation model (DEM) is GIS layer containing information about the elevation of the terrain. A DEM can be represented as both a raster layer containing pixel values of elevation, or as a vector layer in the form of a TIN like in Figure 2-11. The most used representation is in a raster layer, like the example in Figure 2-12.

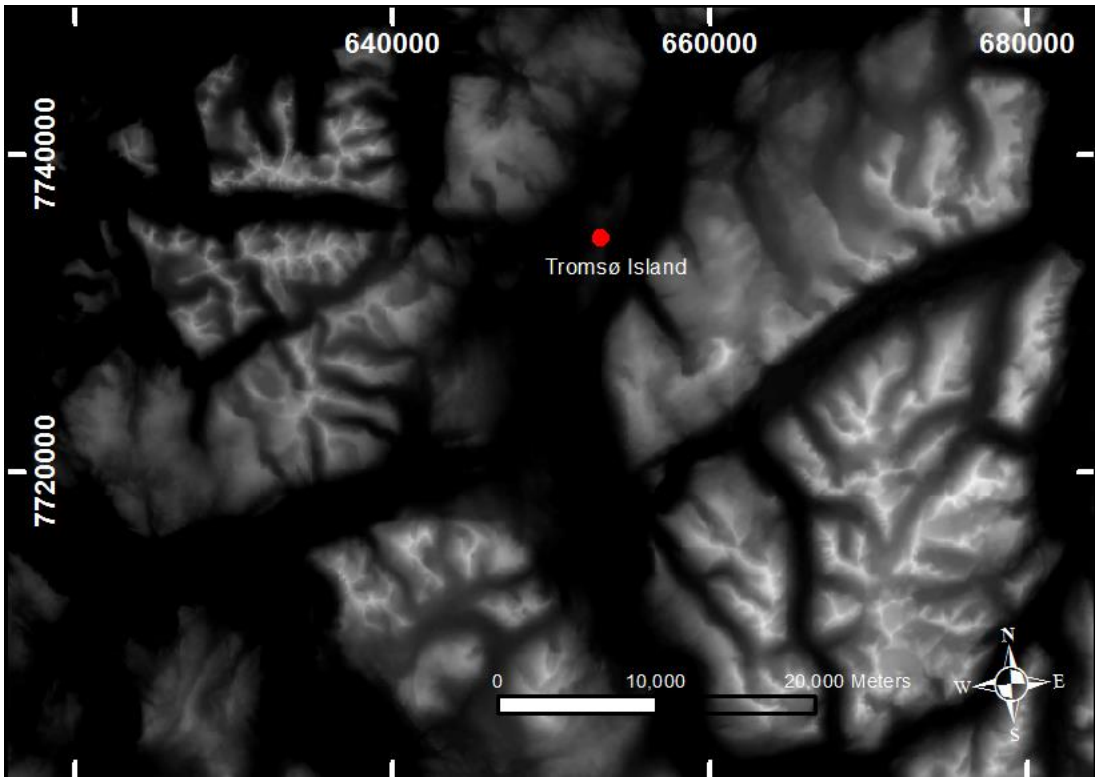

Figure 2-12: DEM10 of the area surrounding Tromsøya island. Created in ArcGIS. Projection: UTM Z-33N.

A DEM can be created by several different techniques, for example LIDAR, as previously mentioned, or photogrammetry. The last years, the use of LIDAR has made it possible to obtain DEMs with resolution up to 8 cells per m^2, thus a resolution of 0.25 m^2. This kind of resolution will severely increase computing times, but also provides DEMs with better details that can be used for applications like rockslide warning mapping. (Polat and Uysal 2015)

DEM is a term that covers both digital terrain model (DTM) and digital surface model (DSM). Note that a DSM is called "digital overflatemodell (DOM)" in Norwegian, which can cause some confusion. Both DTMs and DSMs will be used in this thesis. A DSM represents all types of vegetation and terrain, while a DTM only represents the terrain. This means that a DSM will include terrain features like buildings, trees and chimneys, in contrast to the DTM that represents the surface level. This is illustrated in Figure 2-13.

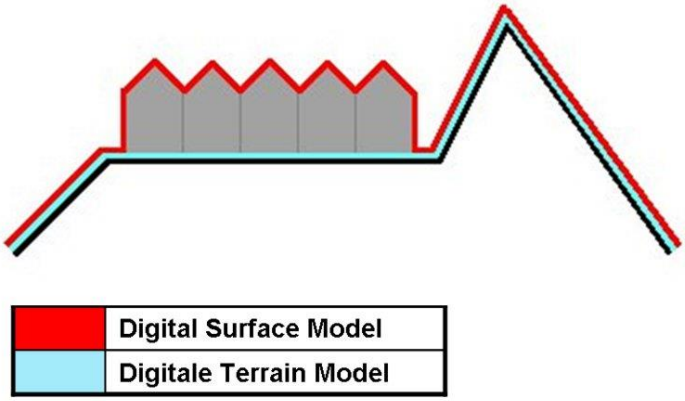

Figure 2-13: The difference between a DSM and DTM. (Defra 2017)

The best resolution of DEMs varies over Norway, but a DTM resolution of 10 meters is available for the whole country. There are available DEMs of Tromsøya with a resolution up to 1 and 0.25 meters. Usually the resolution and type of DEM are written with both included in the name, i.e. DTM10. A resolution of 10 meters means that each pixel in the map is 10x10 meters in the XY plane. The Z plane (elevation) has a standard deviation of $\pm$ 2-3 meters resolution. (Geonorge 2017)

3 Method

3.1 ArcGIS

The GIS program used in this thesis is ArcGIS. The developer of ArcGIS is the Environmental Systems Research Institute, commonly called Esri, which is a private company with headquarters in California. They are the global market leader in GIS, and delivers a variety of solutions within GIS; ArcGIS Desktop, ArcGIS Online and Esri Community, among some of them. (ESRI, About ArcGIS 2017)

This thesis will involve the use of the ArcGIS Desktop version 10.5, and Esri's new ArcGIS Pro software. They are main desktop versions that can use a variety of tools to execute operations on maps and layers. Although they have most of the same properties, they will be used for somewhat different tasks in this thesis.

Several ArcGIS tools will be used during the different processes required in this thesis. While some of them require some to no explanation, others are more complex and important. This includes Esri's Solar Analyst. Solar Analyst includes three tools: Area Solar Radiation (ASR), Point Solar Radiation (PSR) and Solar Radiation Graphics (SRG). They are prominent for this thesis, and include multiple calculations and assumptions that need to be explained. The following subchapter include a thorough explanation of how they work and what it is based on.

3.1.1 Solar Analyst

ASR, PSR and SRG are tools for modeling solar radiation at landscape scales. They are a part of three tools designed in a package called Solar Analyst. Solar Analyst is only available through Spatial Analyst extension for ArcGIS.

Insolation data with high quality for high resolutions is not available for most geographical areas. Because of great differences in insolation within short distances due to differences in topography, point specific measurements like weather station data are not viable to use. The variability in elevation and slope, as well as shadows from topographic elements will create these differences.

According to the creators of Solar Analyst, it is a comprehensive geometric solar radiation modeling tool, and should be able to handle the advanced modelling with greater calculating speed, accuracy and functionality than other tools. (Fu and Rich 1999)

ASR and PSR are calculated the same way, but have a distinction. Area-based models calculate insolation for every pixel in the DEM, while PSR calculate insolation for the chosen pixel. That makes the tools advantageous for different tasks. One of the benefits of using PSR, is that it has very low computing times. The reason for this is the fact that the calculations are point specific, and only calculated for the chosen cells in the DEM. This can be used to compare insolation data with data from a weather station, check global solar radiation on a specific roof, or compare diffuse proportion with direct proportion values. When investigating larger areas, the area-based tool generates values for all cells of the DEM, and the output will be presented in a more dynamical map.

3.1.1.1 Viewshed, Sunmap and Skymap

The design of the Solar Analyst is based on theory concerning viewshed, skymaps, sunmaps and calculation of direct and diffuse solar radiation. SRG can be used to calculate viewshed, skymaps and sunmaps for the chosen location. It is important to note that most tool-related pictures from ArcGIS presented in (Fu and Rich 1999) are from an outdated version of ArcGIS, and therefore no longer applicable. However, the Solar Analyst is still based on the same calculations as in the paper.

Solar Analyst calculations are based on the hemispherical viewshed from each pixel of the DEM. A viewshed is the angular distribution of sky obstruction, i.e. how much of the sky that is obstructed from topographic elements at a certain location. This can be illustrated by an upward-looking hemispherical photograph. As seen in Figure 3-1, heights in topography are obstructing the view closer to the surface. The reason for viewshed to not include the top of the trees can be that it is calculated from a DTM, and not a DSM.

Figure 3-1: Hemispherical viewshed photo with calculated viewshed (yellow inner line). (Huang and Fu 2009)

What Solar Analyst does to create a viewshed is to calculate horizon angles for the input number of directions from the location. The angles are interpolated for all directions, and then converted to a hemispherical coordinate system. Viewshed, sunmap and skymap are created for each pixel in the ASR tool, which is the reason for an increase in computing time for larger areas.

In (Fu and Rich 1999), a mountainous location in California (USA) is used to illustrate the process of making viewshed, sunmap and skymap. For this thesis, similar images are produced with ArcGIS for the location of Holt Weather Station (Chapter 3.3.1). The process of creating the maps will be explained, in addition to what they mean.

The input raster was chosen to be the DTM10 of an expanded area around Tromsøya (Figure 2-12). This was chosen to see if the viewshed would change significantly with a DEM that covers the topography around the island, and whether that could alter the output as opposed to an area of the island alone. The reason for choosing Holt as a location, is because the weather data is collected from the weather station there.

Figure 3-2 show the input tool screen for SRG. The input raster file is the DTM10 of Tromsøya and surroundings. A sky size of 512x512 (resolution for the viewshed), and calculation directions of 64 is enough to represent all sky directions. (Fu and Rich 1999)

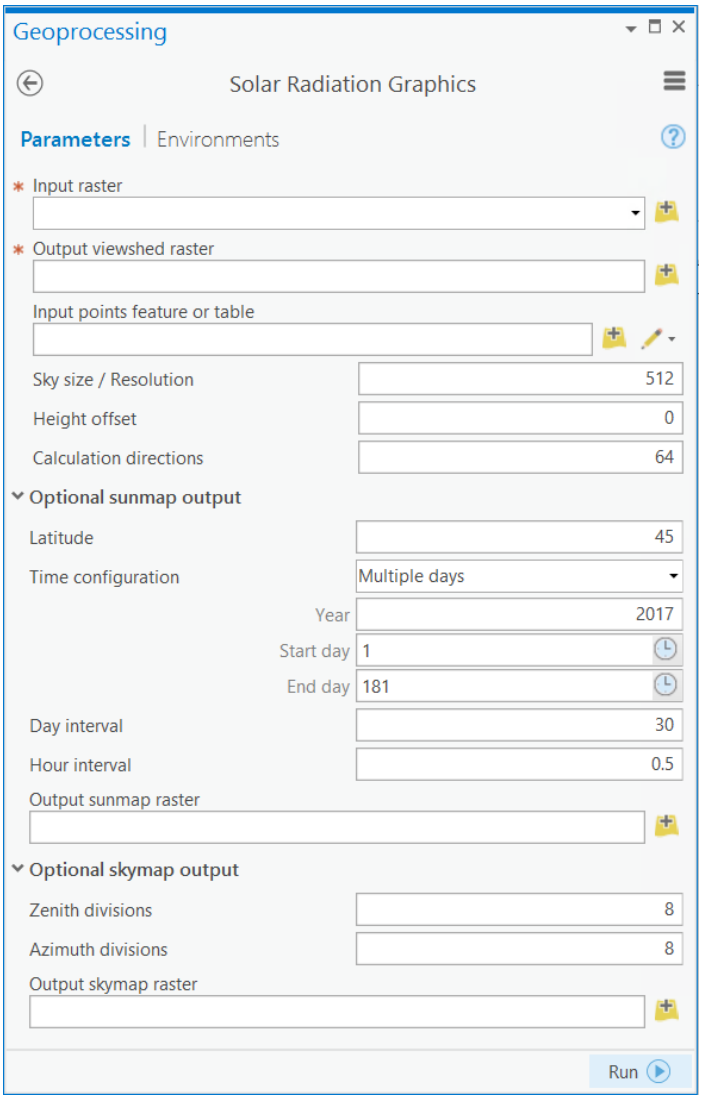

Figure 3-2: Tool screen for Solar Radiation Graphics.

The input in *Optional sunmap output* from Figure 3-2 needs to be altered to get a fitting figure that represents what the user wants to see. In this case, each month should be visible, and it should be possible to differentiate between time of the day. Because of this, a day interval of 30 and an hour interval of 0.5 is chosen. The time configuration should represent half of the year, which makes it possible to see all months without them crossing each other. If the entire year were chosen, months like March and September would cross each other as the sun path is the same. (Figure 3-4 and Figure 3-5). That is why the half-year time configuration is chosen days (days 1-181, and 182-365). Optimally a time configuration between the winter and summer solstice should be chosen, as this is the time the sun is at its highest and lowest during the year. This does not entail any practical difference for the sunmaps produced here, as they are only meant to visualize how the program works.

The *Optimal skymap output* only includes input of zenith and azimuth divisions. These were chosen to be 18 and 16, to represent the sky sectors in the most presentable way. (Fu and Rich 1999)

All hemispherical maps from the Solar Analyst will have east and west directions changed compared to a normal map projection. This is because the viewshed is a picture of what would be seen from a perspective of laying on the ground, looking upwards. Then west is to the right and east to the left. The sun rises in the east and sets in the west.

The first map created is the viewshed in Figure 3-3. Although this viewshed looks like it has only minor obstruction, it is important to note that the sun is very low in the sky for certain times of the year. How the viewshed alters global solar radiation is discussed in Chapter 4.

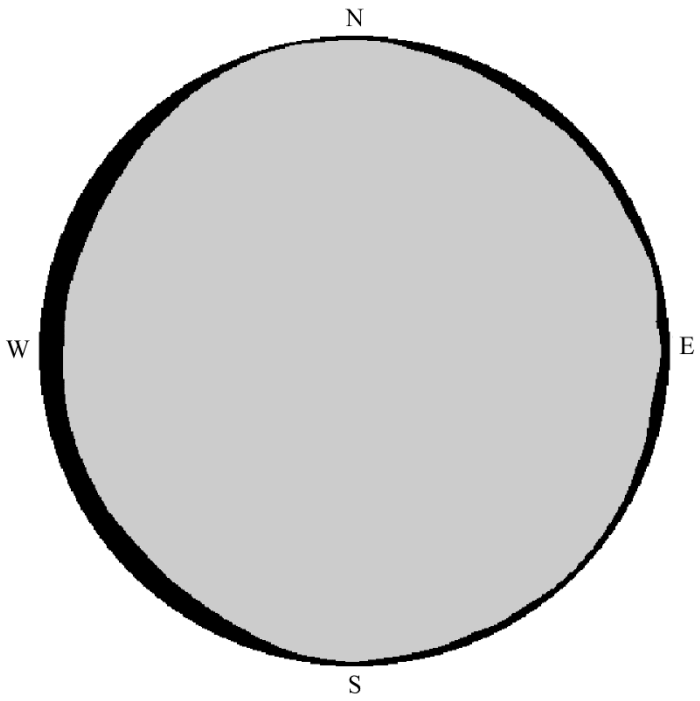

Figure 3-3: Viewshed of Holt. Created in SRG. Note that east and west directions change place.

The next map the tool calculates is the sunmap. A sunmap is the calculated path of the sun in the sky for each month and hour of the day. Note that a solar map and sunmap is not the same thing, and differentiated throughout this thesis. The calculation of a sunmap is based on time of day, latitude and day of the year. The calculated sunmap for Holt is displayed in Figure 3-4 and Figure 3-5.

Figure 3-4 displays months June (the inner circle) to January (the bottom circle close to the south mark), and Figure 3-5 displays July (inner circle) to November (the bottom circle). The first day of each month is marked. The time is displayed because these maps show the position of the sun at a certain time of the day in a certain month. With these maps, it is possible to know where the sun is positioned at any time of the year. Note that as the sun rises in the east, the time intervals move counterclockwise. The sun rises higher on the horizon (closer to the center of the map) for each day of the month in Figure 3-4, and lower for each day of the month in Figure 3-5. So, the 31st of May is placed on the boundary to the 1st of June. Each vertical line break represents half an hour. As an example, for the start of April, the sun will rise at around 05:30 (when not including the viewshed), and set at around 18:30. Sunmaps are used for calculation of direct radiation. Note that December is not visible in Figure 3-5.

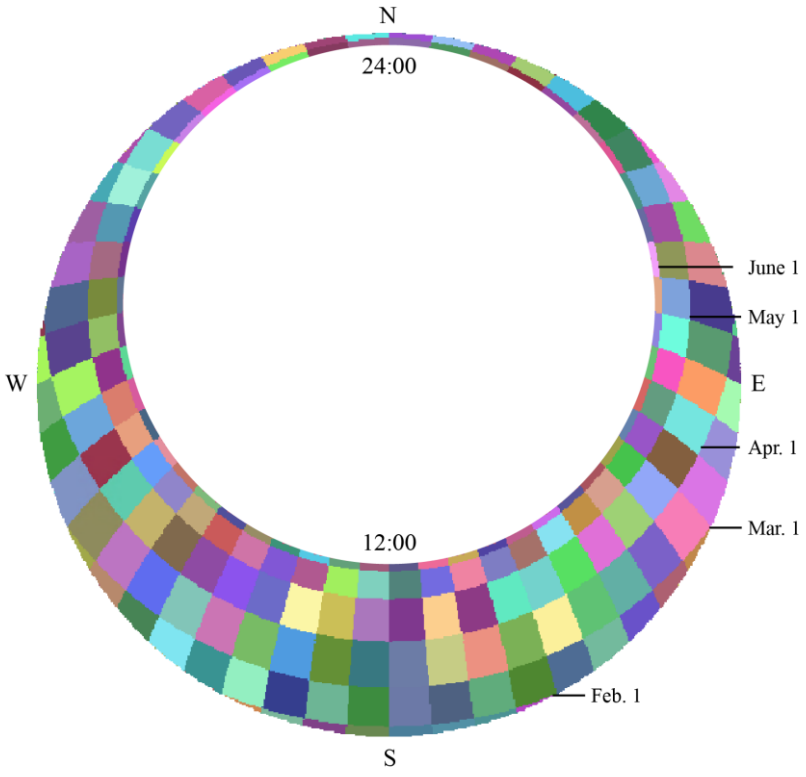

Figure 3-4: Sunmap for the months January to June. The 1st of each month, as well as noon and midnight are marked. Created with SRG in ArcGIS.

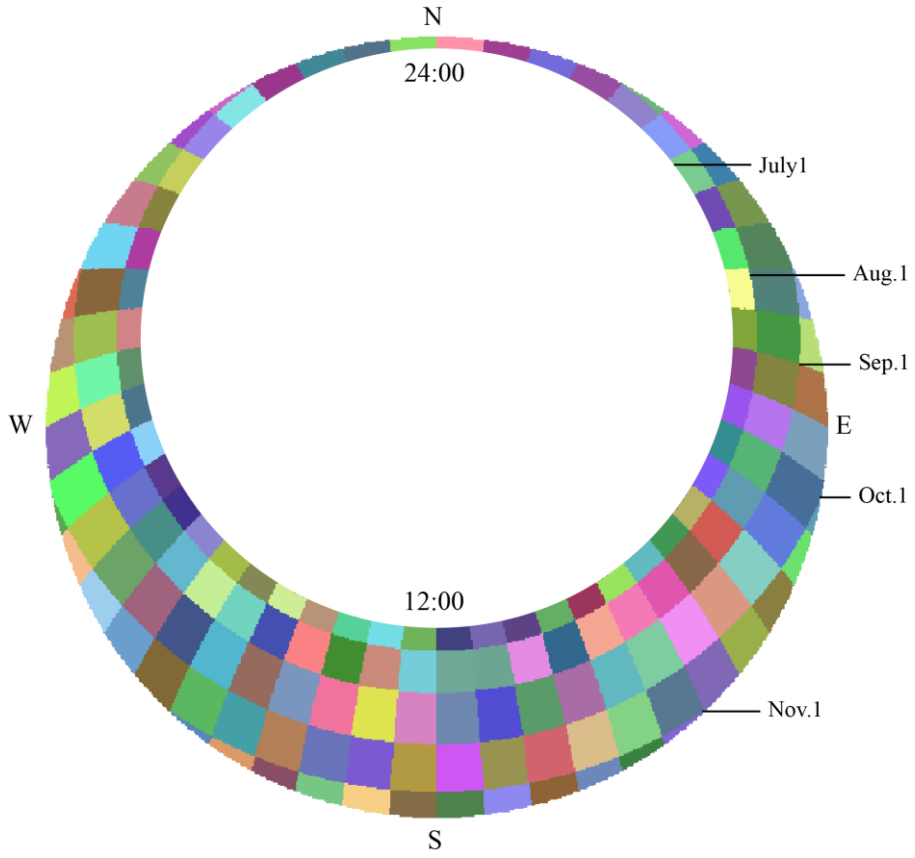

Figure 3-5: Sunmap for the months July to December. The 1st of each month, as well as noon and midnight are marked. Created with SRG in ArcGIS.

The next calculation is a skymap. A skymap divides the sky into azimuth and zenith divisions. Each of these sectors has a unique identification number. For every one of these sectors, the centroid is calculated. The centroid is the geometrical center of mass. The skymap is used for calculation of diffuse radiation.

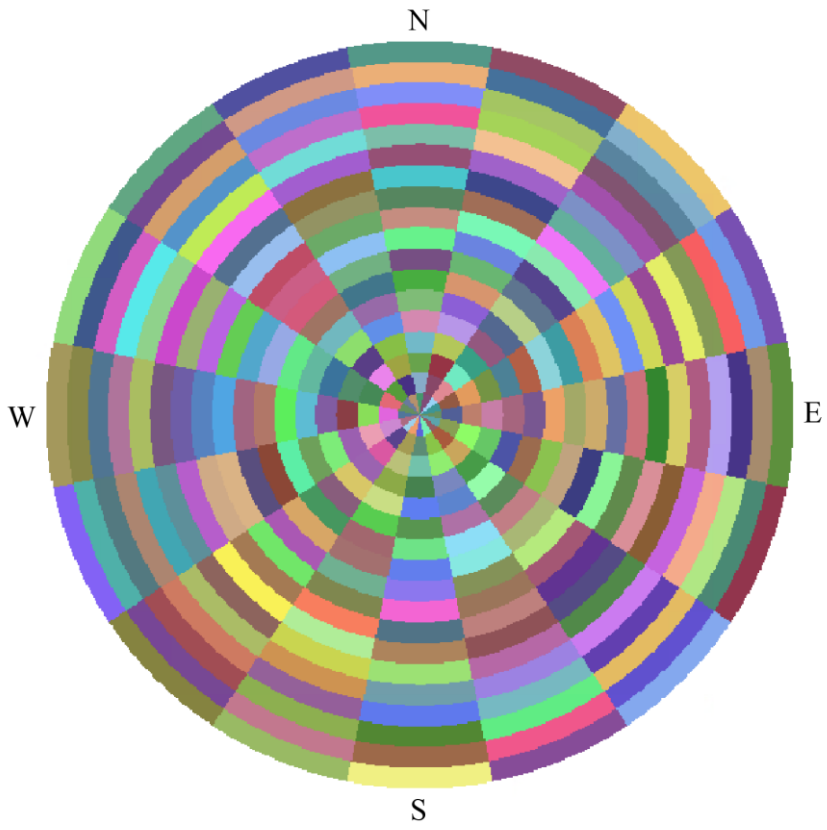

Figure 3-6: Skymap with 16 azimuth divisions and 18 zenith divisions. Created in SRG in ArcGIS.

In calculation for the global solar radiation, the Solar Analyst uses the viewshed combined with these maps. This is displayed in Figure 3-7, Figure 3-8 and Figure 3-9. As seen from these pictures, the viewshed covers some of the sectors. The Solar Analyst uses this representation to find out which sectors in the maps that are fully or partially covered. From the skymap in Figure 3-9, some of the western outer sectors are fully covered by the viewshed and can therefore not be a source for diffuse radiation. For the sectors that are partially covered, a new centroid for the uncovered section is calculated. As for the sunmaps, the representation makes it clear when the sun disappears under the horizon. To use the same example, the new time for the late March sunrise is now close to 06:30, while the sunset happens at around 18:00.

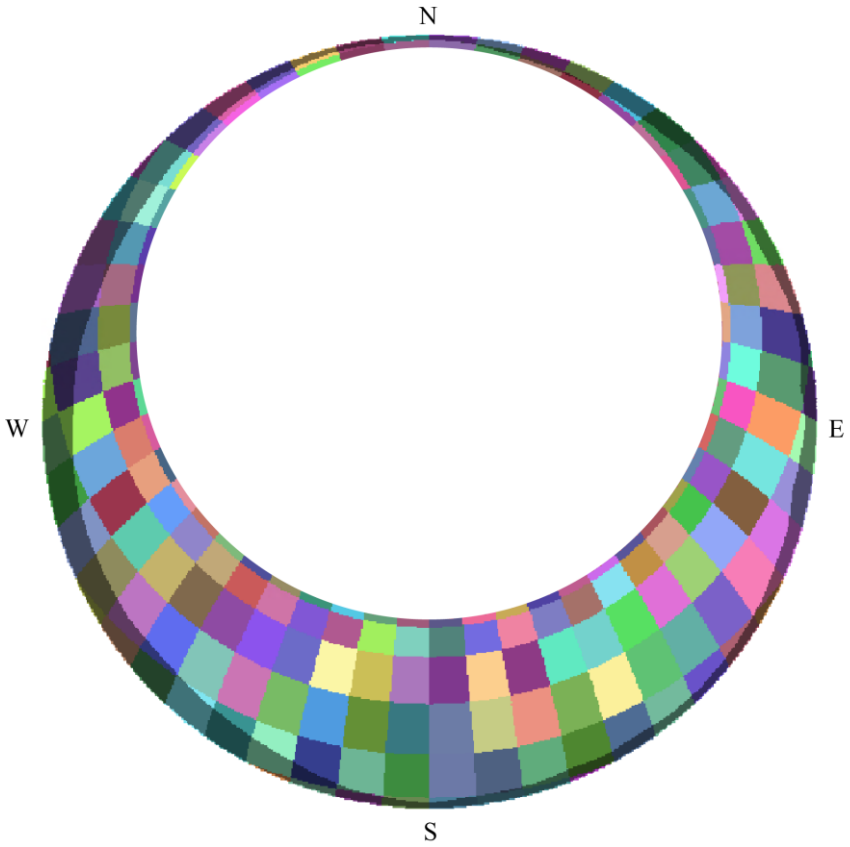

Figure 3-7: Sunmap for January to June with overlaying viewshed. Created in ArcGIS.

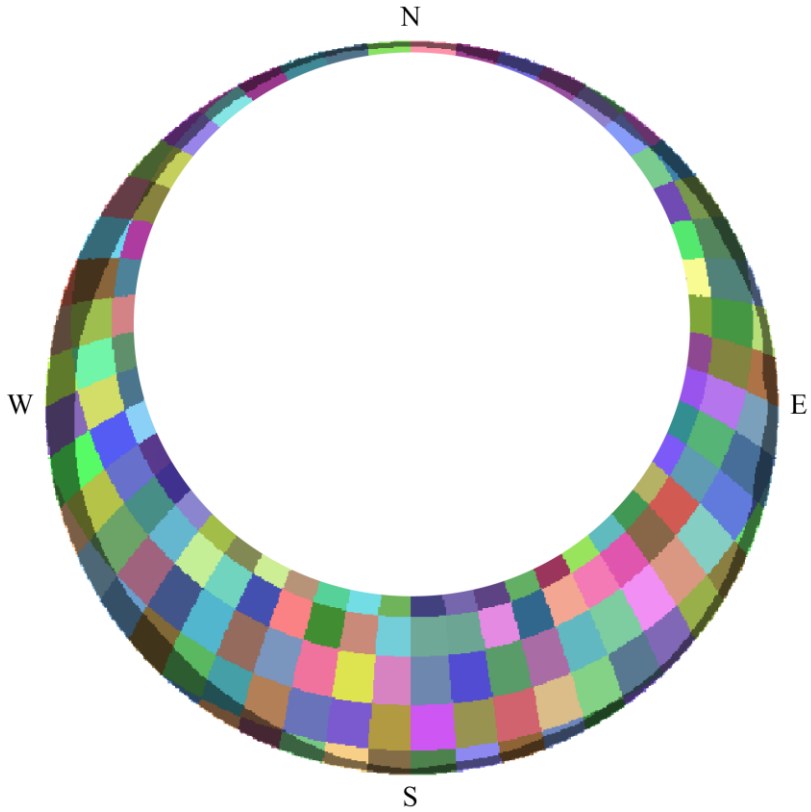

Figure 3-8: Sunmap for July to November with overlaying viewshed. Created in ArcGIS.

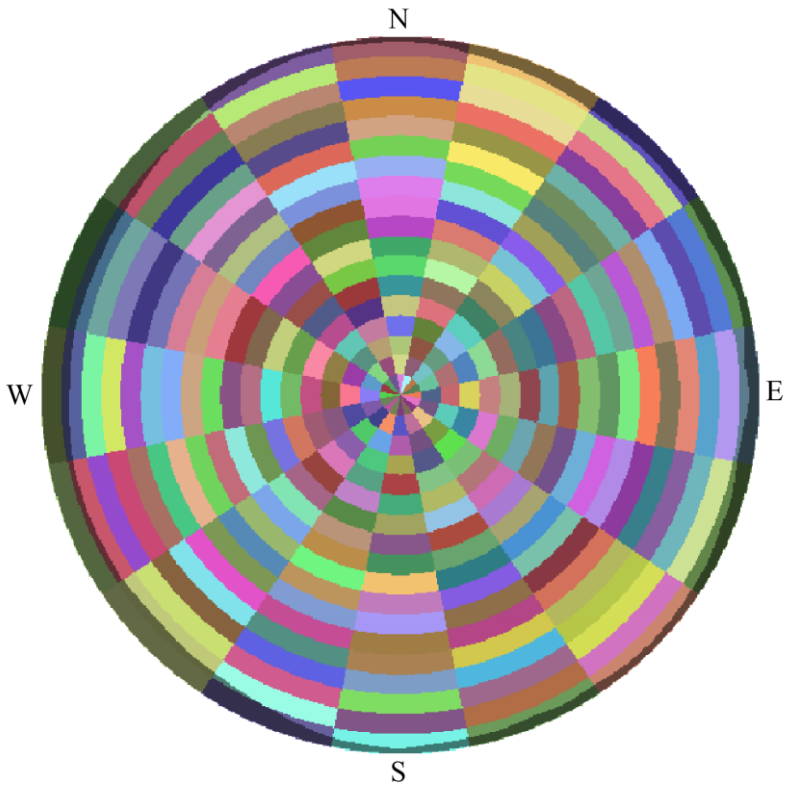

Figure 3-9: Skymap with 16 azimuth divisions and 18 zenith divisions, including overlaying viewshed. Created in ArcGIS.

3.1.1.2 Calculation of Direct Solar Radiation

Direct solar radiation (DIR) is calculated for the sunmap sectors that are not completely obstructed. The process described in (Fu and Rich 1999) is based on a transmission model that accounts for effects like transmittivity and AM.

The total DIR (TDIR) is calculated by taking the sum of the DIR from all sunmap sectors. Each sector is calculated with the use of the zenith angle θ and the azimuth angle α. The azimuth angle is the horizontal angle oriented in the north-south plane, with north as base line. The zenith angle is described in Chapter 2.1.1.

$$TDSR = \sum DIR_{\theta,\alpha} \quad (5)$$

The DIR for each sunmap sector is calculated by the following equation:

$$DIR_{\theta,\alpha} = S_{Const} \times \tau^{m(\theta)} \times SunDur_{\theta,\alpha} \times SunGap_{\theta,\alpha} \times \cos(AI_{\theta,\alpha}) \quad (6)$$

Here, S_{Const} $(\frac{W}{m^2})$ is the solar constant from (1). τ is the transmittivity averaged over all wavelengths for the zenith angle. This can be explained as the fraction of radiation that passes through the atmosphere at the zenith angle. $m(\theta)$ is the relative optical path length. The relative optical path length is the geometric length of the path that light travels, which is different from

the zenith because the atmosphere refracts light. It is calculated by using meteorological tables, together with the elevation (E) and the solar zenith angle (θ).

$SunDur_{\theta,\alpha}$ is the sun duration, i.e. how long time the Sun spends in the sunmap sector.

$SunGap_{\theta,\alpha}$ is the sun gap fraction. This is how much of the sunmap sector is available (or visible) depending on the viewshed over the sunmap (Figure 3-7 and Figure 3-8).

The last input in the equation is $AI_{\theta,\alpha}$. This variable is the angle of incidence between the centroid of the sunmap sky sector and the axis normal to the surface. The incoming solar radiation at the surface is proportional to the cosine of the zenith angle, so multiplying with $\cos(AI_{\theta,\alpha})$ is to account for the effect of surface orientation.

3.1.1.3 Calculation of Diffuse Solar Radiation

Solar Analyst have two different diffuse solar radiation (DIF) models. One is called the uniform diffuse model (UDM), and the other standard overcast diffuse model (SDM). In the UDM, the diffuse radiation will be the same from all sky direction, while the SDM will have a diffuse radiation that varies with the zenith angle. In landscapes with valleys and peaks, the difference between UDM and SDM can increase because the UDM does not distinguish a valley from a peak. This is discussed further in Chapter 3.3.2.

The total DIF (TDIF) is calculated by taking the sum of DIF from all the skymap sectors. Note that the difference from TDIR is that the sum is from the skymap, and not the sunmap.

$$TDIF = \sum DIF_{\theta,\alpha} \quad (7)$$

The diffuse radiation is calculated at its centroid for each sky sector. Equation (8) is the calculation for diffuse radiation.

$$DIF_{\theta,\alpha} = R_G \times P_{diff} \times Dur \times SkyGap_{\theta,\alpha} \times Weight_{\theta,\alpha} \times \cos(AI_{\theta,\alpha}) \quad (8)$$

Here, R_G is the global normal radiation. R_G can be calculated by summarizing the direct radiation from every sector, with a correction for the proportion of direct radiation. As the total proportion of direct and diffuse radiation is 1, the direct proportion is $1 - P_{diff}$. This leaves the calculation as in Equation (9):

$$R_G = \frac{S_{Const} \sum(\tau^{m(\theta)})}{1 - P_{diff}} \quad (9)$$

P_{diff} is the proportion of the diffuse part of global normal radiation, and an important variable in this thesis because it varies greatly from month to month and even day to day. This variable is discussed in Chapter 3.3.2, as it will affect the output results for the thesis depending on how it is changed as input. For normal clear sky conditions, the proportion is around 0.2-0.3, while it reaches around 0.6-0.7 for very cloudy sky conditions. Dur is the time interval, i.e. the input day and hour interval for the tool. $SkyGap_{\theta,\alpha}$ is the proportion (gap fraction) of visible sky for the skymap sector. Note that this is not the same as $SunGap_{\theta,\alpha}$, as it is the proportion of the sky sector and not the sun sector. $Weight_{\theta,\alpha}$ is the proportion of diffuse radiation from a given skymap sector relative to the other sectors. This means that the diffuse radiation from each of the other sky sectors is different depending on which sky sector that is the reference point at that time. $Weight_{\theta,\alpha}$ is calculated differently for UDM and SDM.

$AI_{\theta,\alpha}$ is the same variable as in the calculation for TDIR.

3.1.1.4 Calculation of Global Solar Radiation

Total Global Solar Radiation (TGSR) is the sum of TDIR and TDIF. The calculations above are done for all every pixel on the DEM, which creates a map with GSR for the total area.

$$TGSR = TDIR + TDIF \quad (10)$$

This gives an output with unit Wh/m^2..

3.2 Data Processing

One of the main concerns of making Tromsø Solar Map, was excessive computing times. Oslo Sunmap reported computing times of 24 days total for ASR with a DSM1. With computing time over lengthy periods like that, the creation of a solar map can become impractical. Because of this, a goal was set to reduce computing times together with Section for Digital Research Services at UiT. They designated a computer server for the purpose of logging core load and providing a stronger computer for simulations. A server is a computer designed to process and deliver data to another computer over, in this case, the local network. The specifications for the server is presented in Table 3-1. (Andersen Personal Communication)

Table 3-1: Server Specifications

Model	Dell Precision Rack 7910
Processor	Intel Xeon CPU E5-2623 v3 @3.00 GHz, 4 cores
Memory (RAM)	32 GB
Operating System	64-bit Microsoft Windows Server 2012 R2 Standard

The server supports Hyper Threading, which means that each physical central processing unit (CPU) core can be utilized as two logical CPU cores. This makes the number of cores that can be used for these simulations 8. (Andersen Personal Communication)

It is necessary to note that computing times varies slightly from each simulation to the next one, even with similar inputs and outputs. Reasons for this can be that it is a long time since the last restart or that small tasks are running in the background. That makes these tests more like guidelines, and not a certain answer. Nevertheless, trends in the computing time and the usability of the programs are possible to measure.

To investigate how computing times could be decreased, numerous tests were conducted. For all these tests, the DTM1 of Tromsøya was used together with default values in ASR. To have the same data background, it was calculated for January (days 1-31).

The first tests were to investigate what type of processes in the ASR tool that is the reason for long computing times. These tests were done in ArcGIS for Desktop 10.5. With removing the factor about the resolution of the input raster, because a low resolution would give bad estimations of roofs, two factors were considered: area and time span. The first run done of the whole input DTM1 was completed in 13 hours and 13 minutes. With changing the area input

from the whole Tromsøya to a cell of 2048x2048 meters, the time was reduced to 21 minutes and 9 seconds. So, by reducing the area of the input DEM, it was quickly established that the area is a large factor. The other factor considered was the time span, but by increasing from January to the entire year (days 1-365), the computing time increased to 31 minutes and 46 seconds. These results indicate that computing viewshed, sunmaps and skymaps is the time-consuming part of the calculation, as all calculations are done for each pixel in the DEM whether calculations are done for a single month or the full year. So, reducing the area of the input DEM will reduce computing times.

The second test was to investigate if parallel processing worked in ArcGIS for Desktop 10.5. Parallel processing is a type of computation that divides the problems into smaller problems that can be computed at the same time. This option can be chosen in each tool in ArcGIS under "Environments". Using this option did not change computing times at all. This indicates that ASR only uses one core of the computer at a time, meaning that only 1 out of 8 processor cores are used. This was confirmed by investigating the core usage from the server, as seen in Figure 3-10.

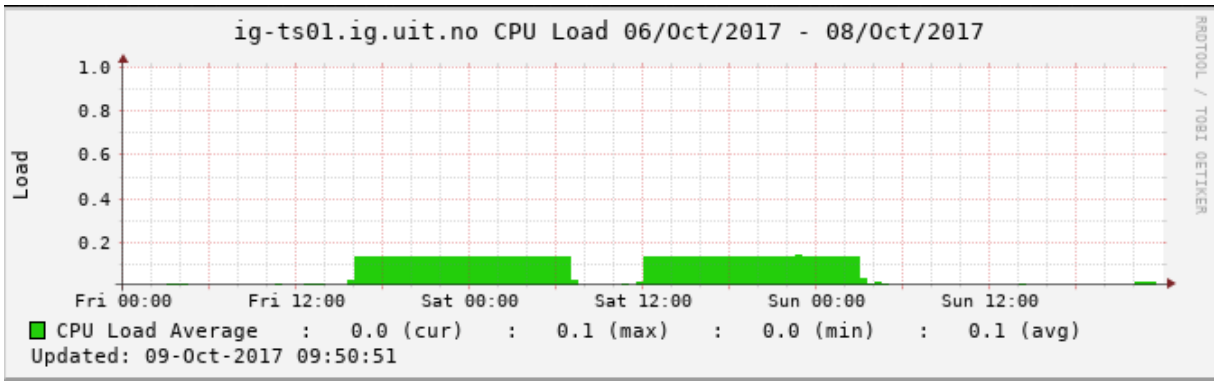

Figure 3-10: Display of core usage from server. The CPU has only been loaded about 13%, which indicates one core used.

The next test was to investigate the differences between computing time of ArcGIS for Desktop 10.5 and ArcGIS Pro. This was done by applying the same 2048x2048 size cell to both programs, with the same conditions. This test showed a computing time of 20 minutes 40 seconds with ArcGIS Pro, which is marginally lower than the other. The output from the maps were the same. It is difficult to say why this is, as the two programs are based on different type of technology. ArcGIS Pro is based on a multithreading technology, which means that it has the ability to use multiple cores at the same time. The option of using multiple cores are also available for ArcGIS for Desktop 10.5 as an extension package called 64-bit Background Geoprocessing. But as is already established, ASR only runs on one core and does not support

parallel processing. By investigating the core usage from the server, this was proven to be true for ArcGIS Pro as well. ArcGIS Pro is more user friendly and it is easier to log computing times. Based on this and the lowered computing time for the cell, ArcGIS Pro were used for all simulations concerning ASR. (ESRI, Background Geoprocessing (64-bit) 2017)

The next task was to utilize all cores of the computer available. With the option of a server, multiple instances of the same program can be opened at the same time. This is possible when using a regular computer as well, although this may require some technical skills. To see if all cores could be utilized, 8 different cells with the same area were used in ArcGIS Pro. During initial tests, some problems occurred. One of them was that the simulation kept running for over an hour, which was not expected. The other issue was that only some outputs were generated. This was solved by creating 8 different folders in the server, where each one of them included the raster they would use and the ArcGIS toolbox, along with a unique geodatabase (GDB). This prevents any of the processes to interact with each other, which can corrupt and delay the process. By using a unique folder for each simulation, the program only writes from and to that folder. A GDB is where the output is written to. Figure 3-11 show from the feedback of the server when all 8 cores were used. The reason for the fragmented graph is because some of the simulations were started at separate times, although at one point (16:00) all of them were simulating at the same time. The computing times were under 25 minutes for all areas.

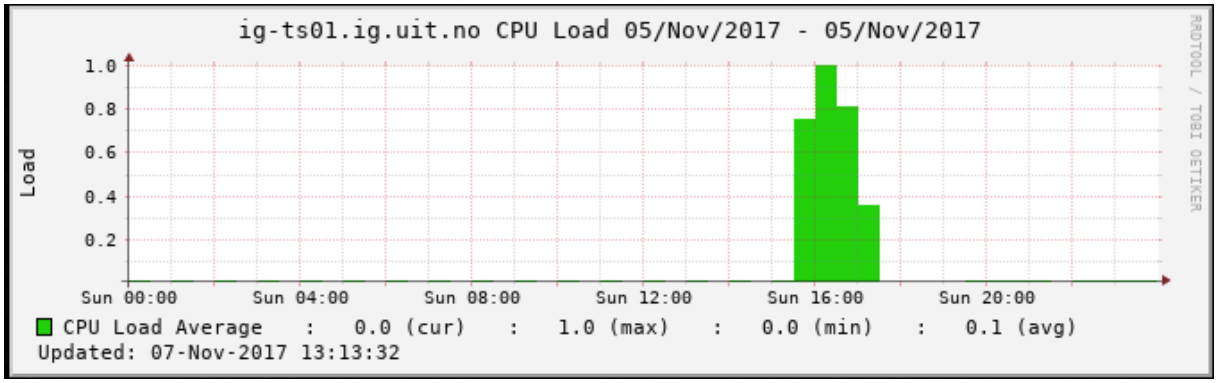

Figure 3-11: Display of core usage from server. The CPU has been loaded about 100%, which indicates all cores used.

By starting all simulations at the same time, the total computing time is expected to be around the same as for one single cell. This last result indicates that the computing time issue can be solved by parting the problem in smaller, independent problems which makes it possible to utilize parallel processing. The DEM of the entire island will be larger than 8 single cells of 2048x2048, but this can be solved by increasing the cell's area or adding them together to consist of 8 areas in total. Ultimately, with 12 servers (one for each month) with 8 processors

each, the whole calculation with a DTM resolution of 1 meter can be finished in hours instead of days.

3.3 Calculation of Diffuse Fraction and Transmittivity

To create a solar map in ArcGIS, certain maps and inputs are necessary. This includes diffusion fraction and transmittivity, because these values display how much of the solar radiation that ultimately reaches the surface, and whether it is diffuse or direct radiation. As no measurements of these values are available for Tromsøya, they need to be calculated by using PSR and weather data.

3.3.1 Holt Weather Station

Holt Weather Station is located at Holt at Tromsøya. This is on the western part of the island, and can be seen in detail in Figure 3-12. The weather station is located at 69°65'38''N, 18°90'95''E.

Figure 3-12 The position of Holt Weather Station. Created in ArcGIS. Projection: UTM Z-33N. Base map: Kartverket, Geovekst og Kommuner – Geodata AS.

Holt Weather Station is operated by Norwegian Institute for Bioeconomy (NIBIO), as a part of the project "Landbruksmeteorologisk Tjeneste", translated as Agriculture-Meteorological Service. The projects main goal is to provide meteorological data for research and notification services. All data from their weather stations is available at the AgroMetBase. (NIBIO 2017)

The weather station is co-operated by Norwegian Meteorological Institute (MET), so both MET and NIBIO provide data. The data from MET can be found at eKlima, their server for historical and real-time observations. This website demands a log-in. (MET 2017)

Holt Weather Station was established in 1987, and measures temperature, precipitation, humidity, wind speed, wind direction, global solar radiation, sun hours and earth temperature. Global solar radiation is the data used in this thesis to calculate diffusion and transmittivity values. The measurement of global solar radiation at Holt is done by a Kipp & Zonen CM11 pyranometer, which gives an output for the mean over the last hour. Few weather stations in Northern Norway measure global solar radiation, and Holt is the only station that measures it at Tromsøya. (Kipp&Zonen 2017)

A pyranometer measures radiation from all angles, but is mounted horizontally. All light entering the glass bulb at the top of the pyranometer is converted from thermal energy into electrical energy, with a strongly light-absorbing black paint. This creates a temperature difference within the pyranometer, which again induces a small voltage. This voltage is measured and transformed into global radiation. Pyranometers usually does not require any power to operate. (Kipp&Zonen 2017)

3.3.1.1 Output Data

In the process of collecting data, some issues arose. Output from both services showed the weather station had periods of down-time and negative or unreasonable output values. This is not necessarily a problem, but it is important to know why these issues occur. Downtime periods for a pyranometer can occur from snowfalls, defaults in the system, dust and lack of maintenance. Some output results showed negative values of -6999.0, which is an obvious error. In addition, some of the data were processed wrong. There are large parts of data values where there is placed a value “0” for the output, when it is supposed to be a non-existing value “NULL”. This is a problem when the data need to be validated. An example is if a full month of February were set to “0” instead of “NULL”, the data could look sufficient even though it is not.

NIBIO provides overview of raw data, by changing the word “controlled” to “raw” in the HTML version of the service output. As the data is not properly fixed at the NIBIO database, there is now a way to control whether it is correct or wrong. This option is not available at eKlima. In addition, NIBIO is the original handler of the data. Because of this, and the fact that

MET does not provide raw data, the NIBIO output is the one used to collect the data output. (NIBIO 2017) (Nordskog Personal Communication)

The small negative values are not non-existing values, but corrections made by the pyranometer. These values occur over measurements that are positive as well, but are hidden in the positive output. The reason for the small negative values are called zero offset, and happens because the pyranometer emits some heat. (Kipp&Zonen 2017)

It was chosen to extract data from the last 10 years. This is large amounts of data that needs to be processed, but this can easily be done with the filter function in Excel. By filtering for year and month, totals can be calculated with the included tools. For the data to be sufficient, each of the year's raw data was investigated. Although this is a time-consuming effort, it is essential that the data collection happens in the right way and the data basis can reflect the actual global solar radiation.

The last 10 years were investigated in this process. This involves the last three months of 2007 until September 30th 2017, to have the same number of months for each calculation. The data from the entire year are removed if there is data missing that can compromise the results. The number of data values compromised by the faults "NULL" and "Negative values <-50" is presented in Table 3-2.

Table 3-2: Percent of missing data from different fault values.

Year	NULL values	Negative values < - 50	% missing
2007*	>1128	0	51%
2008	>2856	0	32%
2009	2	5	<1%
2010	0	1840	21%
2011	2	0	<1%
2012	4	0	<1%
2013**	0	124	
2014	0	0	0%
2015	0	0	0%
2016	4	0	<1%
2017*	1	0	<1%
*) Only specified months			
**) Wrong calibration for pyranometer (Nordskog Personal Communication)			

Based on these results, 7 years were chosen as data basis: 2009, 2011, 2012, 2014, 2015, 2016 and 2017, This gives 6 years of basis, as only the last three months of 2009 and the first 9 months of 2017 are used.

In Excel, all small negative values were removed, and then the total global solar radiation was calculated for each month. This resulted in Table 3-3

Table 3-3: Global solar radiation for each month from selected years. All values in Wh/m^2

Month/year	January	February	March	April	May	June	July	August	September	October	November	December	SUM
2009	x	x	x	x	x	x	x	x	x	16023	1937	13	**17973**
2011	359	8688	28440	68706	142725	155224	126877	106905	53571	14032	868	5	**706399**
2012	487	6955	37009	101799	108525	146165	96858	89471	42360	16262	1321	9	**647221**
2014	934	8094	33408	66729	149403	143762	157321	98662	38904	20597	2209	593	**720615**
2015	975	6628	37113	85292	127519	128751	143393	100134	46266	16556	2002	900	**695531**
2016	1198	8990	43911	114464	126945	110039	113174	89504	43127	15180	2412	480	**669424**
2017	814	9306	37463	108176	126186	161404	122963	84636	61951	X	X	X	**712899**
Average	**795**	**8110**	**36224**	**90861**	**130217**	**140891**	**126764**	**94885**	**47696**	**16442**	**1791**	**333**	**695011**
Highest	1198	9306	43911	114464	149403	161404	157321	106905	61951	20597	2412	900	**829771**
Lowest	359	6628	28439	66729	108535	110039	96858	84636	38904	14032	869	5	**556033**

The average values for each month in Table 3-3 is presented in Figure 3-13.

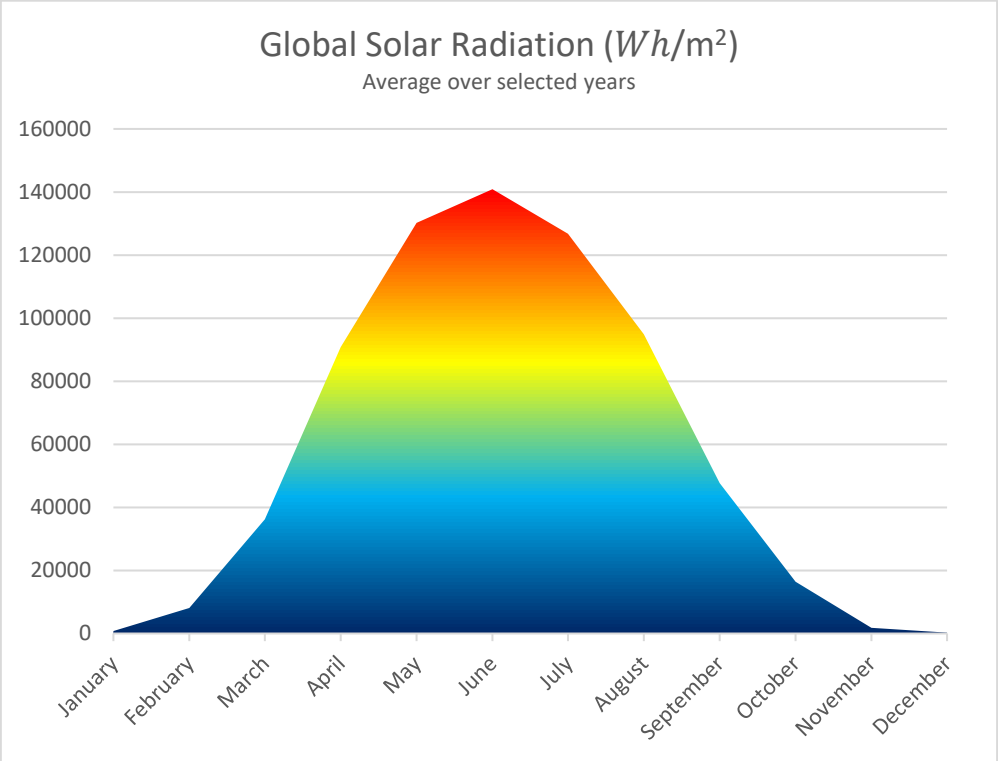

Figure 3-13: Graph of average values of global solar radiation for all months of selected years.

3.3.2 Calculation with PSR and Weather Data

The diffuse proportion of irradiation (D) and transmittivity (T) are of importance for the calculation of global solar radiation. The diffuse fraction value ranges from 0 to 1, and indicates how much of the total global radiation is diffuse radiation. The transmittivity indicates how much of the light that passes the atmosphere, and ranges from 0 to 1, where 1 indicates that 100% of the light passes.

The most ideal way to find the diffuse fraction and transmittivity values would be to measure them with more advanced sensors than the one present at Holt. This way the diffuse could be determined as an average over monthly or daily intervals. These kinds of sensors are expensive, and according to the eKlima website, the only one available in Norway is placed in Bergen. The diffuse values from Bergen would not be fitting to use in Tromsø due to differences in weather, latitude and topography. Because of this, it is necessary to find the value of diffuse radiation in another way.

For the Oslo Solar Map, a combination of weather data from MET and the PSR tool in ArcGIS were used. As one of the objectives of this thesis is to validate and compare the Tromsø Solar

Map with the one from the municipality of Oslo and that neither have measurements of diffuse proportion, the same method has been used here. (Adamou Personal Communication)

To not have even more insecurity.

In the creation of Oslo Solar Map, the UDM were used. This choice was based on Oslo being an urban area, with limited topography surrounding the municipality. As UDM does not distinguish between the different skymaps in calculating diffuse fraction, and no data for diffuse solar radiation were available, there would not be a reason for them to choose SDM. To reduce insecurity and sensibility of the solar map for Tromsøya, the same diffuse model was chosen to be used for further calculations. (Adamou Personal Communication)

3.3.2.1 Points Solar Radiation Tool

Now that the total global solar radiation from Holt is obtained, calculation of D and T values can start. This is done manually by the help of the PSR tool. Here, each of the different values of D and T must be inserted to find fitting input. Note that the values found here are not comparable with the ones in Oslo Solar Map, as the diffusion fraction are site-specific. What is important to note though, is that the diffuse value is likely to be higher in the winter months than the summer months. The reason for this is that the Sun is lower in the sky, which increases the AM value. In locations like Bergen, where there is a lot of precipitation, the T value is expected to be lower than in Tromsø.

In this section, all inputs for PSR is introduced to give an understanding of how they can alter output. PSR finds global radiation from the user-specified location of the input DEM. The PSR tool requires the same input as ASR, except that ASR calculates for the entire DEM. The first part of the default tool screen is presented in Figure 3-14.

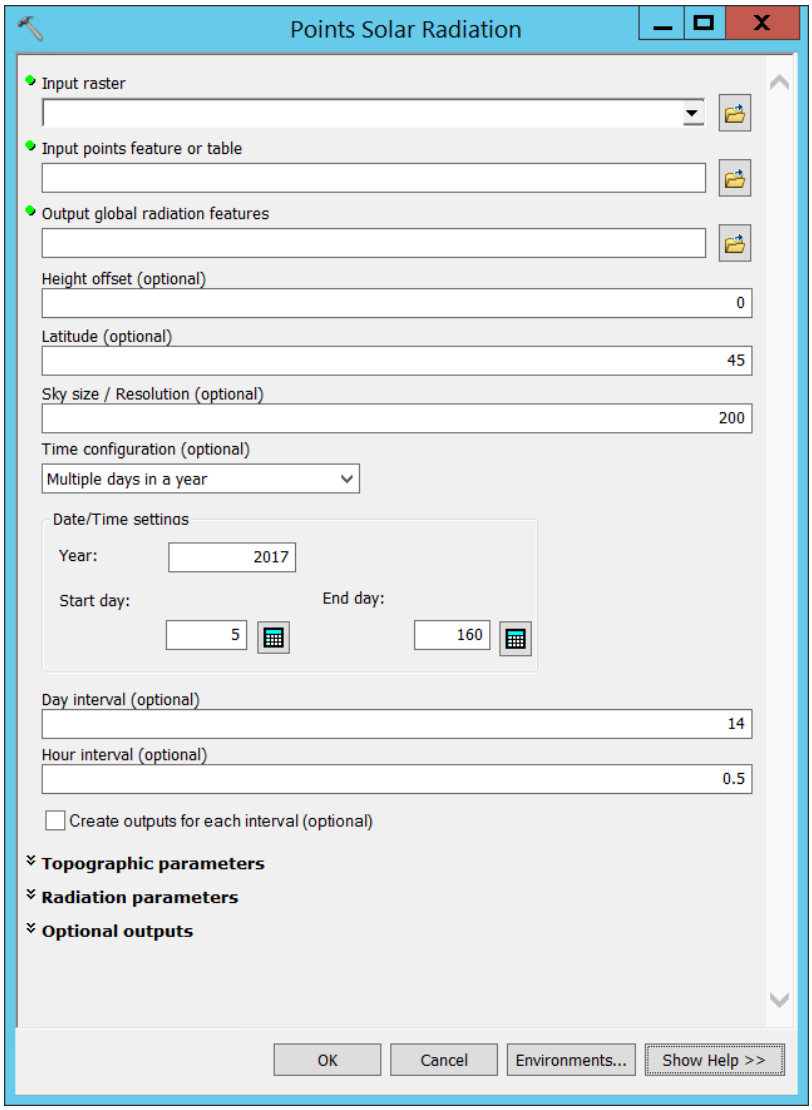

Figure 3-14: Default screen of Points Solar Radiation tool in ArcGIS.

It is important that the inputs used in the PSR tool are the same as later used in ASR. The reason for this is that the requirements set in the tool to define D and T values can change by altering the value. If the inputs in ASR are changed, the D and T values can possibly be wrong compared to the actual values found.

Input raster is a DSM1 of Tromsøya. The same resolution and DEM type were used by Oslo Sun Map.

Input points feature or table: This is the location (or locations) in UTM format where the user wants data from. The specific location used in these calculations is chosen from a spot approximately 3 meters west from the pyranometer at Holt. The location cannot be set to be the exact same place as the pyranometer, because it is placed on a small hill (Figure 3-12). This hill has a non-horizontal topography, which could result in better or worse output. The

chosen spot is at a surface that seems horizontal and does not have trees or other topography close to it compared to what the pyranometer would have. The pyranometer itself and other measurement tools at the weather station could alter the results in some way, but it is seen from Figure 3-3 that this is not the case, as no signs of poles or obstructions can be seen to the east. The reason the obstructions are not there, is because they are lower than what alters the viewshed, which is the top of the island. The coordinates of the chosen location are presented in Table 3-4. They are gathered from the DSM, and are easily found in ArcGIS by moving the cursor over it. The locations coordinates are inserted into notepad (.txt) with a single space between them, to be in the right format for PSR. This is done by writing X and Y on the first line, and the coordinates on the next line. Then the .txt file is used as input points table.

Table 3-4: Coordinates for the chosen location 3 meters west of Holt.

X	Y
651605.529	7732119.407

Output global radiation features: The name of the output file. Needs to be placed in a geodatabase (GDB), where all output from the tools in ArcGIS are put.

Height offset: The height above the DEM surface for where the calculations are to be performed. This is zero by default, and chosen to stay zero because there are only slight differences in height from the pyranometer to the chosen location.

Latitude: This input changes automatically to the middle point of the input DEM. For the DEM used in these calculations, the latitude automatically changes to 69.6699050595104. This is used to calculate how the sunmap will be.

Sky size: This is the cell resolution for the viewshed, skymap and sunmap raster files that is used to calculate direct, diffuse and global radiation. The default, 200 x 200, is sufficient for most purposes, because increasing the sky size will greatly increase computing times but not change accuracy significantly. Changing the cell size from 200 x 200 to 400 x 400 will quadruple computing time, and as that is an issue concerning this thesis, the default cell size was chosen. (Fu and Rich 1999)

Time configuration: There are four choices in this tab, which describe four different calculation methods. The first is *Special days*, which only calculates for summer and winter solstice, in addition to the equinox days. The next one is *Within a day*, where the calculations are done for a specified time period within one day. The third one is called *Multiple days in a year*. This is

the one used for all calculations in this thesis. Here it is possible to choose the full month by selecting the start and end day to be within one month. To use January as an example, the start day would be 1 and the end day would be 31. Note that leap days are included for leap years. Leap days are not of concern for this thesis, as 2017 are used for all calculations. The reason behind this choice is that results in ASR have very small to no changes from year to year. This was figured out in tests when i.e. June in 2016 and June in 2017 gave the same output by a margin of over 99.9%. The fourth and last option is *Whole year with monthly interval*, which calculates the whole year with *day interval* (see below) of one month. This would be possible to use if calculations for this thesis were done with one D and T value for the full year.

Date/Time settings: The user insert the start day and end day of the calculations. Included in Table 3-5 are the start and end days of each month in a non-leap year.

Table 3-5: Day numbers for each month.

Month	1	2	3	4	5	6	7	8	9	10	11	12
Days	1-31	32-59	60-90	91-120	121-151	152-181	182-212	213-243	244-273	274-304	305-334	335-365

Day interval: The day interval for calculations of sky sectors for the sun map. The default value is 14, which means a bi-weekly interval.

Hour interval: Time interval through the day for calculations of sky sectors for the sun map. It has a default value of 0.5 hours.

Create outputs for each interval): By checking this box, there will be created outputs for each interval. If *Whole year with monthly interval* was chosen, then one raster band for each month would be created. This is not necessary for the calculations in this thesis.

The second part of the default tool screen is presented in Figure 3-15. Here, topographic and radiation parameters, as well as optional outputs will be decided.

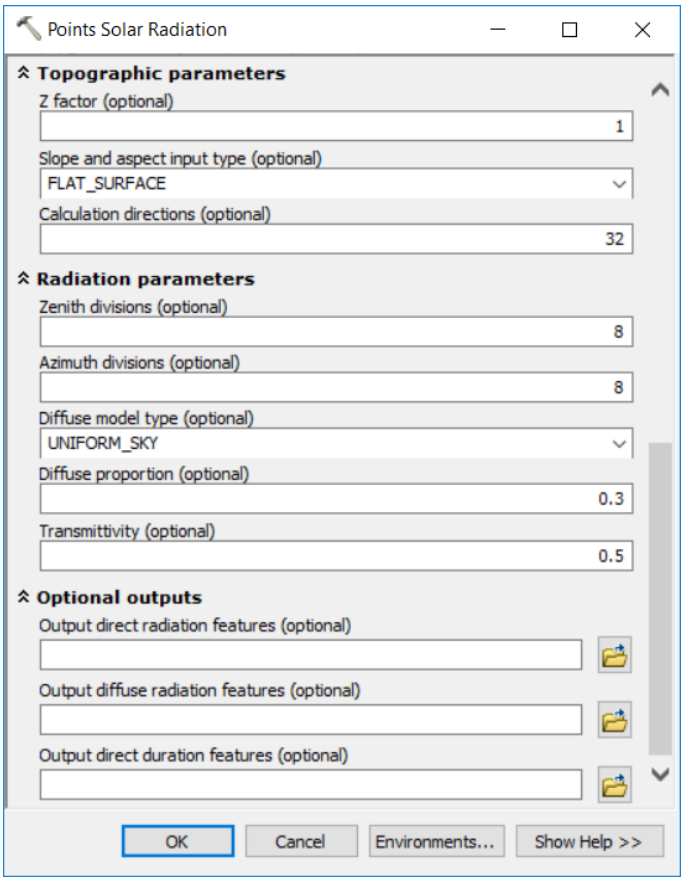

Figure 3-15: Overview of Topographic Parameters, Radiation Parameters and Optional outputs from the Points Solar Radiation tool in ArcGIS.

Z factor: This factor adjusts the units of measurement in the z direction. As the DEM is already in meters, the default value of 1 is good here.

Slope and aspect input type: This tab has two different options. The first, and default, is *FROM_DEM*, which will calculate slope and aspect from the input DEM. The second is *FLAT_SURFACE*, and converts all z-values to zero. *FROM_DEM* will be used in this thesis, as it is necessary to include slope and aspect to calculate differences for surfaces with different orientation.

Calculation directions: The number of azimuth directions used when calculating the viewshed. Valid values are multiples of 8, and the default value of 32 is acceptable for complex topography.

Zenith and azimuth divisions: The number of divisions used to create sky sectors in the skymap. An increased number of zenith and azimuth divisions will have small to no effect on computation time, but will also have small effect on the global solar radiation output. In cases where diffuse radiation is of special interest, the number of divisions should be increased to

16x16. This could be fitting in the case of this thesis, as the study area is far north and the diffuse proportion most likely will differ throughout the year. But when using the UDM, zenith divisions are not of concern, as diffusion is the same from all zenith angles. With 8 zenith divisions, and 8 azimuth divisions, the sky sector will be 11.25 x 45 degrees (as the zenith is maximum 90°, and the azimuth is maximum 360°). (Fu and Rich 1999)

Diffuse model type, *Diffuse proportion* and *Transmittivity* is already discussed.

Output features: The three output features create additional output raster layers for the study area if necessary. There the user can choose output layers of direct, diffuse and direct duration (sun hours).

3.3.2.2 Final Calculation of D and T

The calculation is done by inserting different values of D and T in the PSR tool with the input described above. By using Excel, the values can be set in system. This table is added in Appendix 7.1. By trying out different D and T values, it is possible to investigate which total global radiation concur best with the output of the PSR tool.

The approach used is to start with values of D=0.5 and T=0.5. To use January as an example, the output in this case was $0.005\frac{Wh}{m^2}$. This is way below the insolation data from Holt, which is $795\ \frac{Wh}{m^2}$. By increasing the transmittivity, the output will increase. But even by increasing the T value to 7, the result is still not close to our data from Holt. The next step is to increase the D value to 0.6, and then try with new T values. In the end, the only output that were close to the weather data, was from a diffusion value of 0.9 and transmittivity of 0.8. The chosen value is marked in green, and the closest values are marked in orange.

As seen from Appendix 7.1, August and September had multiple values that could have been chosen. Because of this, and the proximity of the values, some of them were chosen over others. A diffusion value of 0.7 would be strange for August, and what is even stranger is a diffusion of 0.8 for September. This is necessary to address, and it is important to take a look at the outputs from the main simulation in ASR to see if the results there can be correct. This is done in Chapter 4.2.2.

As for December, the tool was not able to calculate any global radiation during the whole month. At Tromsøya, the Sun is not visible in December, but the results from Holt Weather Station show some insolation. Thus, this must be diffused solar radiation that PSR tool are not able to model in this case.

This process is done for each of the months, and give the values presented in Table 3-6.

Table 3-6: Diffuse proportion and transmittivity value for each month.

Month	Diffuse Proportion (D)	Transmittivity (T)
January	0.9	0.8
February	0.6	0.7
March	0.5	0.6
April	0.4	0.6
May	0.5	0.5
June	0.4	0.5
July	0.6	0.4
August	0.3	0.6
September	0.4	0.6
October	0.5	0.7
November	0.7	0.8
December	X	X

3.4 Solar Radiation Modelling

3.4.1 Data Collection

Data collection is an important part of working with GIS. All of the DEMs used in this thesis can be collected at Høydedata. Høydedata is a website where LiDAR data is published as it is produced. The way to collect data from the website is to choose to use polygon to extract the area of choice, and then use the tab "Project". Here, all DEMs of resolutions 1, 10 and 50 meters are available. The 0.25 meters resolution is only available for users with additional rights. Høydedata is administered by Kartverket. (Kartverket 2017)

3.4.2 Data Processing and Sectoring

The DEM used for the simulations in ASR is the DOM1, thus a DSM with 1 meter resolution. When the file is received and uploaded, it needs to be processed to fit with the further requirements. This includes parting it into 8 new areas to reduce computing time.

When ordering a map over Tromsøya from Høydedata, two files are sent. The reason for receiving two files instead of one, is that the maps are saved as packages over larger areas, and Tromsøya is in the middle of two areas. The computing time increases with area, so it is necessary to reduce the DSM to only include the island. The first step to do this is to merge the files to one single file. This is done with one of the Data Management Tools in ArcGIS. The path length (the way to find the tool in ArcGIS Toolbox) is Data Management

Tools/Raster/Raster Dataset/Mosaic to new Raster. Mosaic to new raster default tool screen is presented in Figure 3-16.

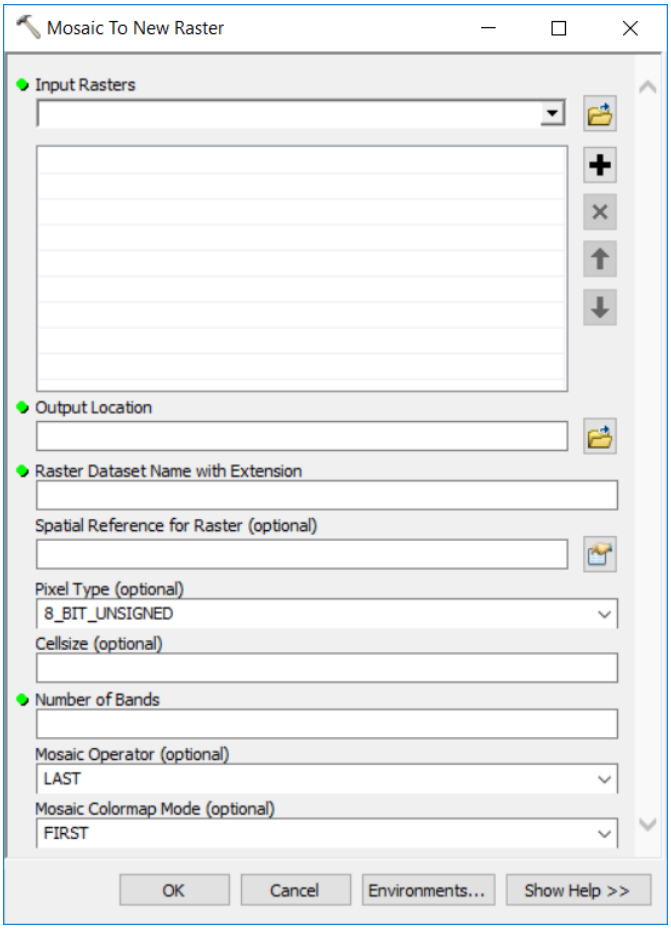

Figure 3-16: Default screen of the tool Mosaic to New Raster in ArcGIS.

What this tool does is to merge rasters together. In this case, the two raster files are added in *Input rasters*. Then, the name with the correct extension (.tif) is added. It Is important to include the *Spatial Reference for Raster*, and UTM Z-33N is used here as well. The *Pixel Type* must be large enough to include all data from the file. As computing times from this tool is not long, it is set to be "64_BIT". *Cellsize* should be 1 meter, as that is what the resolution of the DSM is. *Number of Bands* is one. The *Mosaic Operator* will only have influence in cases where the raster files are overlapping. *Mosaic Colormap Mode* does not have any effect in this task.

When the new file is produced, it is a goal to reduce the area of the file to only include the island. This was done with a tool called "Extraction by polygon". The path length is Spatial Analyst Tools/Extraction/Extraction by polygon. This is a simple tool that lets the user extract a polygon from the input raster by inserting coordinates of the desired area.

The next task is to split the area into new, smaller cells. As the server has 8 processors, 8 areas are optimal. A goal is to give them an area that are approximately the same, so that each simulation will have about the same computing times. For this, the tool “Split Raster” were used. The path length is Data Management Tools/Raster/Raster Processing/Split Raster. The tool gives the user different solutions to how the process of splitting the raster could be done. In this thesis, the split method *SIZE_OF_*TILE was chosen. This option lets the user define a standard size for the new areas. The default value of 2048 was chosen, with an overlap of 250 meters for every cell. There are two reasons for choosing to include overlap. The first is to make sure that no data is lost between each of the cells, and the second is to apprehend the viewshed. If there were no overlap, each cell would calculate viewshed with no topographic obstructions from any of the other cells. This could lead to increased output of global solar radiation. The tool created 17 new cells, with three of them consisting of only water.

The next step is to combine some of the 14 cells to reduce the total to 8. It is important that cells aligned to each other are the ones combined. With the use of *Mosaic to New Raster* again, the final set of 8 areas were created. They are displayed in Figure 3-17.

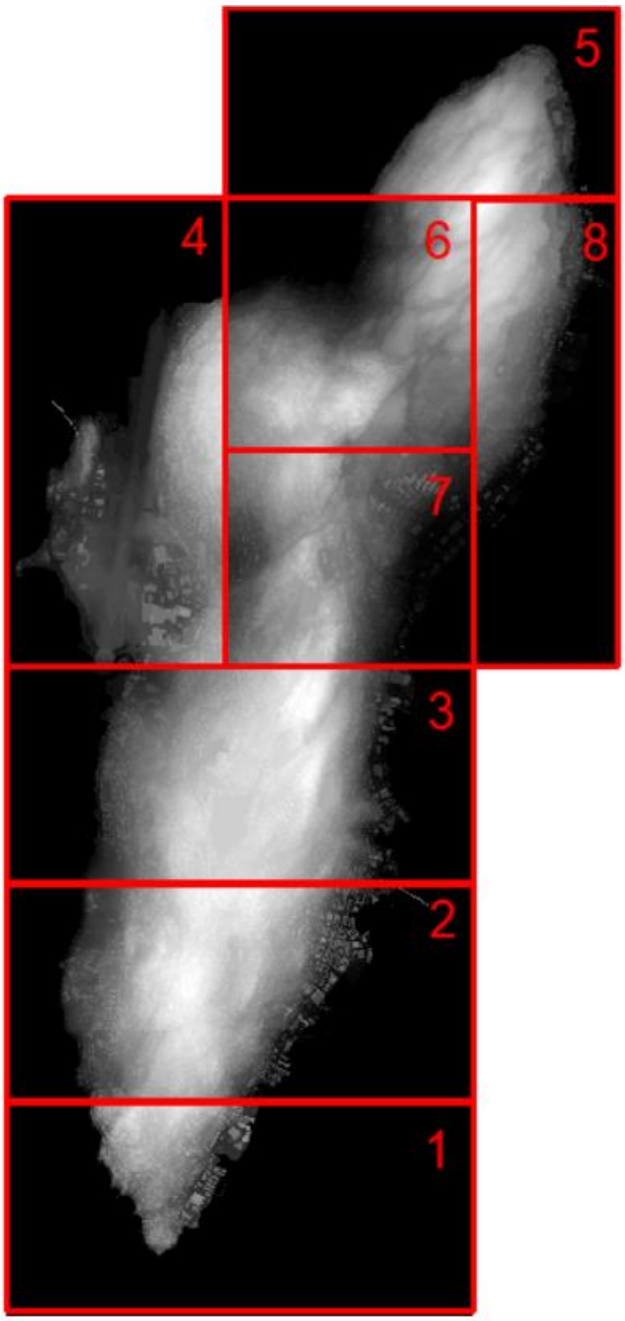

Figure 3-17: Tromsøya parted into 8 sectors.

In retrospect, the split method *NUMBER_OF_TILES* could have been better than the one used. In this method, the user defines how many cells there should be in X and Y direction, thus creating the exact number of tiles and same area. This would also lead to more similar computing times. In addition, the next step of converting the 14 cells to 8 new cells would be unnecessary.

The last step of the map processing is to move each of the 8 files to their own folder in the server as described in Chapter 3.2, to exclude data writing from the same files and to the same location in the GDB.

3.4.3 Creation of the Solar Map

An initial test of ASR for the entire year (days 1-365) in ArcGIS Pro gave the computing times presented in Table 3-7.

Table 3-7: Computing time for first simulation of all areas.

Area no.	Computing time (minutes)
1	145
2	142
3	141
4	147
5	114
6	80
7	78
8	109

This can mean that all simulations for one month can be done in less than 147 minutes, as it is established that computing time increases some for a higher number of days. Thus, a full year could be completed in less than 30 hours. By computing for the whole area for each month, where 1 month had a computing time of 13 hours and 13 minutes, the total time used would be over 158 hours. Thus, parting the area have reduced computing time by more than 5 times.

The next step is to complete all simulations for each month with ASR in ArcGIS Pro. The input for one of these simulations in ArcGIS Pro is presented in Figure 3-18. This particular simulation is for area 1, for January (days 1-31) with D and T from Table 3-6. The rest of the input is default values.

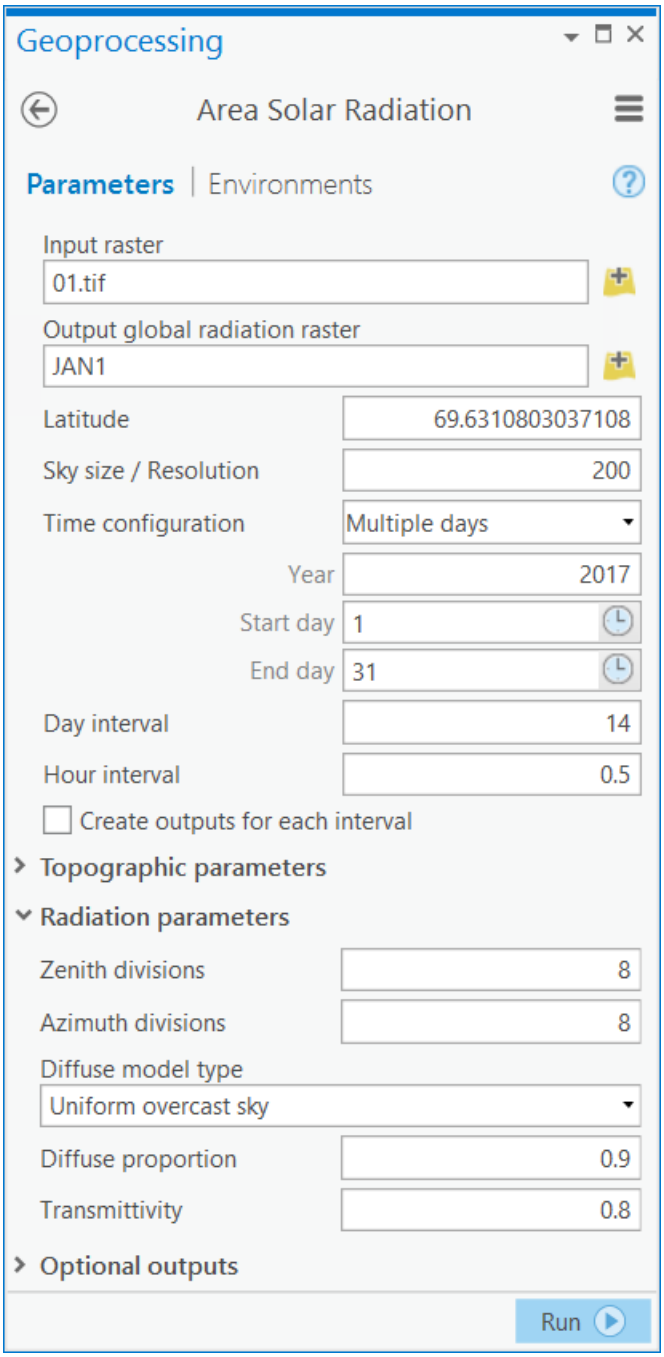

Figure 3-18: Default tool screen of ASR in ArcGIS Pro.

During the process of completing all simulations, the computing time were logged. Due to trouble with some of the months, not all are logged. The reason for this is that the servers are disconnected from the remote server connection, and will not open properly. The only problem with this is that it will not be possible to read and log the computing time. This will not have any effect on the output results, ASR will still run properly and create the solar map. The processing time is logged in Table 3-8.

Table 3-8: Computing time for simulations for each month and area. The value is minutes.

Area no/ Month	January	March	April	May	June	July	Aug	Sept	October	November
1	97	104	110	108	115	113	109	110	102	99
2	98	102	109	106	116	112	107	110	102	97
3	97	101	108	106	113	111	106	110	102	97
4	102	108	113	111	119	115	112	114	112	96
5	76	82	83	84	94	87	84	86	79	75
6	61	54	52	55	60	60	50	60	52	49
7	47	52	55	55	62	57	56	59	50	52
8	72	78	83	83	85	84	81	82	75	72

The next process in creating the map is to merge all maps created for each month into a single map. This is done with the *Mosaic to New Raster* tool. Now that the cells have overlap, it is necessary to pay attention to the input of *Mosaic Operator*. The *Mosaic Operator* decides what will happen to the overlapping cells from each of the maps. The operations to choose between for the overlap sections are presented in Table 3-9.

Table 3-9: Overview of Mosaic Operators in Mosaic to New Raster tool in ArcGIs.

First	The value from the cell in the first input raster will be chosen
Last	The value from the cell in the last input raster will be chosen
Blend	The value for the new cell will be calculated by a horizontally weighted calculation of the overlapping cells
Mean	The new value will be the mean of the cell values
Minimum	The minimum value for the overlapping cells will be chosen
Maximum	The maximum value for the overlapping cells will be chosen
Sum	The sum of the cells will be the new cell value

The operations considered were *Maximum* and *Minimum*. The reason for this is that one of the call values for the overlapping area should be used, and not a new calculated value that would alter the results in one way or the other. Both operations were tested, and *Minimum* was chosen to be used. This is discussed in Chapter 4.2.1.1. All monthly solar maps are included in Appendix 7.2.

The final process is to merge all areas together to one single raster. Again, the *Mosaic to New Raster* tool is used. This time, the *Mosaic Operator Sum* is used. This operation sums the value for all 11 overlapping cells, and creates a final solar map.

4 Results and Discussion

4.1 Final Solar Map

The results from the final solar map is presented in Figure 4-1.

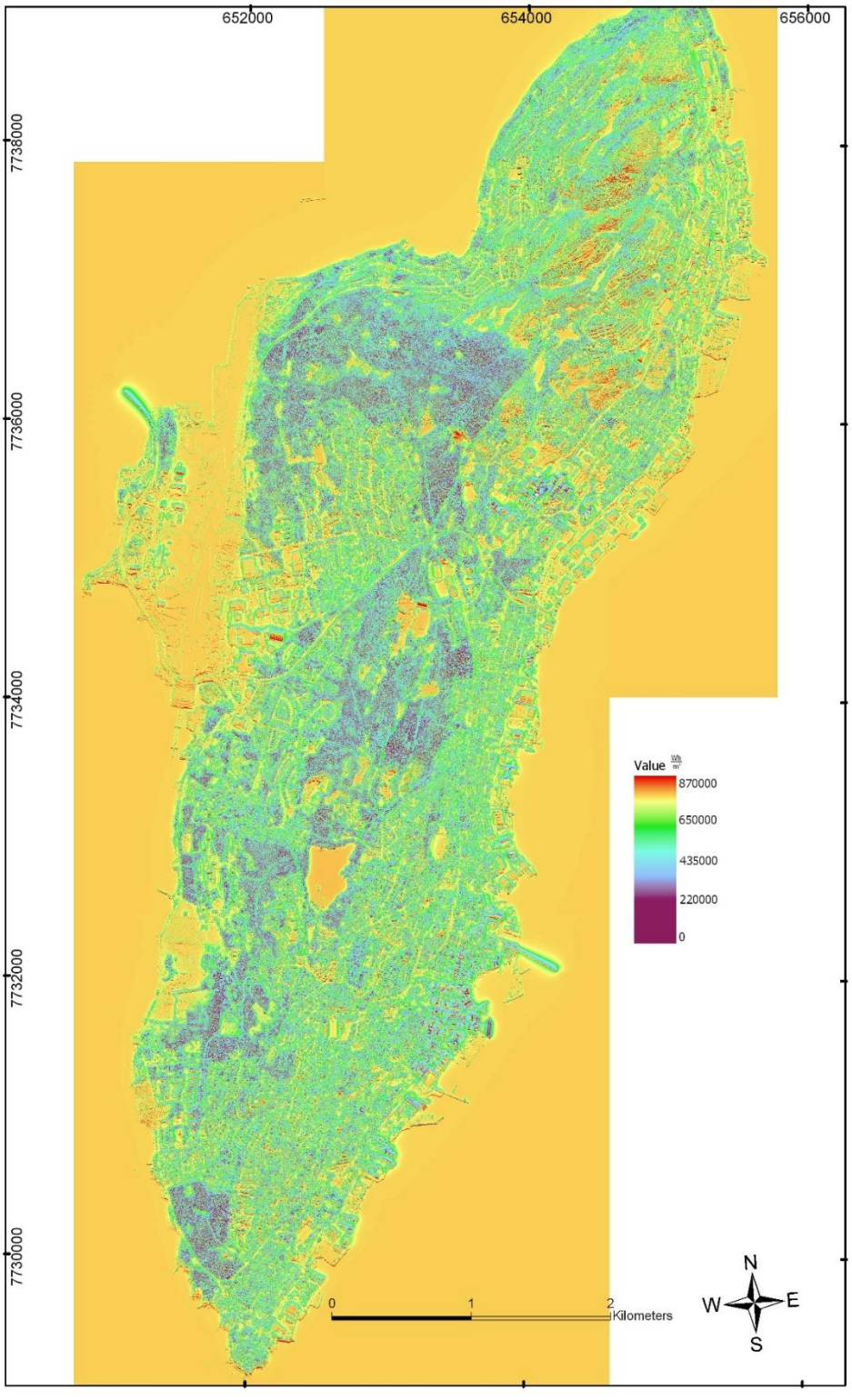

Figure 4-1: Solar map for Tromsøya. Legend in $\frac{wh}{m^2}$. Projection: UTM Z-33N.

It is difficult for the reader to investigate Figure 4-1 in its current form, without the ability to present an interactive map that makes it possible to zoom in and out over the area. This is solved by investigating some of the interesting locations in the map.

The maximum cell value of the map is 869 kWh/m^2 for one year, while the mean is 598 kWh/m^2. By creating a map in ArcGIS that only includes certain values, it will be possible to locate the areas in the solar map with highest values. Presenting the map in its original boundaries is not practical in the format of this report, so a few focus areas have been located. The first map in each case is presented with a stretched format legend to show the surroundings. The second map only show values above 800 kWh/m^2.

Figure 4-2 show the sports hall Tromsøhallen, located close to the middle of the island. The hall has a south-west orientation (note that the northern arrow is pointed to the true north, not straight Y direction. There are three more halls like this at Tromsøya, and they have the same orientation and great output values. Tromsøhallen is on top of the island, at an elevation above 100 meters.

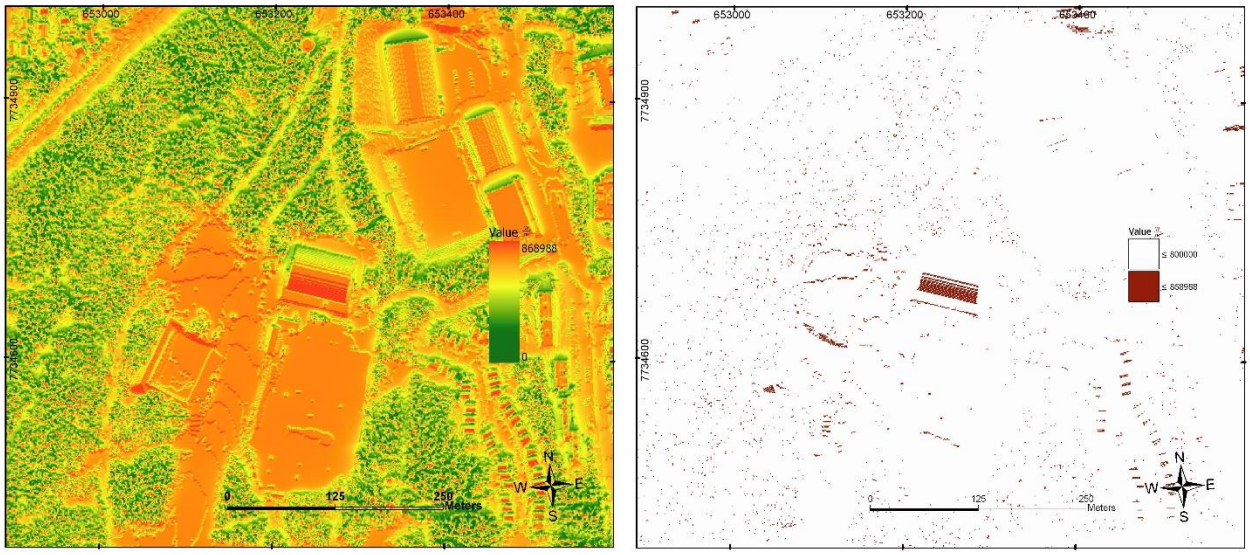

Figure 4-2: Focus area Tromsøhallen. Left map has a stretched legend which varies from 0 to 869 kWh/m^2. Right map only shows values above 800 kWh/m^2 in red. Created in ArcGIS. Projection: UTM Z-33N.

Figure 4-3 shows a section over Åsgård Hospital and residential buildings. The roofs with high global radiation values are orientated south. Buildings in the eastern part of the picture, right above the legend, have a west-east orientation and no clear areas of output over 800 kWh/m^2.

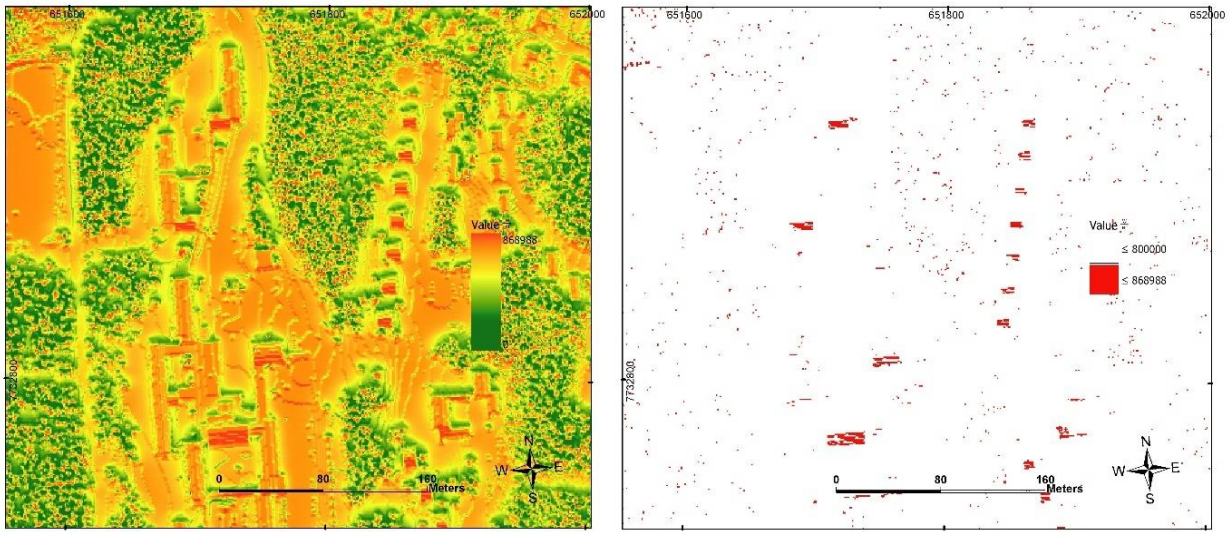

Figure 4-3: Overview of Åsgård Hospital (mid-west part of the map) and residential buildings (mid-east part of the map). Left map has a stretched legend which varies from 0 to 869 kWh/m^2. Right map only shows values above 800 kWh/m^2 in red. Created in ArcGIS. Projection: UTM Z-33N.

Figure 4-4 show a section of Fagereng. Here, clear differences between south orientated roofs and roofs at west-south-west or south-east orientations have lower global radiation values.

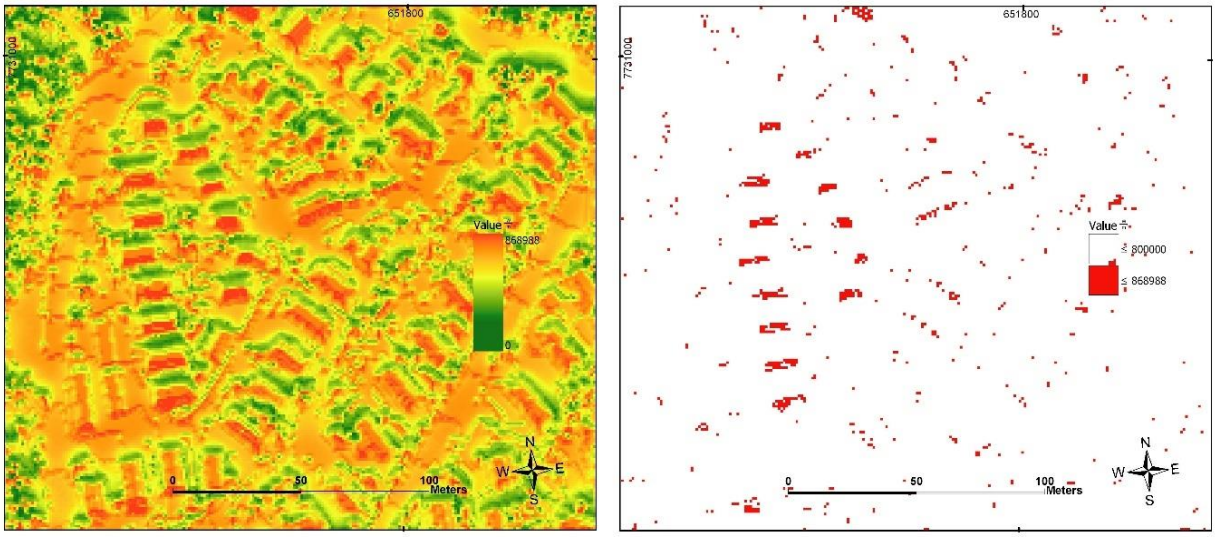

Figure 4-4: Overview of residential buildings at Fagereng. Left map has a stretched legend which varies from 0 to 869 kWh/m^2. Right map only shows values above 800 kWh/m^2 in red. Created in ArcGIS. Projection: UTM Z-33N.

4.1.1 Monthly Solar Maps

The partial outputs of monthly solar maps are included in Appendix 7.2. November and January have different legends than the other months, because the values are too low to visualize the map. What can be seen in these maps is that areas of forest have large distortion in values, and is visible as clouded parts of the maps. In addition, areas with tall buildings close together show lower values then the areas around it. One of these areas is the University of Tromsø Campus.

In the June solar map, the shading from buildings can be seen easily. Some surfaces are completely obstructed by buildings, and have very low values. This is displayed in Figure 4-5.

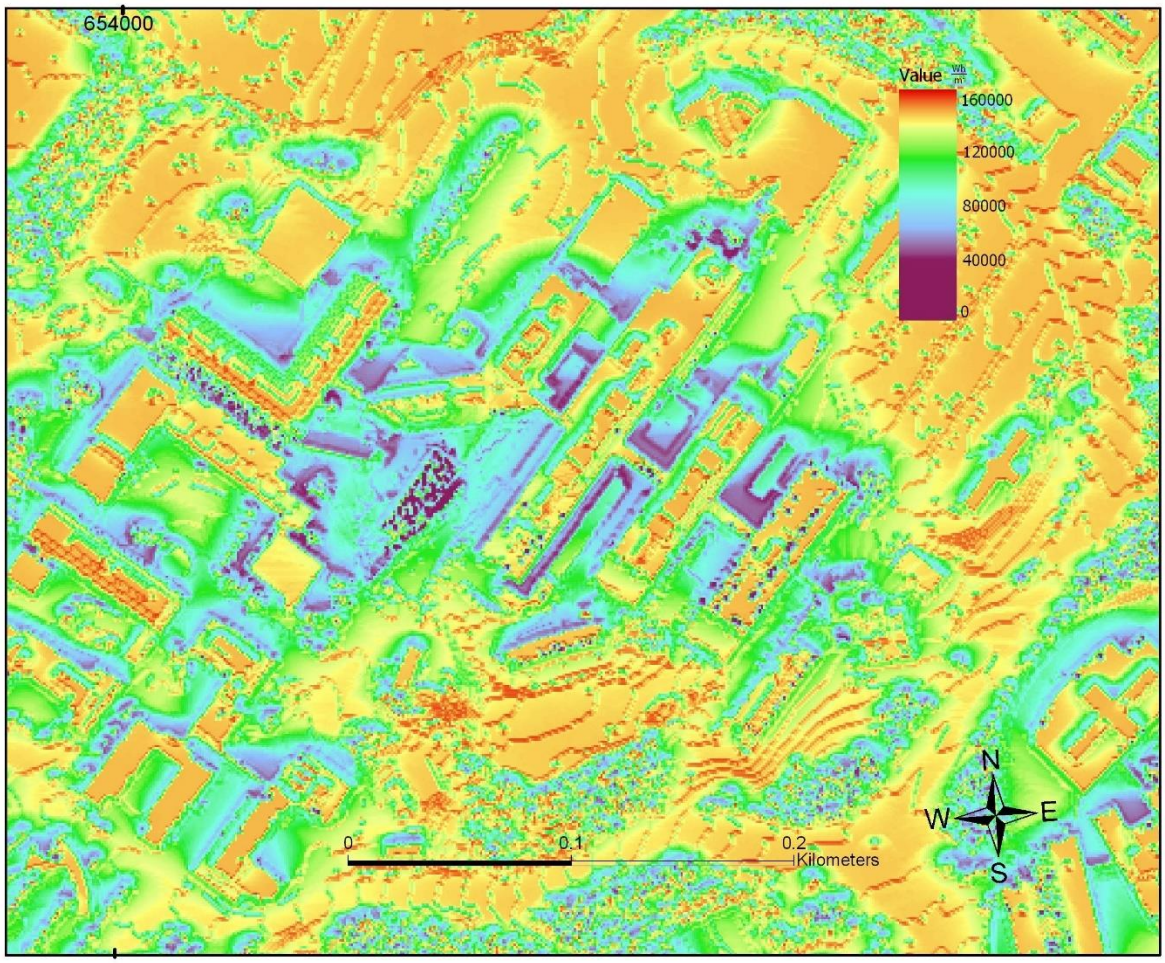

Figure 4-5: Overview of the University of Trosmø Campus area. Solarmap for June. Created in ArcGIS. Projection: UTM Z-33N

Another interesting aspect to look at is how shading varies between the months. In FIGURE, a football field just east of Tromsøhallen is displayed for the months June and February. Here, the shading over the football field is long for February, as the global solar radiation appear to be better further north on the field. In the map for June, only some shading is seen close to the south-west corner. These effects appear because the sun is lower in the sky in February.

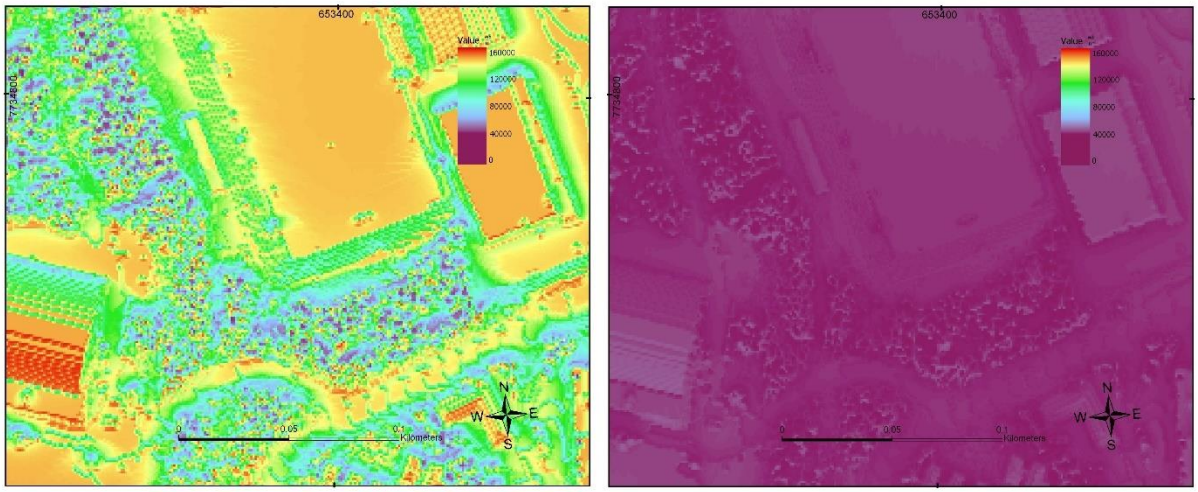

Figure 4-6: Shading effects for June (left map) and February (right map). Created in ArcGIS. Projection: UTM Z-33N

4.1.2 Global Radiation Output Validity

One of the ways to validate the final solar map, is to investigate the output values with weather data and other sources. This is necessary to investigate if the process of making the map were correct, and see if the results make sense.

The weather data obtained from Holt weather station, and presented in Table 3-3, show an average yearly output of global solar radiation of 695 kWh/m^2. This value is measured from a horizontal surface. This indicates that open, horizontal surfaces in the map should comply with that value. By checking in ArcGIS pro for values at a lake (Prestvannet), the sea, and at Holt, the values in Table 4-1 found.

Table 4-1: Output cell values for picked horizontal locations.

Location (elevation (meters))	Cell value (W/m^2)
Holt (13)	692260
Prestvannet (96)	706340
Sea west of island (0)	696943
Sea east of island (0)	697068

The values in Table 4-1 indicates that the horizontal measurement of global solar radiation in the solar map matches each other. There is no surprise that the value at Holt is close to the measurements from the weather station, but it was necessary to investigate if no mistakes were done during the determining of diffusion fraction and transmittivity, in addition to processing the map.

With the result presented from PVGIS in Chapter 2.1.3, it is possible to comment the results further. The horizontal surface values are close to the values from the obtained solar map for

Tromsøya. The values for an optimally inclined surface are higher than the highest values from the map. This can indicate that although correct for horizontal surfaces, the D and T values are too low. This is further discussed in the next section.

4.2 Sensitivity Analysis

4.2.1 Consequences of Sectoring

It is necessary to address issues concerning viewshed when dividing the total area into smaller areas. As known, this removes shading from the other cells when calculating viewshed. In urban areas with low topography, overlapping the cells can be enough to represent viewshed in a reasonable way. But it can also be a wrong representation because tall buildings just outside the overlap area will not be considered for the viewshed. This gives a viewshed with less obstruction and better output than expected. If a tall building is placed directly to the south from a location that is just outside the overlap section, the output could be considerably lower and not necessarily suitable for a solar panel.

In Figure 4-7, two viewsheds for DSM1 (a) and DTM1 (b) is shown to compare how the resolution and type of DEM alters the viewshed. What could be expected is that the DSM will have a viewshed with more obstruction than the DTM, as it includes all topography. This can be seen in Figure 4-7 a), where there is obstruction from north north-west from a tree. It can also be seen that the DTM1 viewshed has no shading from the west, even though Figure 3-3 had so.

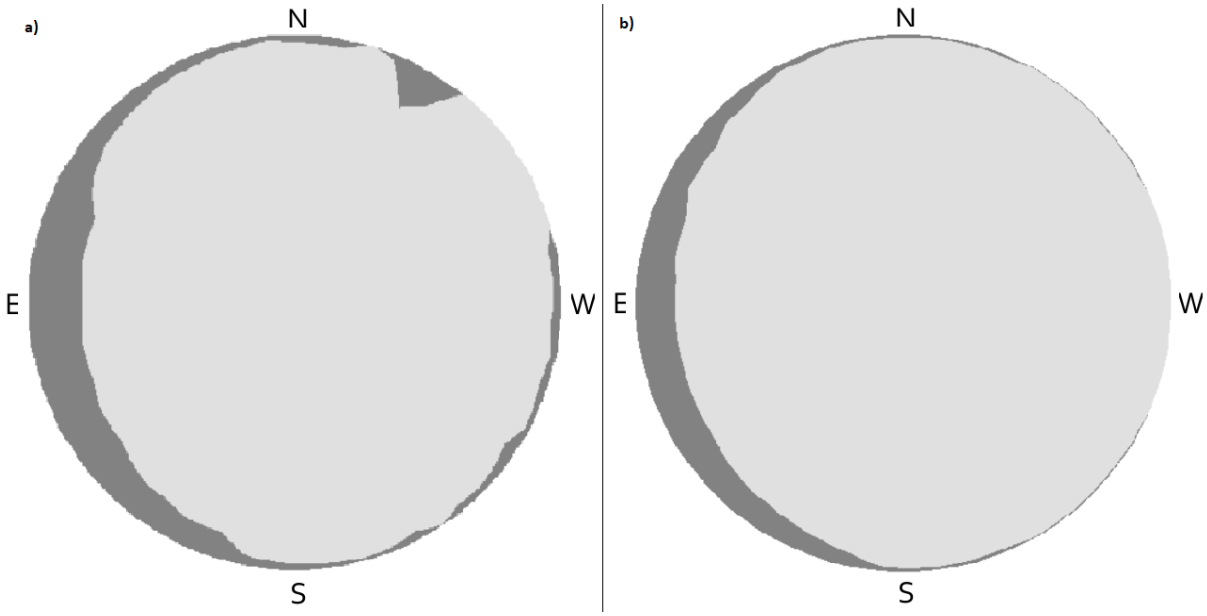

Figure 4-7 a) Viewshed from Holt with DSM1. b) Viewshed from Holt with DTM1. Created in GSR.

The same thing applies when a full map is divided into multiple sectors. This can cause better output of global solar radiation than expected, because there is less shading from topography. A viewshed for the same location in sector 1 and 2 (Figure 3-17) were calculated in SRG. The results are displayed in Figure 4-8. What can be seen here is that the viewshed is altered by the sector it is calculated for. Because of this, the viewshed will never include obstructions from the other sector. This makes the output value better than what it should be.

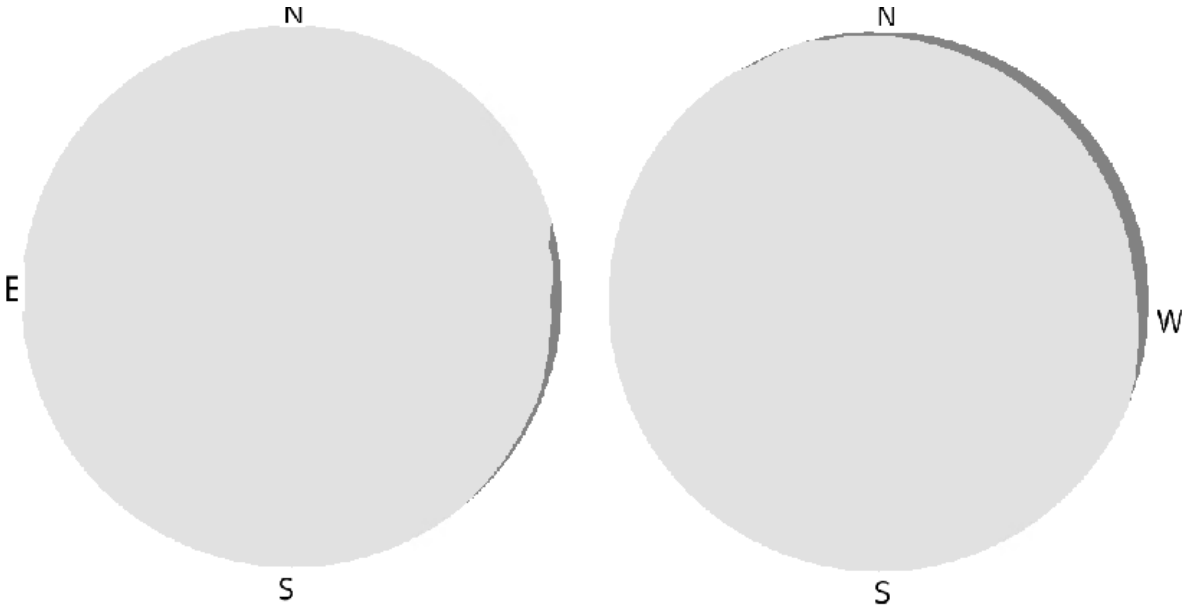

Figure 4-8: Left viewshed is for area 1, right for area 2. The viewsheds are altered by what section they are in. Created in ArcGIS.

4.2.1.1 Cell Overlap

In Chapter 3.4.2, it was considered whether to use the *Mosaic Operator Maximum* or *Minimum.* With testing both operations for the solar map of June, it was figured out from Figure 4-9 and Figure 4-10 that there is a clear difference in the transition between the overlap for each sector. The location marked is a location west on Tromsøya. It is clear that some of the calculated values for the roof is wrong. Figure 4-9 shows the simulation with the operator *Maximum.* What has happened here, is that the *Maximum* operator includes the highest calculated values for each sector. As known from the last section, the viewsheds alter the output for each section to be better than it is. In Figure 4-10, the operator *Minimum* is used. When using *Minimum,* no signs for an overlay can be seen, because the lowest value for the overlap is the one used.

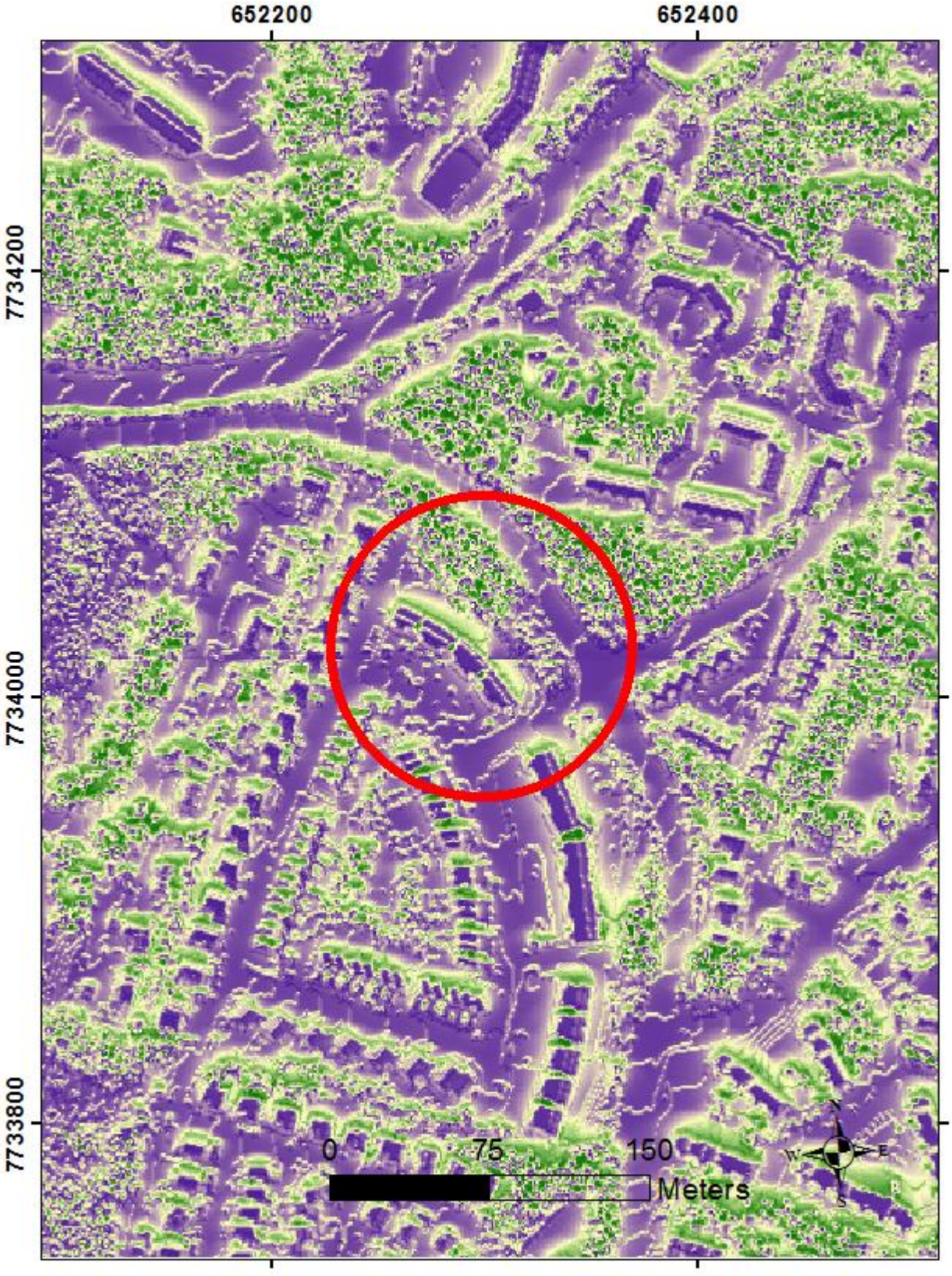

Figure 4-9: A location west on Tromsøya showing overlap section differences. This map was created with Mosaic Operator Maximum. Created in ArcGIS. Projection: UTM Z-33N

Figure 4-10: A location west on Tromsøya showing no signs of overlap section differences. This map was created with Mosaic Operator Minimum. Created in ArcGIS. Projection: UTM Z-33N.

4.2.2 Diffusion Fraction and Transmittivity

The method with using PSR to estimate D and T value are difficult to evaluate without having the possibility to use measured data of the diffuse fraction. From the table in Appendix 7.1, it can be seen that some values are very close to each other. This could indicate that by changing these values, the output of the map could be changed in positive or negative direction.

When deciding D and T for August and September, two combinations gave close to the same global solar radiation. Because of this, it was necessary to investigate both of them in the form of a solar map to see the difference. The solar map with different D and T for September is included in Figure 4-11 and Figure 4-12. Figure 4-11 was created with a D fraction of 0.4 and T value of 0.6, while Figure 4-12 had a D fraction of 0.8 and T value of 0.4. As seen from the figures, the output varies significantly, with better values from the first figure. This indicates that determining D and T values are of importance, and that the way used to determine them are not necessarily valid. The top value for the map in Figure 4-11 is 76 kWh/m^2, with a mean of 39 kWh/m^2, while Figure 4-12 had a top value of 54 kWh/m^2 and mean of 41 kWh/m^2. Based on the results of the top values, the first map was chosen to be input for the finished map. The values for south facing roofs decrease with higher diffusion fraction, and a D of 0.8 is most likely not correct for September.

The same test was done for August. Here, the first map was created with a D fraction of 0.3 and T value of 0.6. The second map had a D fraction of 0.7 and a T value of 0.4. The top value for the first map were 120 kWh/m^2, with a mean of 83 kWh/m^2. The second map had a top value of 102 kWh/m^2 and mean of 70 kWh/m^2. The first map was chosen in this case as well, based on the same conclusions as for September.

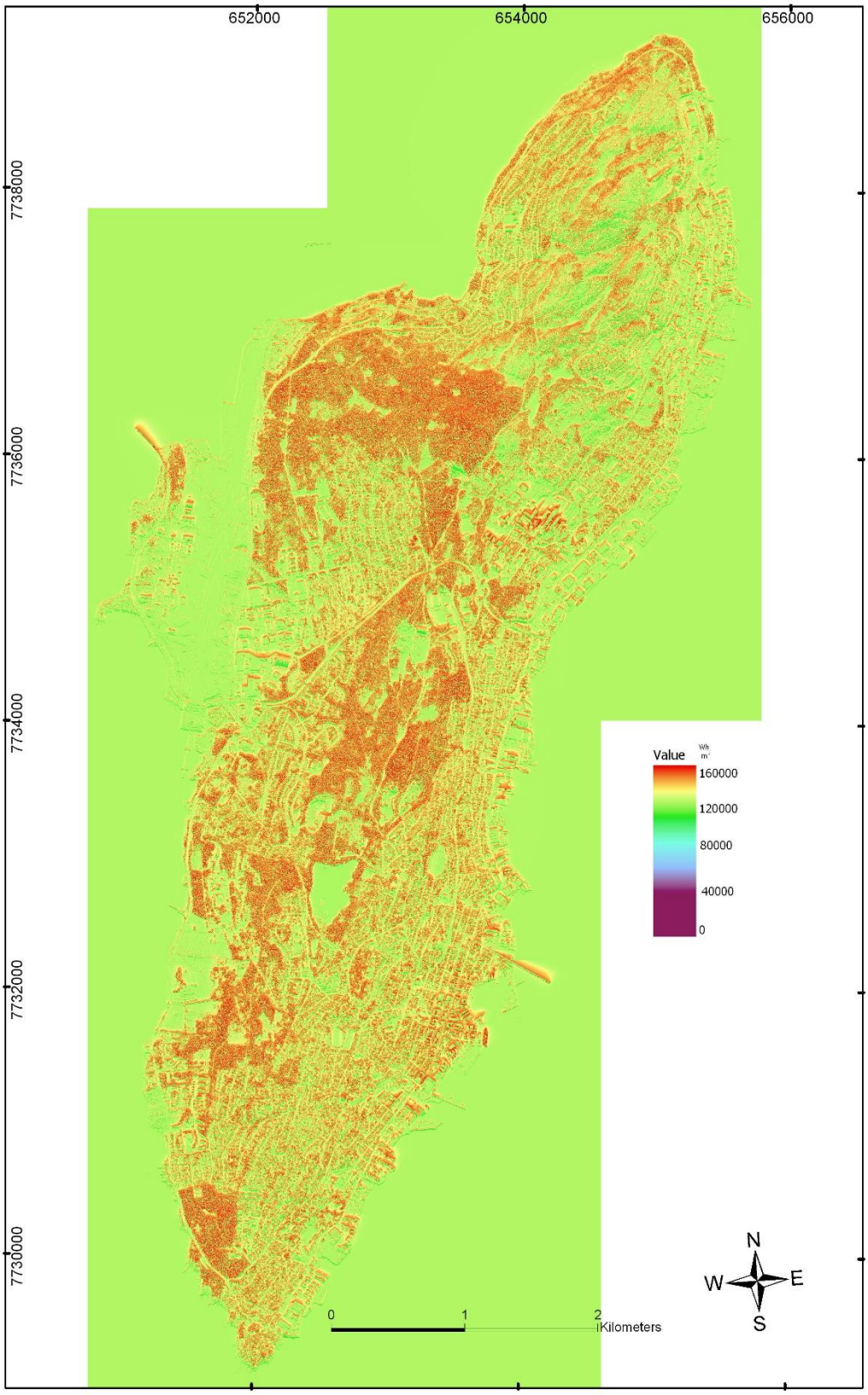

Figure 4-11: Solar map of September with D=0.4 and T=0.6. Legend display is from 0 to 160 kWh/m^2. Created in ArcGIS. Projection: UTM Z-33N.

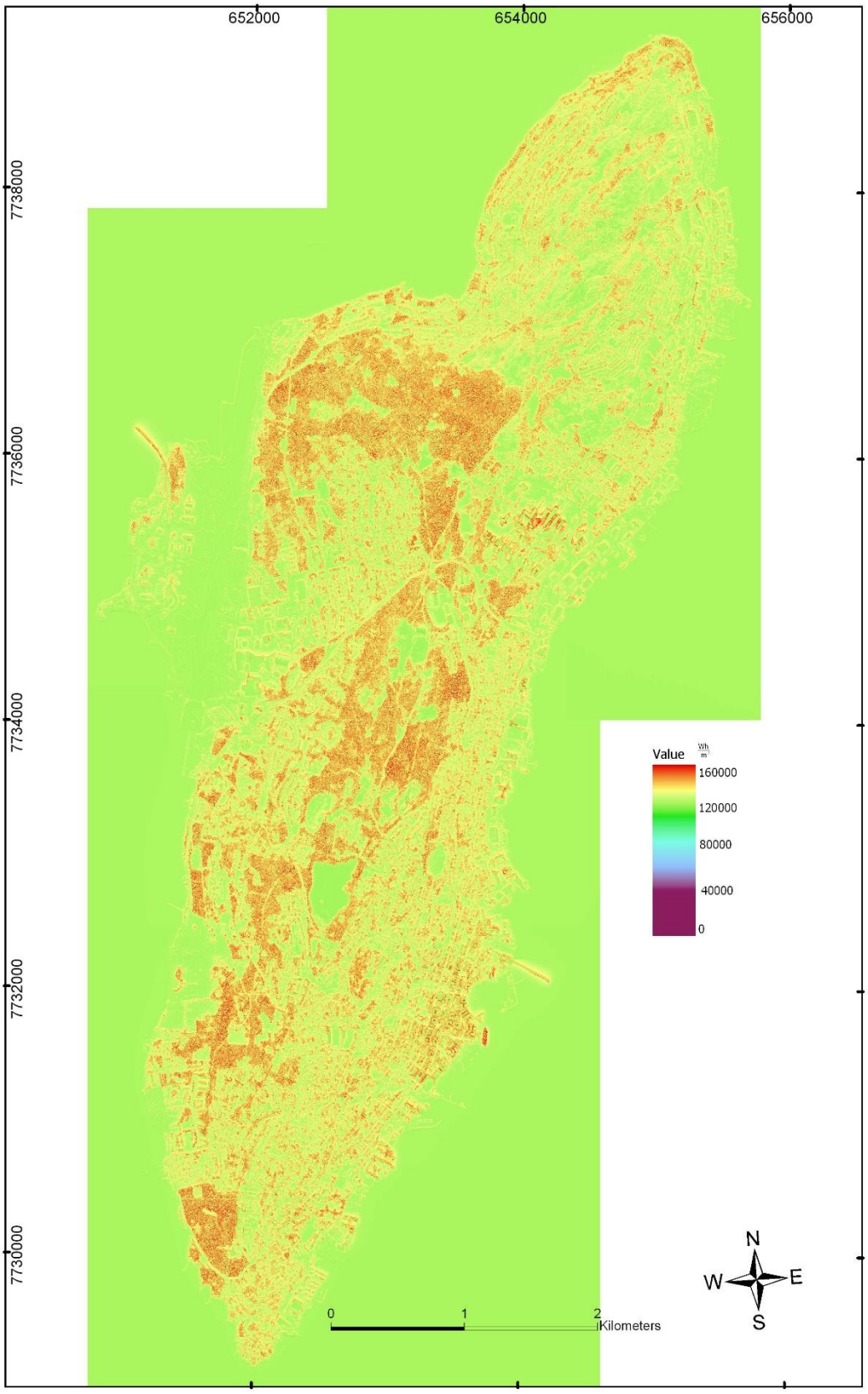

Figure 4-12: Solar map of September with D=0.4 and T=0.6. Legend display is from 0 to 160 kWh/m^2. Created in ArcGIS. Projection: UTM Z-33N.

This indicates that months with low diffusion fraction will have better top values compared to months with high diffusion fraction. This way, the result could be altered in a positive direction, by only choosing values with low diffusion fraction. The fact that this is possible makes the result difficult to authenticate, although the decisions are based on what most likely is the correct values.

In addition, the solar map for December was not possible to make. The program could calculate any global solar radiation for Tromsøya. As seen in the sunmaps in Chapter 3.1.1.1, December is not visible at all. This could have made the program believe that no outputs were possible.

4.3 Computing Time

Via personal communication with the creators of Oslo Solar Map, the total computing time for a solar map for all months and sectors with DSM1 were found to be 24 days. For DSM0.5, the computing time was reported to increase to 1 year, and therefore close to impossible to make. Their simulation was run in a batch between two computers. The specifications of the computers used are presented in Table 4-2. Batch is the process of writing a script so that when one simulation is finished, the other one automatically starts. With this process, it seems like only one core at each computer is running at the same time, instead of utilizing all cores. Unlike the UiT server, the machines used by Oslo Solar Map does not support Hyper-Threading. (Adamou Personal Communication)

Table 4-2: Specifications for both computers used by Oslo solar map.

Model	Dell (unknown model)
Processor	Intel(R) Core(TM) i5-3470 CPU @3.20 GHz, 4 cores
Memory (RAM)	8 GB
Operating System	64-bit Microsoft Windows 7 Professional Service Pack 1

When comparing the results of computing times with the ones in Oslo, it is important to keep in mind that the area they use is a lot larger. They parted the municipality into 56 tiles of 2000x2000 meters resolution and 250 meters overlap. With 56 tiles instead of 8, the computing time will increase. It is difficult to say why parting the area into 56 tiles would benefit the simulation, except the ability to get a clear overview of when each and one tile are finished. By changing the area to the number of processors, or run several simulations on enough computers to compute more areas at the same time, computing time would be reduced. (Adamou Personal Communication)

Oslo reported that each of the 56 tiles used approximately 1 hour of computing time. As each tile is run for every month, this is 672 hours (28 days) of computing time. If running two computers in parallel had worked properly, this computing time should have been reduced to 336 hours, but the total computing time were reported to be approximately 24 days (576 hours). It is difficult to say why this occurred, but it can be that the batch script was not properly set up, that some of the processes stopped each other's progress, or that there was a waiting time between each simulation. To draw any more conclusions from this would be mere speculation.

If an assumption is made that each of these two computers have 4 cores, utilizing all cores would reduce the total to 84 hours. Reducing the areas into cells have not necessarily saved computing time for Oslo Solar Map, because the computing power has not been utilized.

As this type of computing power is not available for most institutions like municipalities and learning institutions, a solution suggested by Section for Digital Research Services can be to rent a cloud service. Although not tested yet, a cloud service could make it possible to rent a powerful server and do all main simulations there. With this option, the possibility to part the area into even smaller parts and utilize more cores is an option, thus reducing simulation time further. (Andersen Personal Communication)

If a DSM0.5 was used for the main simulations in this thesis, the computing time would have an estimated increase of 4 times, as there are 4 times as many cells. It is unclear why Oslo Solar Map estimated an increase from 24 days to 1 year from DSM1 to DSM0.5, but it might be a consequence of their batch script. As Tromsøya is quite small in area, it would be possible to do simulations with a higher resolution. With 8 cores available, simulations for each month would be approximately 8 hours, and the map would be finished in 96 hours.

Another reason for reducing computing time is the aspect of updating the map. With new weather measurements, higher resolution on DEMs, or changes in D and T values, large parts of this process would have had to be done over again. If computing times is lowered, this is not a significant issue. In opposition, low computing times can cause opportunities for more testing and validation of the result.

5 Conclusion

5.1 Conclusion

A solar map of Tromsøya have been created using Solar Analyst tools in ArcGIS. The process of making the map has been thoroughly explained. The process includes understanding how the Solar Analyst tools calculate global solar radiation and how different input alters the final map. Solar Analyst require input of diffusion fraction (D) and transmittivity value (T), which have an important effect on the results. These values were calculated by combining weather station measurements with calculation in the Solar Analyst tool Points Solar Radiation. Although, this way of calculating diffusion fraction and transmittivity have some disadvantages, as several different varieties of D and T values can fit the requirements. This a

The solar map shows that southward-facing roofs have global solar radiation values of over 800 kWh/m^2, which can indicate good potential for solar modules.

One of the main issues in the creation of the solar map with this process was excessive computing times. It was quickly established that the tools in Solar Analyst only utilizes one core of the central processing unit. Through sectoring the area and utilizing all cores with the use of a server, the computing time for a single month was reduced from over 13 hours to less than 2 hours. By using this process, simulating solar maps will reduce computing time from several days to hours. This is advantageous for updating maps and test different outputs, in addition to increasing the resolution and area of the map.

5.2 Further Work

5.2.1 Solar Energy Output

The ultimate goal for creating a solar map is to determine energy yield for solar modules. The results from the map are better suited in terms of how much a solar module could produce with these results. So, by translating the output values to solar energy output, the solar map would be more suited for people that considers installing a solar energy system.

In addition, case studies for certain locations within the map can be done with solar energy output. A suggested case study is investigating the solar energy system potential for rooftops at the campus of the University of Tromsø. The university has a newly installed solar energy system, and data from the map can be compared with the output.

5.2.2 Map Extension to Tromsø Municipality

Computing times are decreased using the process described in this thesis. This will make expansion of the map easier. One of the initial goals of this thesis was to map the whole of Tromsø Municipality, and this will be easier with the new technique of utilizing all cores of the central processing unit.

In addition, the reduced computing time makes it possible to make a solar map with higher resolution. This is a natural step forward, and will make it possible to see small changes within small distances, i.e. a chimney on top of a roof.

5.2.3 Include Buildings and Facades

Oslo Solar Map is rendered with the use of NT3D-builder from GEODATA, together with building data. This makes map only include values for roofs, and also makes it more appropriate and pleasant for the ones viewing it. In addition, NT3D-builder can be used to create a 3D solar map, with possible mapping of global solar radiation of facades. Rendering the map using NT3D-builder is a necessary step before possibly publishing the map and make it possible for everyone to use it.

6 Bibliography

Adamou, Stefanie. "E-mail: stefanie.adamou@pbe.oslo.kommune.no." *Oslo Plan- og Bygningsetat*, Personal Communication.

Andenæs, E., B.P. Jelle, K. Ramlo, T. Kolås, J. Selj, and S.E. Foss. "The influence of snow and ice coverage on the energy generation from photovoltaic solar cells." *Solar Energy* 159 (2018): 318-328.

Andersen, Rolf. "E-mail: rolf.andersen@uit.no." *Section for Digital Research Services*, Personal Communication.

Andrews, J. H., and S. Kais. "Theoretical limits of photovoltaics efficiency and possible improvements by intuitive approaches learned from photosynthesis and quantum coherence." *Renewable and Systainable Energy Reviews* 43 (2015): 1073-1089.

Andrews, J., and N. Jelley. *Energy Science: Principles, technologies and impacts.* Oxford University Press, 2007.

Barstad, Endre. *Fornybar.no.* 2016. http://www.fornybar.no/solenergi/ressursgrunnlag/solenergiressursen-i-norge.

Brennan, M.P., A.L. Abramase, R.W. Andrews, and J.M. Pearce. "Effecs of spectral albedo on solar photovoltaic devices." *Solar Energy Materials and Solar Cells* 124 (2014): 111-116.

Christensen, Arnfinn. *Science NordicArnfinn Christensen.* 2012. http://sciencenordic.com/bright-future-solar-energy-north.

Defra. 2017. http://adlib.everysite.co.uk/adlib/defra/content.aspx?id=2RRVTHNXTS.96RYU2KJZWFLU (accessed December 2017).

Dubey, S., J.N. Sarvaiya, and B. Seshadri. "Temperature Dependent Photovoltaic (PV) Efficiency and Its Effect on PV Production in the World - A Review." *Energy Procedia* 33 (2013): 311-321.

ESRI. *About ArcGIS.* 2017. http://www.esri.com/arcgis/about-arcgis (accessed December 2017).

—. *Background Geoprocessing (64-bit).* 2017. http://desktop.arcgis.com/en/arcmap/10.3/analyze/executing-tools/64bit-background.htm (accessed December 2017).

ESRI Norsk Brukerkonferanse. *Oslo Solkart.* 2017. https://www.kartverket.no/globalassets/arkiv/kartkontor/oslo/ptuoa/esri_brukerkonferanse_stea20170126.pdf (accessed December 2017).

ESRI. *What is a TIN surface.* 2017. http://desktop.arcgis.com/en/arcmap/10.3/manage-data/tin/fundamentals-of-tin-surfaces.htm (accessed December 2017).

—. *What is GIS?* ESRI ArcGIS. 2017. http://www.esri.com/what-is-gis/howgisworks (accessed December 2017).

—. *What is raster data.* 2017. http://desktop.arcgis.com/en/arcmap/10.3/manage-data/raster-and-images/what-is-raster-data.htm (accessed December 2017).

Fu, P., and P.M. Rich. "Design and implementation of the Solar Analyst: an ArcView extension for modeling solar radiation at landscape scales." *Proceedings of the Nineteenth Annual ESRI User Conference*, 1999.

Geonorge. *DTM 10 Terrengmodell (UTM33).* 2017. https://kartkatalog.geonorge.no/metadata/kartverket/dtm-10-terrengmodell-utm33/dddbb667-1303-4ac5-8640-7ec04c0e3918 (accessed December 2017).

Google Project Sunroof. 2017. https://www.google.com/get/sunroof.

Honsberg, C., and S. Bowden. "PV Education." 2015.

Huang, S, and P Fu. "Modeling Small Areas Is a Big Challenge - ESRI." *ArcUser*, no. Spring (2009): 28-31.

IEA-PVPS. "A Snapshot of Global Photovoltaic Markets 2016." 2017.

Kartverket. *Høydedata.* 2017. https://hoydedata.no/LaserInnsyn/ (accessed December 2017).

Kipp&Zonen. *Instruction Manual CM11 Pyranometer and CM14 Albedometer.* Edited by Kipp & Zonen. 2017. https://www.google.no/url?sa=t&rct=j&q=&esrc=s&source=web&cd=2&cad=rja&uact=8&ved=0ahUKEwiBpuPKpezXAhXkAJoKHf59DXQQFggvMAE&url=http%3A

%2F%2Fwww.kippzonen.com%2FDownload%2F48%2FCM-11-Pyranometer-CM-14-Albedometer-Manual&usg=AOvVaw2CXD_N9sXdFAfKfLnZTFUO.

MET. *eKlima.* Edited by Norwegian Meteorological Institute. 2017. http://eklima.met.no/.

NASA. *Earth Observatory.* 2017. https://earthobservatory.nasa.gov/Features/RemoteSensing/remote_08.php.

NIBIO. *AgroMetBase.* Norwegian Institute for Bioeconomy. 2017. http://lmt.bioforsk.no/agrometbase/getweatherdata.php (accessed November 2017).

Nordskog, Berit. "E-mail: berit.nordskog@nibio.no." *NIBIO*, Personal Communication.

PBE. *Oslo Solkart.* Edited by Unit for Planning and Thematic Maps. Departmant for Planning and Buildings. 2017. https://www.oslo.kommune.no/politikk-og-administrasjon/miljo-og-klima/solkart-for-oslo/#gref.

Polat, N, and M. Uysal. "Investigating performance of Airborne LiDAR data filtering algorithms for DTM generation." *Measurement* 63 (2015): 61-68.

Portland State University. 2017. http://web.pdx.edu/~jduh/courses/geog493f12/Week04.pdf (accessed December 2017).

PVGIS. *Photovoltaic Geographic Information System.* European Commision. 2017. http://re.jrc.ec.europa.eu/pvgis/apps4/pvest.php.

PVGIS5. *Photovoltaic Geographic Information System 5.* 2017. http://re.jrc.ec.europa.eu/pvgis.html.

Quaschning, Volker. "Understanding Renewable Energy Systems." Earthscan, 2005.

Sengupta, M., et al. "Best Practices Handbook for the Collection and Use of Solar Resource Data for Solar Energy Applications." 2015.

Solanki, C. S. *Solar Photovoltaics: Fundamentals, Technologies and Applications.* 2nd ed. Delhi: PHI Learning Private Limited, 2011.

Solkart.no. *Solkart.no.* Sivilingeniør Carl Christian Strømberg AS and Norkart AS. 2016. https://solkart.no/?side=omsolkart.

Stockhols Stad. *Stockholms Solkarta.* Stockholms Stad Energi och-klimatrådgivningen. 2017. http://www.stockholm.se/ByggBo/Leva-Miljovanligt/Stockholms-solkarta/.

Wikimedia. *Wikipedia.* 2017.
https://commons.wikimedia.org/wiki/File:Simple_vector_map.svg.

7 Appendix

7.1 Values for Diffusion Fraction and Transmittivity

Table 7-1: Tests for different D and T value, for each month. Cells marked in green show chosen values, while cells marked in orange is the next best. Blue cells indicate values that had to be tested.

		January	February	March	April	May	June	July	August	September	October	November	December
		794.9167	8110.483	36223.92	90860.95	130217	140890.9	126764.4	94885.3	47696.38	16441.52	1791.45	333.35
	Day	(1-31)	(32-59)	(60-90)	(91-120)	(121-151)	(152-181)	(182-212)	(213-243)	(244-273)	(274-304)	(305-334)	(335-365
D	T												
0.2	0.6					121538	147398.4	138450.5	86221.36				
0.2	0.7							187069.1	121457.8				
0.3	0.5				45064.5	101942.5	119117.6	116766.3	66941.95	21103.58			
0.3	0.6	0.069994			77626.98	138632.6	166993.5	157220.7	99509.49	36325.47			
0.3	0.7	1.681177								58507.74			
0.4	0.4	0.000042											
0.4	0.5	0.002982			53634.55	112537.6	146259.5	137071.9	78553.65				
0.4	0.6	0.106554		26308.81	87120.12	161425.4				44311.12	5630.885		
0.4	0.7	2.569402	4115.231	46557.34							13046.15		
0.5	0.4				39076.05		108666.8	100890.7	64062.53				
0.5	0.5	0.005204		17498.97	65632.62	134279.5	162710	165499.7	103419.7		3262.577		
0.5	0.6	0.157737	1907.273	33540.17	106601					55539.03	7460.135		
0.5	0.7	3.812918	5622.198								17399.91		
0.6	0.3	0											
0.6	0.4	0.000091				108267.8	133737.7	124451.7	73691.77				
0.6	0.5	0.00655		23053.32	87000.13	166892.4	200853.4		119194.6	41479.94			
0.6	0.6	0.234511		44387.22	135822.2					72350.89	10204.01		
0.6	0.7	5.678191	7882.648	79425.09							23930.55	102.082	
0.6	0.8	132.253										1029.077	
0.6	0.9	1888.535										8851.99	

		January	February	March	April	May	June	July	August	September	October	November	December
		794.9167	8110.483	36223.92	90860.95	130217	140890.9	126764.4	94885.3	47696.38	16441.52	1791.45	333.35
	Day	(1-31)	(32-59)	(60-90)	(91-120)	(121-151)	(152-181)	(182-212)	(213-243)	(244-273)	(274-304)	(305-334)	(335-365
0.7	0.3	0.000001				83192.98	105677.6	97129.23					
0.7	0.4	0.000141			78265.99	143064	175522.5	163720.1	98499.62	29657.14	1861.674		
0.7	0.5	0.010119		32310.57	117756.8					57328.21	14777.13		
0.7	0.6	0.362468	3918.159										
0.7	0.7	8.786979	11650.06									156.801	
0.7	0.8	173.18										1582.68	
0.7	0.9	2931.181											
0.8	0.3	0.000001			54286.51								
0.8	0.4	0.000241			105302.8					45909.33	2995.601		
0.8	0.5	0.017255	2209.316								9170.044		
0.8	0.6	0.618383	6431.767								23923.38		
0.8	0.7	15.00456	19184.9									312.606	
0.8	0.8	296.077										2689.887	
0.8	0.9	5016.474											
0.9	0.3												
0.9	0.4		970.887										
0.9	0.5	0.038664	13972.56										
0.9	0.6	1.386128											
0.9	0.7											594.551	
0.9	0.8	681.838											0
0.9	0.9	11272.35											

7.2 Solar Map Each Month

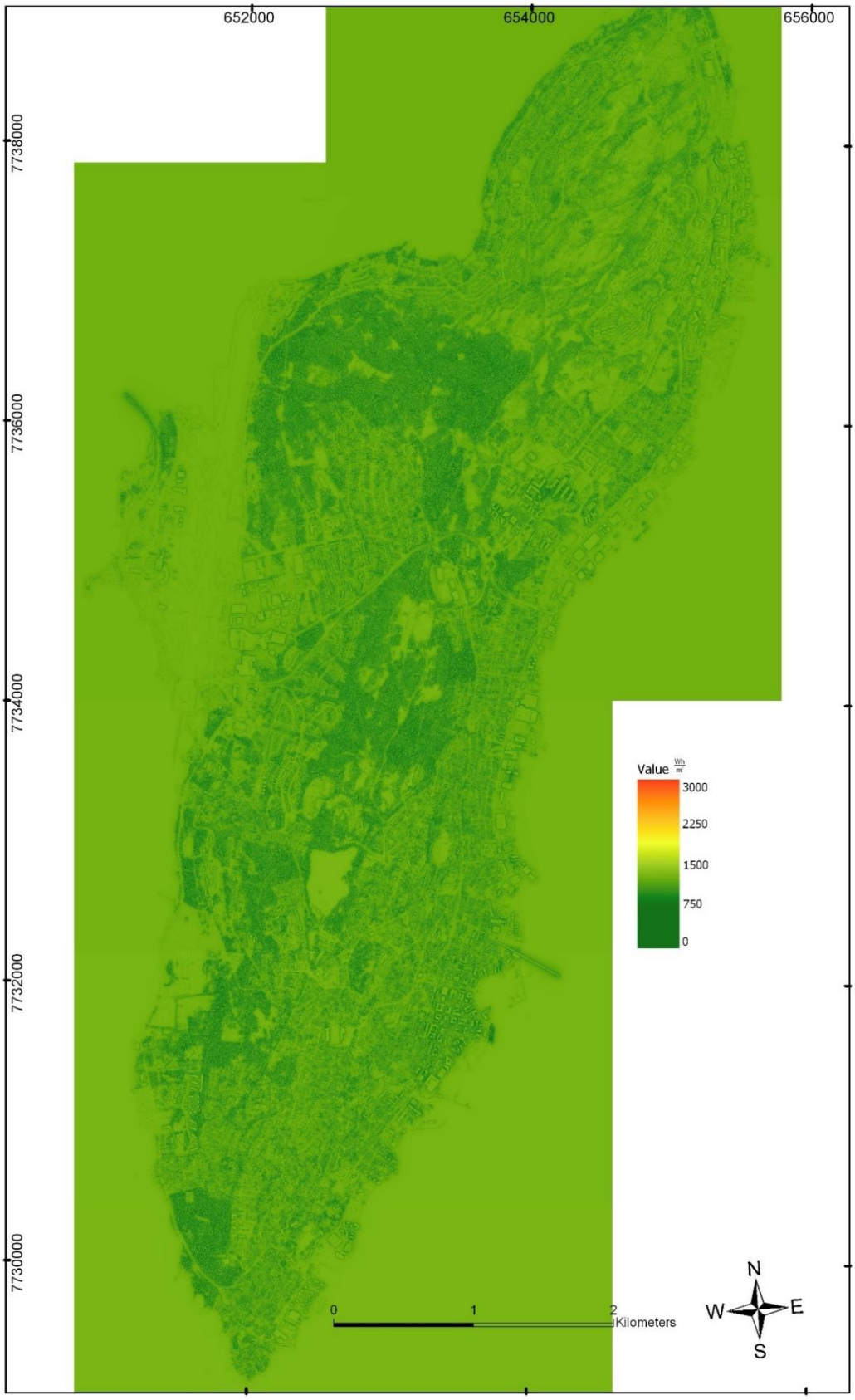

Figure 7-1: Solar map for January, with legend values varying from 0 to 3 kWh/m^2. Created in ArcGIS. Proj: UTM Z-33N

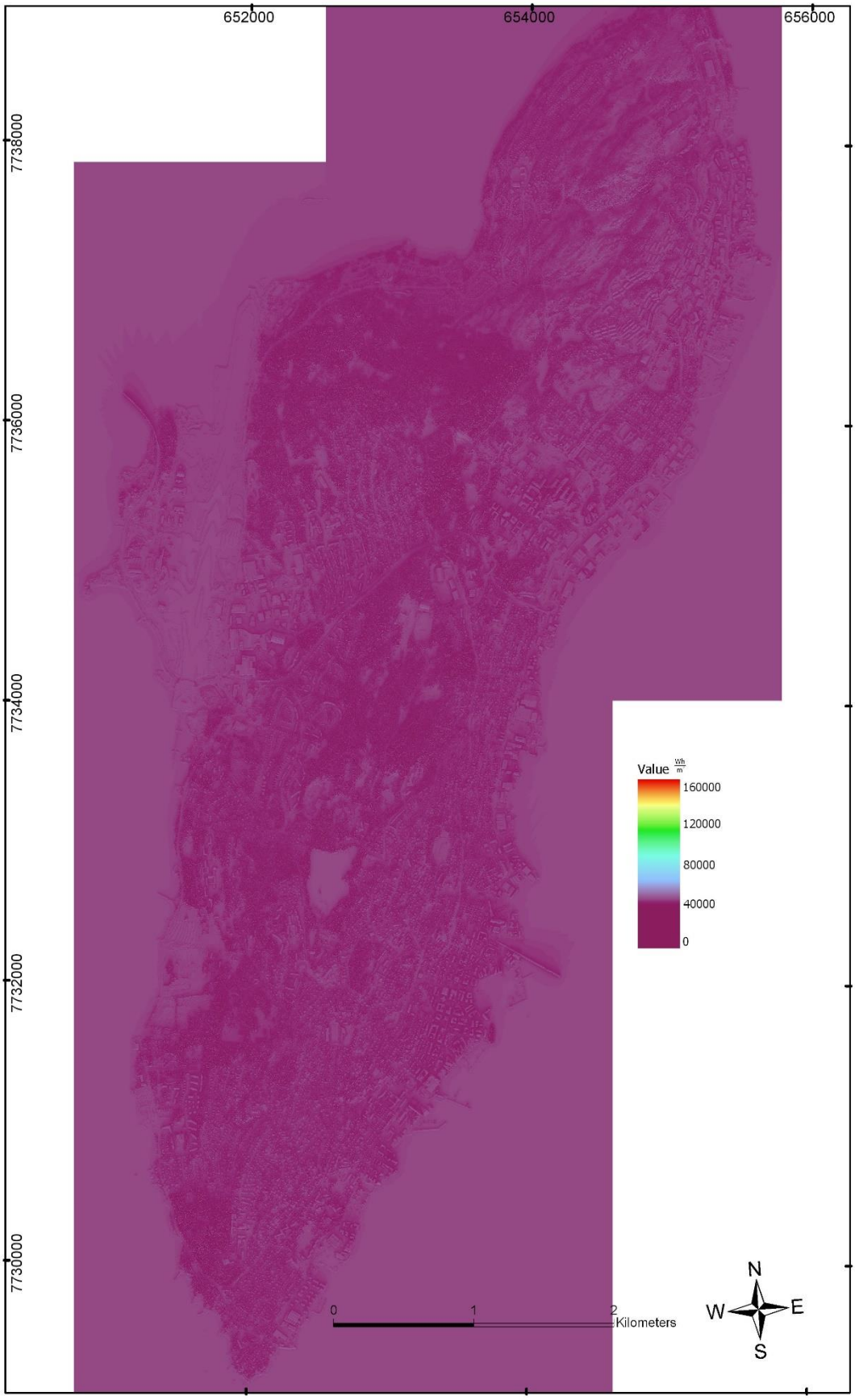

Figure 7-2: Solar map for February, with legend values varying from 0 to 160 kWh/m^2. Created in ArcGIS. Proj:UTM Z-33N

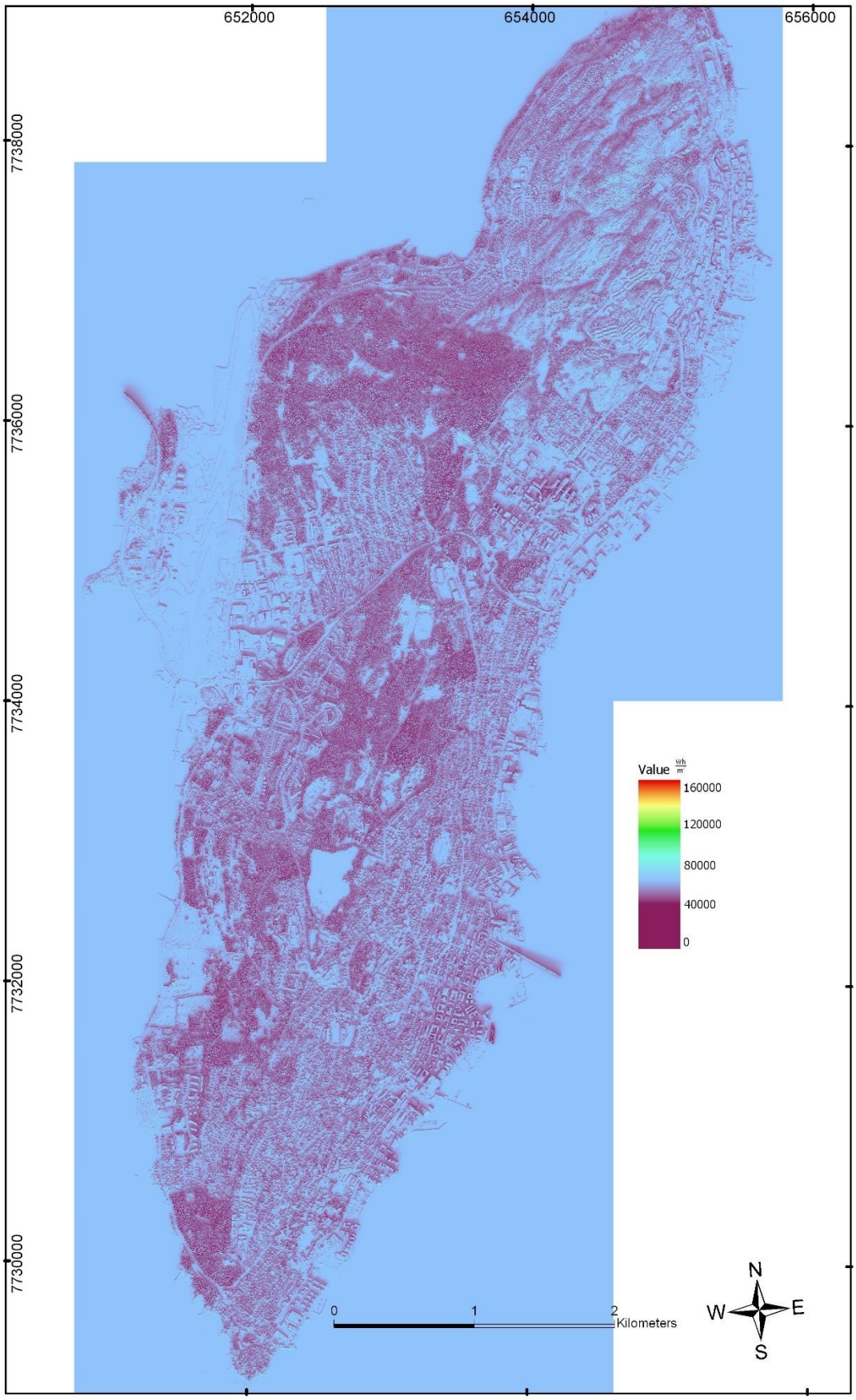

Figure 7-3: Solar map for March, with legend values varying from 0 to 160 kWh/m^2. Created in ArcGIS. Proj:UTM Z-33N

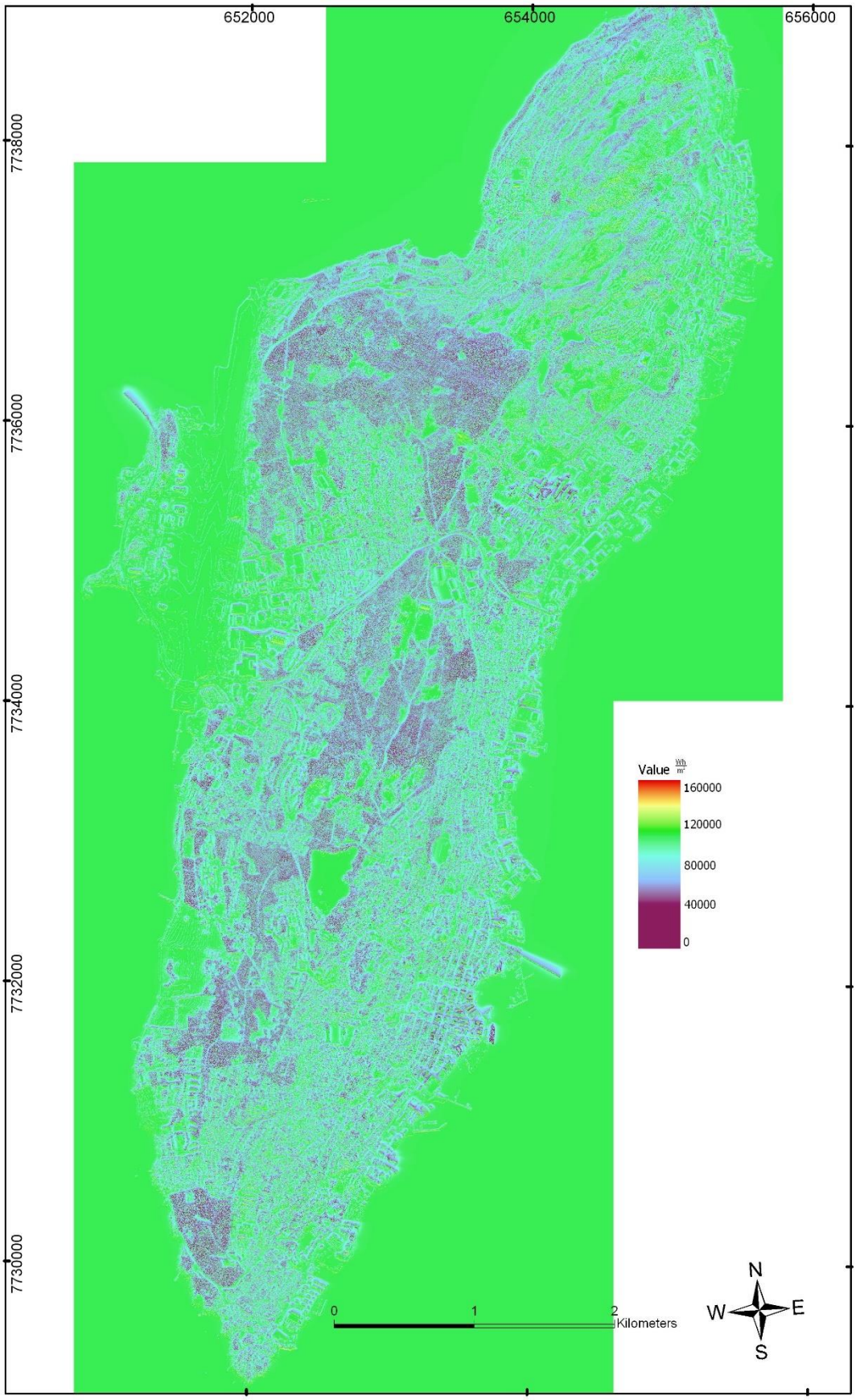

Figure 7-4: Solar map for April, with legend values varying from 0 to 160 kWh/m^2. Created in ArcGIS. Proj:UTM Z-33N

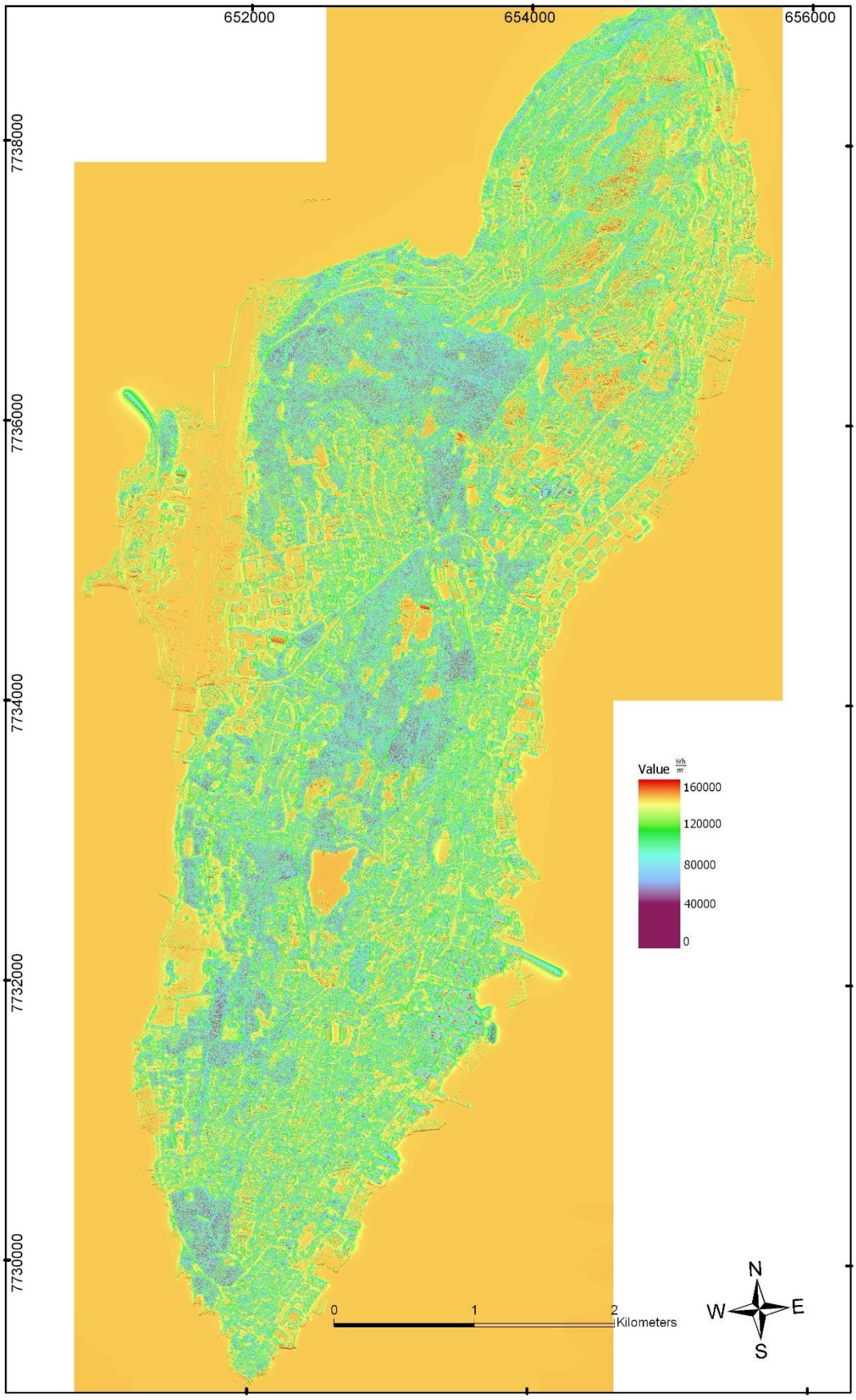

Figure 7-5: Solar map for May, with legend values varying from 0 to 160 kWh/m^2. Created in ArcGIS. Proj:UTM Z-33N

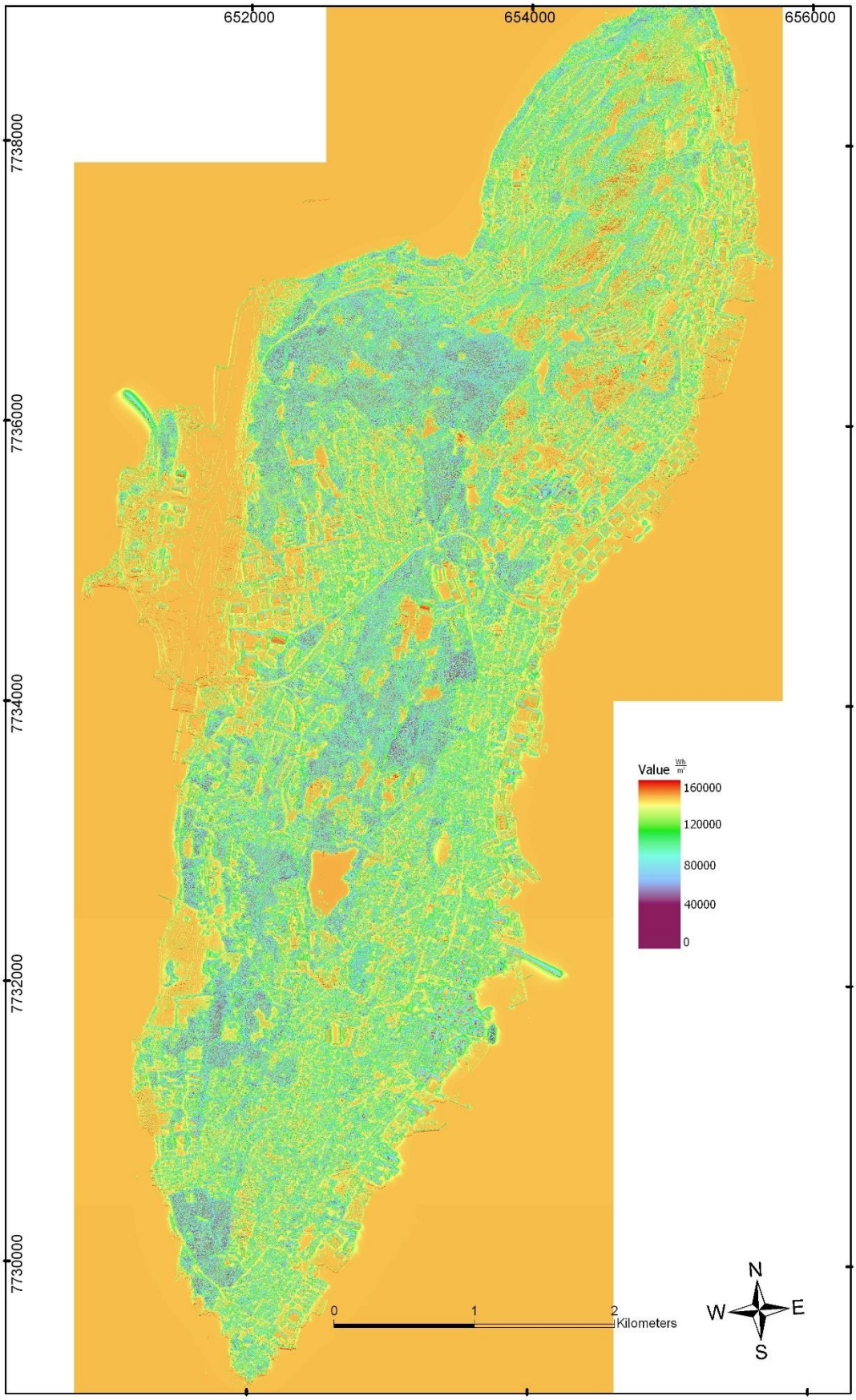

Figure 7-6: Solar map for June, with legend values varying from 0 to 160 kWh/m^2. Created in ArcGIS. Proj:UTM Z-33N

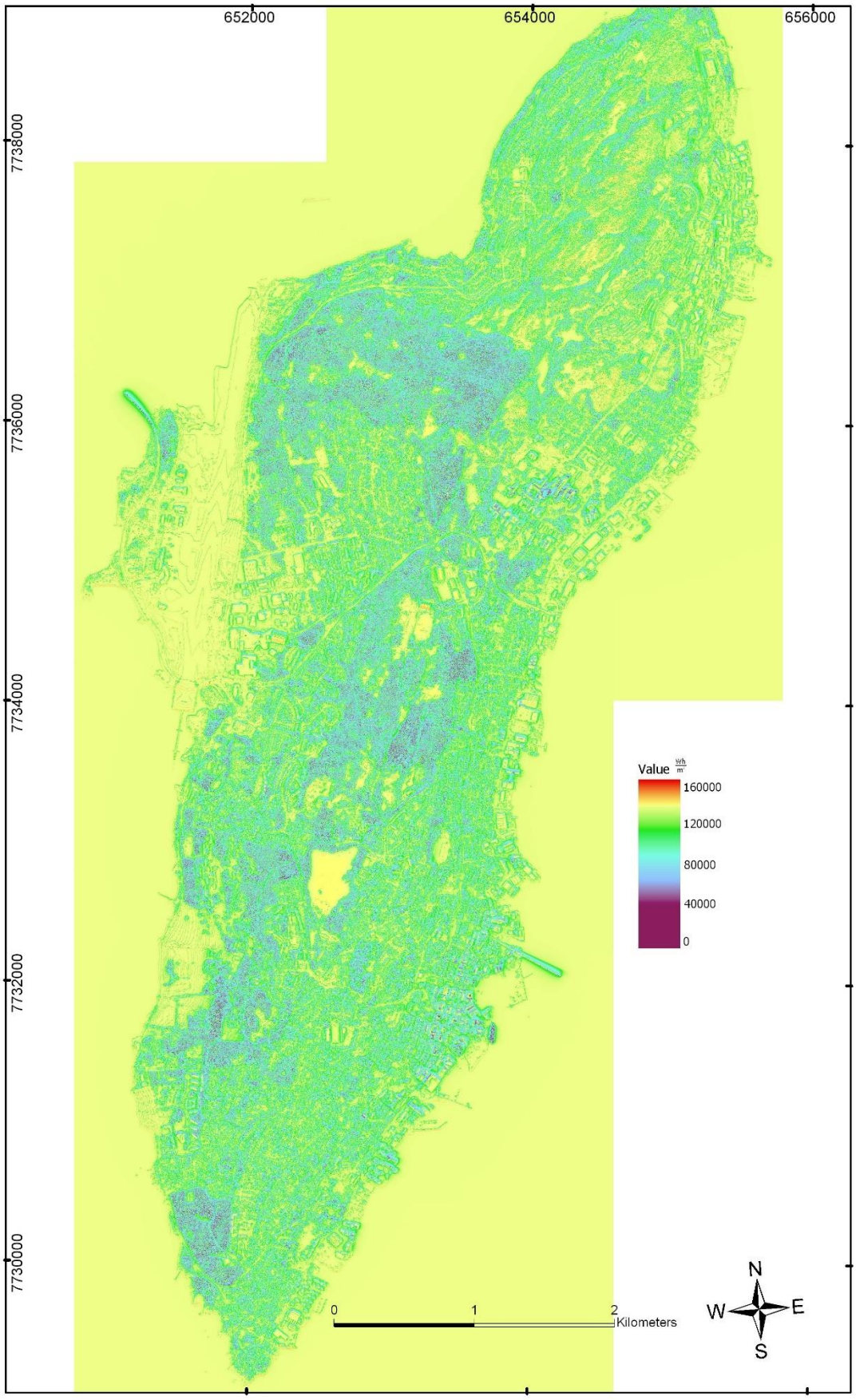

Figure 7-7: Solar map for July, with legend values varying from 0 to 160 kWh/m^2. Created in ArcGIS. Proj:UTM Z-33N

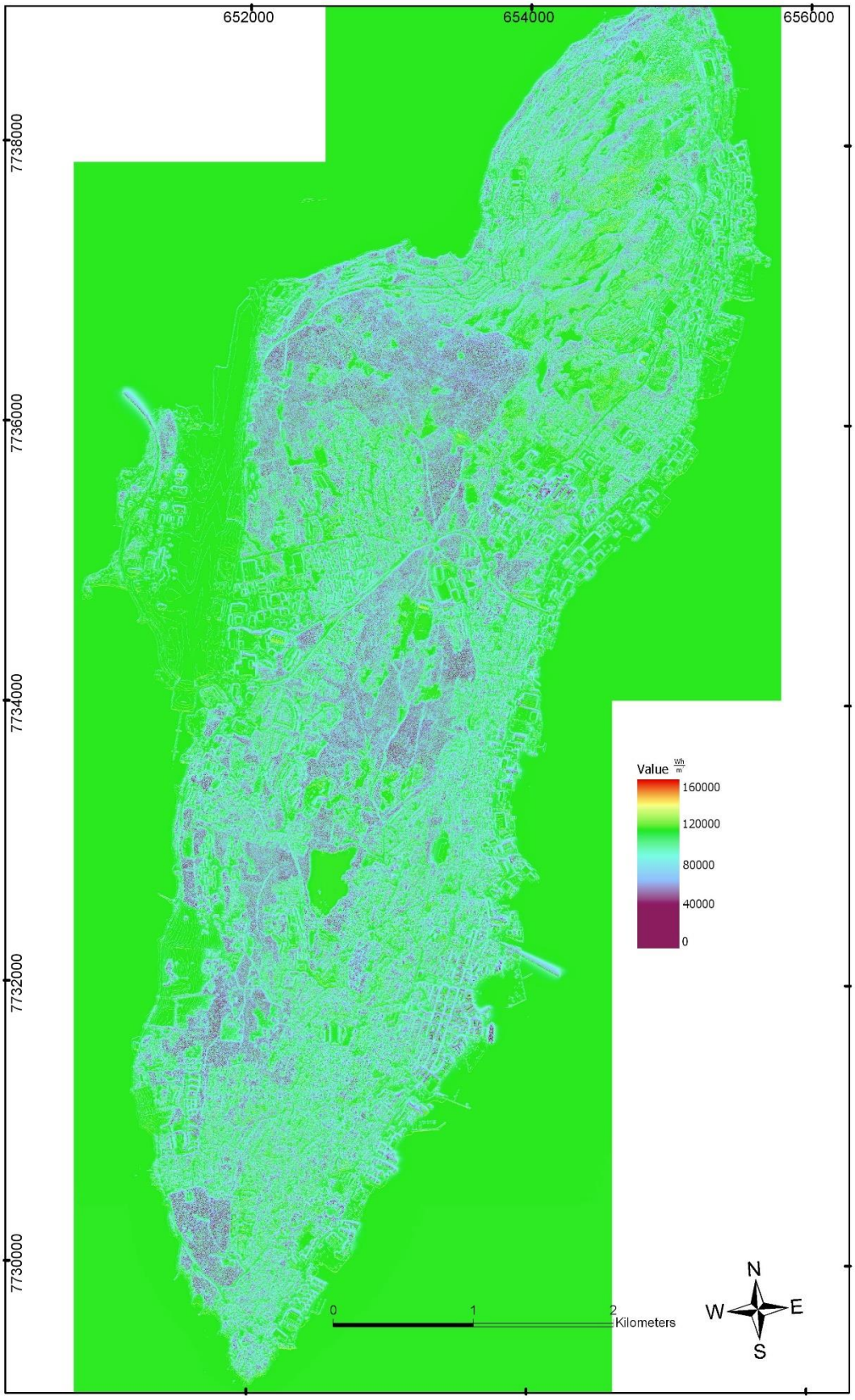

Figure 7-8: Solar map for August, with legend values varying from 0 to 160 kWh/m^2. Created in ArcGIS. Proj:UTM Z-33N

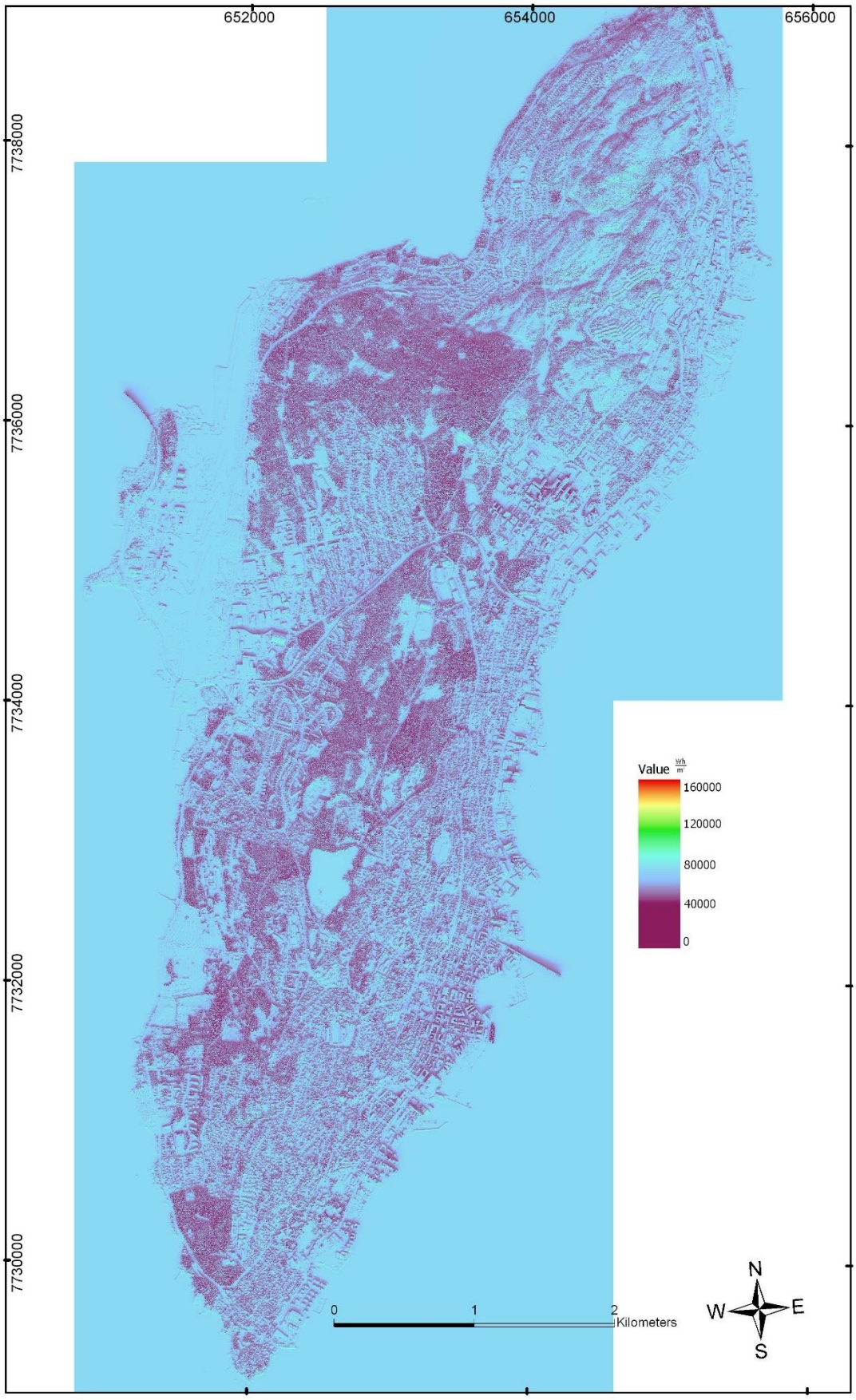

Figure 7-9: Solar map for September, with legend values varying from 0 to 160 kWh/m^2. Created in ArcGIS. Proj:UTM -33N

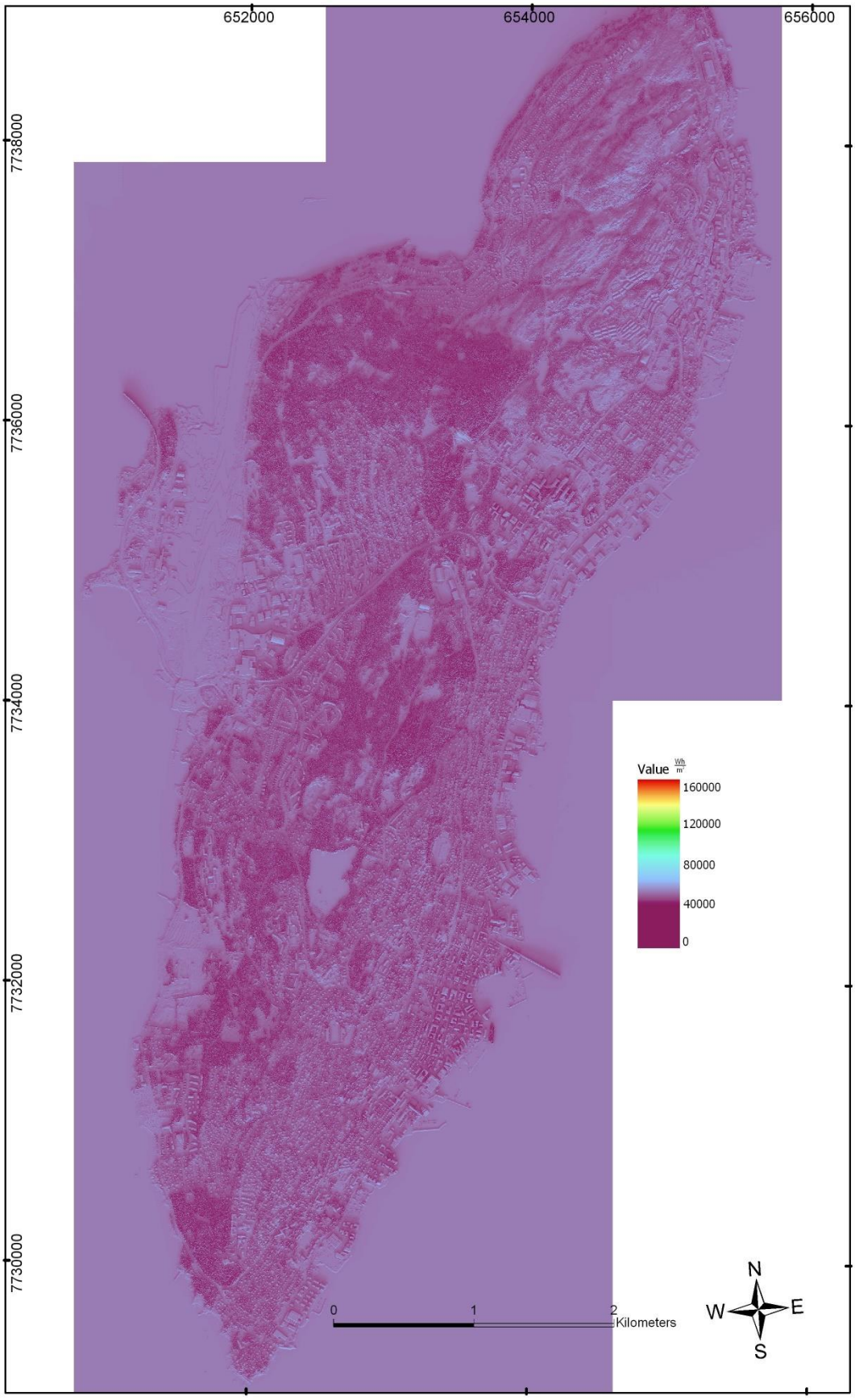

Figure 7-10: Solar map for October, with legend values varying from 0 to 160 kWh/m^2. Created in ArcGIS. Proj:UTM Z-33N

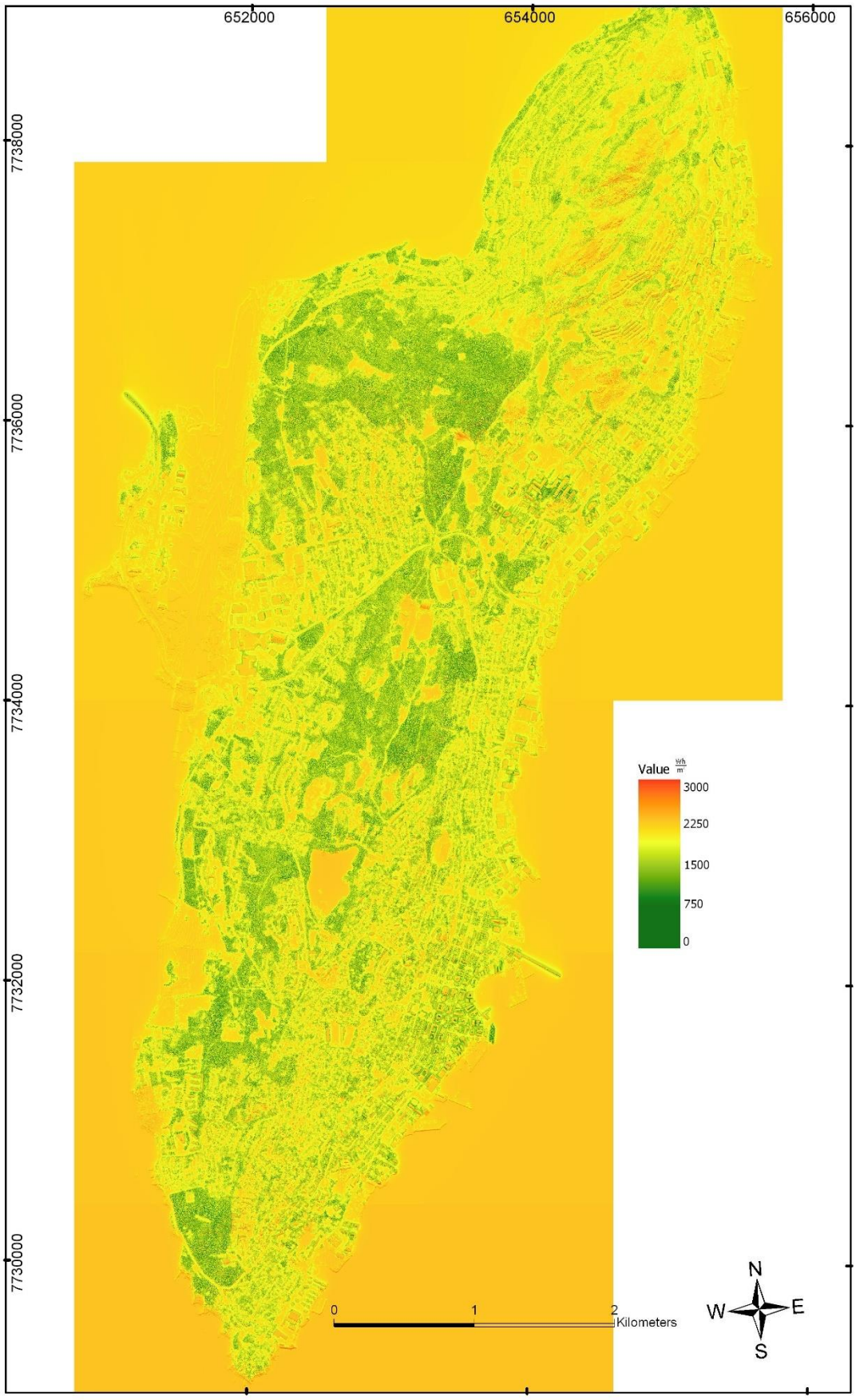

Figure 7-11:Solar map for November,with legend values varying from 0 to 160 kWh/m^2. Created in ArcGIS. Proj:UTM Z33N